

Lars Marius Mikalsen
Kasper Haugaard Thorsen

Improved Energy Dissipation in Stepped Spillways – Hydraulic Model Study Applying Bubble Image Velocimetry

Utforming av og energihåndtering i
trappetrinnsflomløp - modellforsøk med Bubble
Image Velocimetry

Master's thesis in Civil and Environmental Engineering

Supervisor: Leif Lia

Co-supervisor: Elena Pummer, Asli Bor Türkben

June 2023

Lars Marius Mikalsen
Kasper Haugaard Thorsen

Improved Energy Dissipation in Stepped Spillways – Hydraulic Model Study Applying Bubble Image Velocimetry

Utforming av og energihåndtering i
trappetrinnsflomløp - modellforsøk med Bubble
Image Velocimetry

Master's thesis in Civil and Environmental Engineering
Supervisor: Leif Lia
Co-supervisor: Elena Pummer, Asli Bor Türkben
June 2023

Norwegian University of Science and Technology
Faculty of Engineering
Department of Civil and Environmental Engineering



Norwegian University of
Science and Technology



MASTEROPPGÅVE

Kandidat: *KASPER HAUGAARD THORSEN OG LARS MARIUS MIKALSEN*

Tittel: **UTFORMING AV OG ENERGIHANDTERING I
TRAPPETRINNSFLOMLØP – MODELLFORSØK**

1 BAKGRUNN

Flomløp til dammar må utformast for å leie store og små flommar sikkert forbi dammen og andre konstruksjonar. Dei fleste flomløp er utforma for ein spesifikk kapasitet, og i dei fleste tilfelle må energien som finnast i flomvatnet takast ut av vatnet før vatnet når tilbake i elveløpet. Dette kallast ‘energidreping’ på norsk, sjølv om ordet ikkje kling særleg i kommunikasjon med andre. Ulike former for energidreping nyttast for ulik topografi, ulike damtyper, ulike vassføringar osv. Sidan Noreg i hovudsak har svært god bergkvalitet, har energidreping i flomløp ikkje fått særleg merksemd. Internasjonalt har det stort fokus og mange sofistikerte løysingar har blitt utvikla gjennom tidene.

Denne masteroppgåva vil undersøke utforming og energidreping for flomløp som er bygd med trappetrinn nedstraums overløpsterskelen. Det skiljast mellom to typar; Små trinn (som i ei vanleg trapp) og store trinn (som lange kar). Energidrepinga i slike trappetrinn kan også gå føre seg på minst to måtar; med auka ruhet frå trappetrinna (som om du sklir ned ei trapp) eller som fullstendig energiomsetning i kvart trinn (som i eit vasstandssprang). Skiljet mellom dei måtane går i hovudsak på einingsvassføring i høve til utforming av kvart trinn, men i mange tilfelle kan skilnaden mellom funksjon bli liten. Litteraturen på flomløp med trappetrinn er ikkje særleg godt utvikla, spesielt ikkje for val av ingeniørmessige gode løysingar. Det er såleis eit ønskje frå kraftutbyggerar og andre om eit betre kunnskapsgrunnlag for utforming av trappetrinn i flomløp.

Modellering og berekning av energinivå i vatn er spesielt krevjande der det er store vasshastigheter kombinert med luftmeddriving, som i eit flomløp. Luftinnblanding er ikkje råd å skalere rett korkje i fysiske modellforsøk eller i CFD, så forsøka må ta omsyn til det. Val av oppsett, skala, metodikk osv. må veljast ut frå kva som er formålet med oppgåva og resultatata bør gjerast mest mogeleg generelle og relevante for framtidige prosjekt.

2 HOVEDPUNKT I OPPGÅVA

Arbeidet vil ha med seg følgjande hovudpunkt:

1. Litteraturstudie på flomløp med trappetrinn
2. Gjennomgang av eksisterande flomløp med trappetrinn, i Noreg og internasjonalt
3. Planlegging, utforming og etablering av modellforsøk i Vassdragslaboratoriet for uttesting av
 - Ulik utforming og storleik på trappetrinn
 - Ulik skala
 - Varierende funksjon og detaljutforming
4. Simulering/kartlegging av strøymingsforhold på dei valte løysingane i pkt. 3
5. Testing av følgjande forhold med fysisk modell
 - a. Strømningsituasjon
 - b. Energiomsetning
 - c. Total energidreping
 - d. Sikkerhet og risiko for feilfunksjon
6. Samanlikning av resultat frå fysiske forsøk med andre forsøk/simuleringar
7. Vurdering av praktiske forhold mop. bygging
8. Diskusjon og konkludering
9. Rapportering

Det kan kome forslag til endringar i oppgåva og det må vurderast av studentane i samråd med rettleiarane.

3 RETTLEIING, DATA OG INFORMASJON

Professor Leif Lia vil vere hovudrettleiar og Dr. Elena Pummer og Dr. Asli Bor Türkben vil vere medrettleiarar. Teknikarar i Vassdragslaboratoriet vil vere tilgjengelege under arbeidet, men det vil også vere aktuelt å løyse mange av dei praktiske utfordringane sjølve. Diskusjon med og bidrag frå kollegaer og medarbeidarar i NTNU, Sintef, NVE, rådgivande ingeniørfirma og kraftselskap er tilrådd. Bidrag som nyttast i rapporten skal refererast på rett måte.

4 RAPPORTFORMAT, REFERANSER OG ERKLÆRING

Oppgåva skal skrivast i eit tekstbehandlingsprogram slik at figurar, tabellar, foto osv. får god rapportkvalitet. Rapporten skal innehalde eit samandrag, ei innhaldsliste, ei litteraturliste og opplysningar om andre relevante referansar og kjelder. Oppgåva skal leverast i B5-format som .pdf i Inspira og trykkast i tre eksemplar som sendast direkte frå trykkeri til faglærer/institutt. Samandraget skal ikkje gå over meir enn 450 ord både på norsk og engelsk

Masteroppgåva skal ikkje leverast seinare enn 11. juni (20 veker).

Trondheim, 13. januar 2023



Leif Lia
Professor

ABSTRACT

Energy dissipating structures that can handle changing hydrological conditions without jeopardizing dam safety is crucial. Stepped spillways are a type of energy dissipator that has regained interest since the introduction of roller compacted concrete (RCC). This physical hydraulic model study seeks to optimize parts of the design, operation and modelling of stepped spillways, focusing on feasible measures and practical methods.

Stepped spillways have been studied thoroughly both in physical models, numerical models and in practice lately, particularly the transitions of flow regimes in addition to modification of step geometry has been subject of investigation. It was decided to focus on the skimming flow regime, two-phase flow conditions, and simple measures of improving energy dissipation in this study. Bubble image velocimetry (BIV), in addition to combining and comparing experimental data with prototype data that is available, were also methods chosen to proceed with.

Two scaled physical hydraulic models in Froude similitude were constructed in the Norwegian Hydrotechnical Laboratory at the Norwegian University of Science and Technology in Trondheim. It was determined that the models corresponded well with established theory. Crest splitters were installed to further increase energy dissipation, and the hydraulic jump method was applied to measure the residual energy level. State of the art BIV was also employed to investigate flow characteristics.

Data measurements from the experimental program were conclusive by large, and a great deal of different phenomena was observed and discussed. The data obtained from BIV is extremely dense in information, with remarkable levels of detail, which is ideal for studying highly turbulent two-phase flow. Severe scale effects were also observed, both in air entrainment and in energy dissipation, as anticipated.

The study found crest splitters to be a practical and cost-effective measure to improve energy dissipation, in addition to reducing the length of inception and cavitation potential, leading to a higher allowable maximum unit discharge. Higher discharges must be investigated along with optimization of splitter geometry in further studies. BIV seem like best practice to study two-phase flow at certain conditions, but must be validated. Combining prototype data with model studies has great potential and should be investigated further. The importance of a large scale model must also be emphasized, which is also relevant for the use of BIV.

SAMMENDRAG

Utforming av hydrauliske konstruksjoner som sikrer tilstrekkelig energihåndtering ved flomsituasjoner er avgjørende i møte med framtidens klima. Trappetrinnsflomløp er en type energidreperkonstruksjon som har fått mye oppmerksomhet siden introduksjonen av valsebetong, da kombinasjonen gir en enkel og kostnadseffektiv byggeprosess. Dette studiet benytter fysiske modellforsøk for å optimalisere utforming, drift og modellering av trappetrinnsflomløp, med fokus på byggbare og praktiske løsninger.

Trappetrinnsflomløp har i nyere tid blitt studert grundig i fysiske modeller, numeriske modeller og i praksis, da spesielt overgangen mellom forskjellige strømningsregimer, samt modifikasjon av trappetrinnsgeometri. I dette studiet er det valgt å fokusere på strømningskarakteristikk ved høye vannføringer, luft-vann strømning, og metoder for å øke energiuttaket ved hjelp av enkle og byggbare løsninger. Metoder som ble valgt er blant annet videobasert hastighetsmetri (BIV), i tillegg til det å kombinere fysiske modellforsøk med data fra prototyp.

To skalerte fysiske modeller ble bygget ved hjelp av Froudes modellov i Vassdragslaboratoriet ved NTNU i Trondheim. Innledende forsøk fastslo at modellene samsvarte godt med eksisterende teori. Strømningssplittere ble installert for å øke energiuttaket, hvor nedstrøms energinivå ble beregnet ved hjelp av vannstandsspranget. Toppmoderne BIV ble benyttet for å studere strømningsbildet.

Måleseriene viser entydighet, og mange fenomener blir observert og diskutert. Data innhentet med BIV er svært detaljert, og inneholder ekstremt mye informasjon, noe som er ideelt når man studerer turbulent tofase strømning. Tydelige skalaeffekter på luftmedrivning og energidreping ble også observert, som forventet.

Studien fastslår at strømningssplittere er et byggbart og kostnadseffektivt tiltak for å øke energiuttaket i flomløpet, i tillegg til å øke naturlig luftmedrivning og redusere kavitasjonsfare. Dette fører videre til en økt grense på maksimal enhetsvannføring. Større vannføringer burde undersøkes sammen med optimalisering av utformingen av strømningssplittere i videre studier. BIV er vurdert til å være den beste fremgangsmåten for å studere luft-vann strømninger under visse forhold, men metoden må valideres i hvert enkelt tilfelle. Kombinasjonen mellom fysisk modellering og data fra prototyp er lovende, og burde fokuseres på i videre studier. I tillegg må viktigheten av stor skala understrekes, både for å minimere skalaeffekter, men også for bruken av BIV.

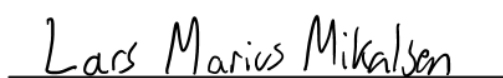
PREFACE

This master's thesis of 30 ECTS is the final work of our 2-year master's degree program in Civil and Environmental Engineering at the Norwegian University of Science and Technology in Trondheim. The thesis work is a cooperation between Kasper Haugaard Thorsen and Lars Marius Mikalsen as a continuation of Mikalsen's pre-feasibility study on energy dissipation structures in a project for Scatec ASA.

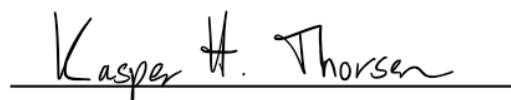
The topic of stepped spillways with additional elements for increased energy dissipation has been a topic of research during the last decades. As former craftsmen, Lars Marius as a plumber and Kasper as a concrete worker respectively, this topic was chosen on account of a desire to reduce the gap between theoretical research and more feasible engineering solutions, in addition to the wish of conducting physical hydraulic modelling.

We want to express our gratitude to the staff and co-students at the Department of Civil and Environmental Engineering among other persons in the industry, domestically and abroad, for short or long discussions, both professional and non-professional. Thanks to our supervisor Prof. Leif Lia for leading and guiding us with his vast knowledge, and to our co-supervisors Assoc. Prof. Elena Pummer and Dr. Asli Bor Türkben for regular feedback. Thanks to Scatec ASA represented by Øyvind Engelstad and Dr. Hanne Nøvik for encouragement and emphasizing the importance of designing feasible solutions. Thanks to the expert on stepped spillways hydraulics Dr. Matthias Kramer of UNSW Canberra for willingly sharing his experience in hydraulic physical modelling, in addition to Prof. Nils Reidar Bøe Olsen for his valuable insights regarding numerical modelling.

Thank-you to our loved ones from far south in Denmark to far north in Norway.



Lars Marius Mikalsen



Kasper Haugaard Thorsen

Trondheim, June 9, 2023

CONTENTS

Abstract	i
Sammendrag	ii
Preface	iii
Contents	iv
List of Figures	vi
List of Tables	vii
List of Symbols	viii
1 Introduction	1
1.1 Background	1
1.2 Purpose and limitations	2
1.3 Scope of the thesis	2
2 Theoretical Framework	3
2.1 Stepped spillways	3
2.1.1 Definition sketch	3
2.1.2 Flow regimes on a stepped chute	5
2.1.3 Transition of flow regimes	6
2.1.4 Inception of free-surface aeration	7
2.1.5 Air entrainment and cavitation potential	9
2.1.6 Flow depths	11
2.1.7 Flow velocities	11
2.2 Energy dissipation	13
2.2.1 Roberts splitters	13
2.2.2 Hydraulic jump	14
2.2.3 Stepped spillways	14
2.3 Review of hydraulic studies	15
2.4 Physical hydraulic modelling	18
2.4.1 Similarity and scale effects	18
2.4.2 Physical measuring methods	19
2.5 Resulting research method	23

3	Experimental Setup	25
3.1	Experimental facilities	25
3.1.1	Flume system layout	25
3.1.2	Entrance conditions	26
3.1.3	Standard stepped spillway models	27
3.1.4	Stepped spillway models with crest splitters	29
3.1.5	Tailwater adjustment and outflow conditions	30
3.2	Measuring instrumentation	30
3.2.1	Discharges	31
3.2.2	Image-based velocimetry	31
3.2.3	Flow depths	33
3.3	Experimental program	34
4	Results	35
4.1	Flow characteristics	35
4.2	Onset of air entrainment	41
4.3	Energy dissipation	42
4.4	Velocity profiles	45
4.5	Qualitative visual observations	48
5	Discussion	49
5.1	Effect of crest splitters	49
5.1.1	Energy dissipation	49
5.1.2	Length of inception	50
5.1.3	Flow regimes	50
5.2	Application of BIV	51
5.2.1	Velocity profiles	51
5.2.2	Uncertainty and error sources	52
5.2.3	Other observations	53
5.3	Scale effects	54
5.3.1	Air-water flow	54
5.3.2	Length scale magnitude	54
5.3.3	Other error sources	55
6	Conclusions	57
6.1	Key findings	57
6.2	Recommendations for future research	58
	References	59
	Appendices:	I
A	Laboratory Data	II
A.1	D-flume measurements	II
A.2	C-flume measurements	VI
B	PIVlab Settings	IX

LIST OF FIGURES

2.1.1 Definition sketch of stepped spillways in skimming flow conditions.	4
2.1.2 Representation of nappe, transition, and skimming flow regimes.	5
2.1.3 Empirical relations for the onset of flow regimes on stepped spillways.	7
2.1.4 Empirical relations for the length of inception on stepped spillways.	8
2.2.1 Wadi Dayqah main dam, Oman.	13
2.3.1 Physical model of stepped spillways with triangular protrusions.	15
2.3.2 Sketch of a selection of different stepped spillway configurations.	16
2.4.1 Positioning of the hydraulic jump downstream stepped spillways.	22
3.1.1 D-flume experimental setup.	25
3.1.2 C-flume experimental setup.	26
3.1.3 D-model in D-flume.	28
3.1.4 C-model in C-flume.	28
3.1.5 Crest splitters positioning and design.	29
3.2.1 Experimental setup for the D-model.	30
3.2.2 Comparison of original and pre-processed frame in PIVlab.	32
3.2.3 Ultrasonic sensors positioning in D-flume.	33
4.1.1 Side view of skimming flow in the stepped spillway models.	35
4.1.2 Deflecting nappe in C-model.	36
4.1.3 Velocity vectors in D-model obtained from BIV analysis.	36
4.1.4 Velocity magnitude in D-model obtained from BIV analysis.	37
4.1.5 Streamlines in D-model obtained from BIV analysis.	37
4.1.6 Comparison of flow regimes in both models	38
4.1.7 Comparison of streamlines in D-model obtained from BIV analysis.	39
4.1.8 Transitions between skimming regime and deflecting nappe regime.	40
4.2.1 Comparison of inception point location with empirical relations.	41
4.3.1 Energy dissipation in D-model.	42
4.3.2 Energy dissipation in C-model.	43
4.3.3 Energy grade line in D-model.	44
4.4.1 Velocity profiles in D-model compared with power-law approach.	45
4.4.2 Velocity profiles in D-model compared with mixing layer theory.	46
4.4.3 Surface velocities compared with ideal fluid flow.	47
4.5.1 Region of low pressure on spillway surface in D-model.	48

LIST OF TABLES

2.1.1 Description of notation used in stepped spillway sketch	4
2.1.2 Summary of coefficients used to fit the power law.	12
2.4.1 Recommended criteria for stepped spillways model scaling.	18
3.1.1 Overview of model and prototype dimensions.	27
3.1.2 Crest splitters design parameters.	29
3.3.1 Summary of parameters and ranges in the experimental scheme. . .	34
A.1.1 D-flume measurements data - series 1 - basecase.	II
A.1.2 D-flume measurements data - series 2 - basecase.	III
A.1.3 D-flume measurements data - series 3 - basecase.	III
A.1.4 D-flume measurements data - series 1 - splitters.	IV
A.1.5 D-flume measurements data - series 2 - splitters.	IV
A.1.6 D-flume measurements data - series 3 - splitters.	V
A.2.1 C-flume measurements data - series 1 - basecase.	VI
A.2.2 C-flume measurements data - series 2 - basecase.	VI
A.2.3 C-flume measurements data - series 3 - basecase.	VII
A.2.4 C-flume measurements data - series 1 - splitters.	VII
A.2.5 C-flume measurements data - series 2 - splitters.	VIII
A.2.6 C-flume measurements data - series 3 - splitters.	VIII
B.0.1 Overview of settings in PIVlab.	IX

LIST OF SYMBOLS

Roman symbols

A	Cross section area [m^2]
B_f	Flume width [m]
\bar{C}	Depth-averaged air concentration [-]
C_b	Air concentration at the pseudo-bottom [-]
C_{bi}	Air concentration at the pseudo-bottom at the point of inception [-]
\bar{C}_i	Mean air concentration at point of inception [-]
D_h	Hydraulic diameter [m]
f	Darcy-Weisbach friction factor [-]
F_i	Inception Froude number, $F_i = q_w / \sqrt{g(h_s/l_s)k_s^3}$ [-]
Fr	Froude number, $Fr = u / \sqrt{gz}$ [-]
F_*	Roughness Froude number, $F_* = q_w / \sqrt{g \sin(\theta)k_s^3}$ [-]
g	Gravity acceleration [m/s^2]
H	Local energy head [m]
H_0	Head above crest [m]
H_{90}	Dimensionless mixture flow depth, $H_{90} = z/z_{90}$ [-]
h_c	Critical depth, $h_c = \sqrt[3]{q_w^2/g}$ [m]
H_{dam}	Dam head crest above downstream toe [m]
H_f	Height of flume [m]
h_s	Height of the step [m]
k_s	Normal height of the step [m]
L_e	Characteristic mixing layer length scale [m]
L_i	Longitudinal distance from the top of the crest to the inception point [m]
L_j	Length of the hydraulic jump [m]
l_s	Length of the step [m]
L_u	Longitudinal distance from the top of the crest to the beginning of the quasi-uniform region [m]
L_x	Longitudinal distance from the top of the first step [m]
n	Power-law exponent [-]
N_s	Number of steps along the chute [-]
P_0	Pressure at flow surface [N/m^2]
P_v	Vapor pressure [N/m^2]
Q	Water discharge [m^3/s]
Q_{max}	Maximum water discharge [m^3/s]
q_w	Unit water discharge [m^2/s]
R_1	Upstream radius 1 for ogee weir [m]

R_2	Upstream radius 2 for ogee weir [m]
Re	Reynolds number [-]
R_h	Hydraulic radius [m]
u	Streamwise water velocity [m/s]
\bar{u}	Time-averaged streamwise velocity [m/s]
u_0	Mean streamwise water velocity [m/s]
u_1	Incoming velocity to the hydraulic jump [m/s]
u_2	Outgoing velocity from the hydraulic jump [m/s]
u_{90}	Air-water mixture velocity at the flow depth z_{90} [m/s]
u_{FS}	Free-stream velocity [m/s]
u_{if}	Inflection point velocity [m]
u_m	Air-water mixture velocity [m/s]
\bar{u}_m	Time-averaged mixture velocity [m/s]
u_{min}	Minimum velocity of the mixing layer [m/s]
u_{ML}	Mixing layer velocity [m/s]
V	Volt [V]
v_c	Critical velocity [m/s]
W	Weber number [-]
x	Longitudinal streamwise distance from the top of the crest [m]
x_i	Dimensionless distance from the inception point, $x_i = (x - L_i)/z_{m,i}$ [-]
x_s	Longitudinal distance between two step edges [m]
y	Coordinate normal to the flume bottom or river bed [m]
y_x	Vertical distance from downstream dam toe to pseudo-bottom [m]
Y	Conjugate flow depth in the hydraulic jump [m]
z	Coordinate and flow depth normal to the chute or pseudo-bottom [m]
z_{90}	Flow depth with 90% air concentration [m]
z_{if}	Inflection point elevation above pseudo-bottom [m]
$z_{m,i}$	Mixture depth at point of inception [m]
z_w	Equivalent clear water flow depth [m]

Greek symbols

α	Kinetic energy correction coefficient due to non-uniform velocity [-]
δ	Boundary layer thickness [m]
$\frac{\Delta H}{H_0}$	Relative energy loss [%]
η	Correction factor for the singular loss when the flow changes direction from the stepped spillway to the horizontal bed [-]
θ	Angle of the slope of the chute [°]
λ_F	Length scale factor in Froude similitude [-]
ν	Kinematic viscosity [m^2/s]
ρ_m	Density of air-water mixture [kg/m^3]
ρ_w	Density of water [kg/m^3]
σ_c	Cavitation index [-]
σ_{cr}	Critical cavitation index [-]
σ_{sur}	Surface tension between water and air [N/m]

Abbreviations

ADV	Acoustic Doppler velocimeter
BIV	Bubble image velocimetry
CFD	Computational fluid dynamics
CP	Conductivity probe
EPFL	École polytechnique fédérale de Lausanne
FPS	Frames per second
IP	Inception point
NTNU	Norwegian University of Science and Technology
OF	Optical flow
PIV	Particle image velocimetry
RCC	Roller compacted concrete
SPH	Smoothed-particle hydrodynamics
UNSW	University of New South Wales
USBR	United States Bureau of Reclamation
XPS	Extruded polystyrene

Index

1	Characteristics in the upstream cross-section of a hydraulic jump
2	Characteristics in the downstream cross-section of a hydraulic jump
90	Characteristics at 90% air concentration
<i>b</i>	Characteristics at the pseudo-bottom
<i>c</i>	Characteristics of critical flow
<i>i</i>	Characteristics of the inception point
<i>if</i>	Characteristics of the inflection point
<i>m</i>	Mixture air-water flow characteristics
<i>u</i>	Characteristics of the fully developed region (quasi-uniform region)
<i>w</i>	Clear water characteristics

INTRODUCTION

1.1 Background

As a result of a changing climate, we are experiencing an increase in the frequency and intensity of extreme weather events, which lead to more flooding, in addition to floods exceeding design flood values. More frequent, and more severe flooding leads to more stress on dams, and their associated energy dissipating structures.

Controlled energy dissipation is crucial for a spillway because erosion can lead to catastrophic failure for the associated dam. Constructing steps on the face of the spillway is useful to help dissipate the energy stored in the dam during the release of water, in addition to aerating the water. Some of the earliest documented use of stepped spillways in hydraulic design dates to 700 BC, in water supply systems for the ancient Assyrian city of Nineveh in upper Mesopotamia, today known as Mosul, Iraq (Ruff et al. 2002). The utilization of this technology is well documented for dams and weirs all over the world since then (Chanson 1994b).

The introduction of Roller Compacted Concrete (RCC) in dam construction has renewed the interest in stepped spillways as an energy dissipation structure because the construction technique of RCC favors stepped spillways (Khatsuria 2004). In dam construction, RCC is placed in horizontal layers using paving equipment and then compacted with vibrating roller equipment. This construction method leads to several advantages compared to using traditional concrete, predominantly rapid construction and reduced cost.

Stepped spillways are compatible with both concrete and gabion as construction materials. RCC is sometimes also used as an overlay on embankment dams for overtopping protection, a practical solution to the problem of insufficient capacity due to increasing design floods. There are several advantages of stepped spillways besides providing cost-efficient energy dissipation. The implementation of stepped spillways decreases the need for other energy dissipation measures, in practice, this often results in a reduction of the length of the stilling basins downstream. Introduction of two-phase air-water flow in stepped spillways also gives other advantages like re-aeration and reduced cavitation potential.

1.2 Purpose and limitations

Besides being crucial for dam safety, optimization of the design of hydraulic energy dissipation structures can reduce material usage and total cost in dam projects. Achieving a cost-effective, feasible design in a two-dimensional approach has massive potential, as this design can be applied for the full length along the dam axis. The main purpose of this study is to further utilize and optimize the main advantage of stepped spillways in RCC dams, complimentary energy dissipation.

There is often a difference between theoretical research and practice. Bridging the gap between hydraulic research and practical engineering solutions can contribute to dam safety, and improve standard design solutions. This study aims to apply and develop established theory to improve practice for stepped spillway design, operation, and modelling.

The field of study was limited by resources available, as well as the time at hand. It was not feasible to investigate all design parameters for stepped spillways in this research, some needed to be set constant in order to investigate others thoroughly. Instruments and computational capacity that was accessible for the study also set conditions for the field of research. More specific limitations are discussed in section 2.5.

1.3 Scope of the thesis

The first part of this study was to evaluate current practice in regard to stepped spillway design and operation, in addition to a review of hydraulic studies to investigate state of the art stepped spillway modelling. The field of study starts quite broad, and then more exact topics are picked. The most comprehensive and time-consuming part of this research was to construct and validate stepped spillway physical scale models. After the design and construction of the models, it was crucial that the models corresponded to the current established theory before proceeding with further research.

The new study focused on practical, cost-effective, and feasible measures to improve energy dissipation in stepped spillways, both in new projects and at existing spillways. Accurately measuring and determining flow characteristics is crucial to evaluate different designs, therefore this was also a central part of the study. Different scales of the models were also employed, in addition to prototype data, in order to investigate scale effects. An alternative perspective to traditional physical hydraulic modelling, such as other simulations, implementing new technology or numerical modelling was also included, which is explained thoroughly through the report.

THEORETICAL FRAMEWORK

2.1 Stepped spillways

During the last four decades, there has been carried out numerous investigations and studies on the hydraulics of stepped spillways, both in numerical models, in physical models, and in practice. Other than the practical restriction of the unit discharge $q_w < 30 \text{ m}^2/\text{s}$ due to the cavitation risk for higher discharges on stepped spillways, the implementation of stepped spillways seems to have great potential in many scenarios. Although stepped spillways can be a suitable alternative for energy dissipation in many projects, it is often difficult to precisely estimate and document the actual energy dissipation at a wide range of discharges and operating conditions for a given design (Mikalsen 2022).

In particular, the interactions between a stepped spillway and another energy dissipator, for example a stilling basin, can be hard to predict because of current issues in modelling turbulence and two-phase air-water flows, two governing processes in stepped spillways hydraulics. Because of these issues regarding modelling of stepped spillways hydraulics, Chanson (2021b) is questioning the accuracy of both numerical models and physical models in the absence of full-scale validation. A well known integral method used to determine the interaction of water and air for two-phase flows in prototypes is particle image velocimetry (PIV). A modified technique, known as bubble image velocimetry (BIV) has also been in use lately, in addition to the optical flow (OF) method. However, using these methods on prototypes to acquire validation data with satisfying quality can be a challenge (Zhang and Chanson 2018).

2.1.1 Definition sketch

Figure 2.1.1 illustrates the flow over a stepped spillway, the flow direction is from the left to the right. The figure also presents the notation used in this report, along with a corresponding table explaining the notation.

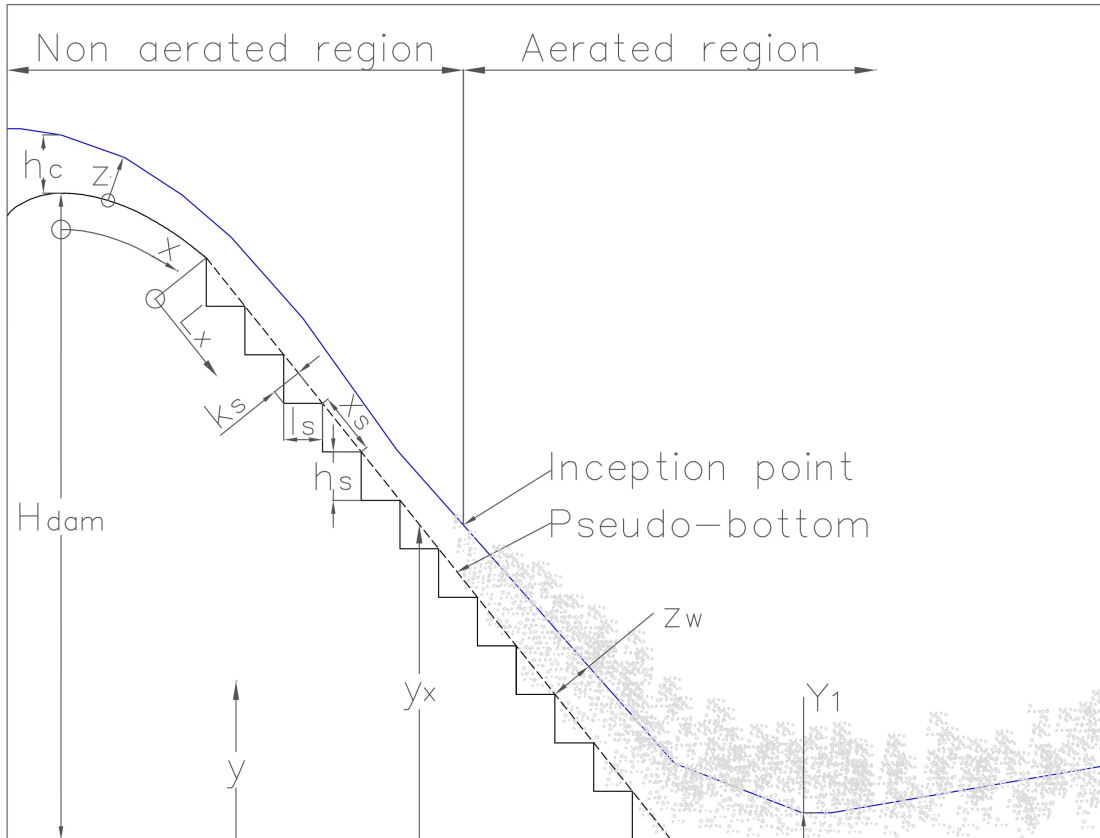


Figure 2.1.1: Definition sketch of a stepped spillway in skimming flow conditions.

The definition sketch is to scale. Table 2.1.1 gives a description of the notation used in the definition sketch.

Table 2.1.1: Description of notation used in stepped spillway sketch (figure 2.1.1)

Notation	Description
h_c	Critical flow depth
H_{dam}	Dam head crest above downstream toe
h_s	Height of the step
k_s	Normal height of the step
l_s	Length of the step
L_x	Longitudinal streamwise distance from the top of the first step
x	Longitudinal streamwise distance from the crest
y	Coordinate normal to the flume bottom or river bed
Y_1	Incoming flow depth to the hydraulic jump
y_x	Vertical distance from the dam toe to the pseudo-bottom
z	Coordinate and flow depth normal to the chute
z_w	Equivalent clear water flow depth

2.1.2 Flow regimes on a stepped chute

The behavior of flow over a stepped chute is classified depending on the flow conditions. In current literature, the flow regime is defined as nappe flow for low flow rates, transitional flow for intermediate flow rates, or skimming flow for high flow rates. A physical definition sketch of the different flow regimes (André 2004) can be observed in figure 2.1.2.

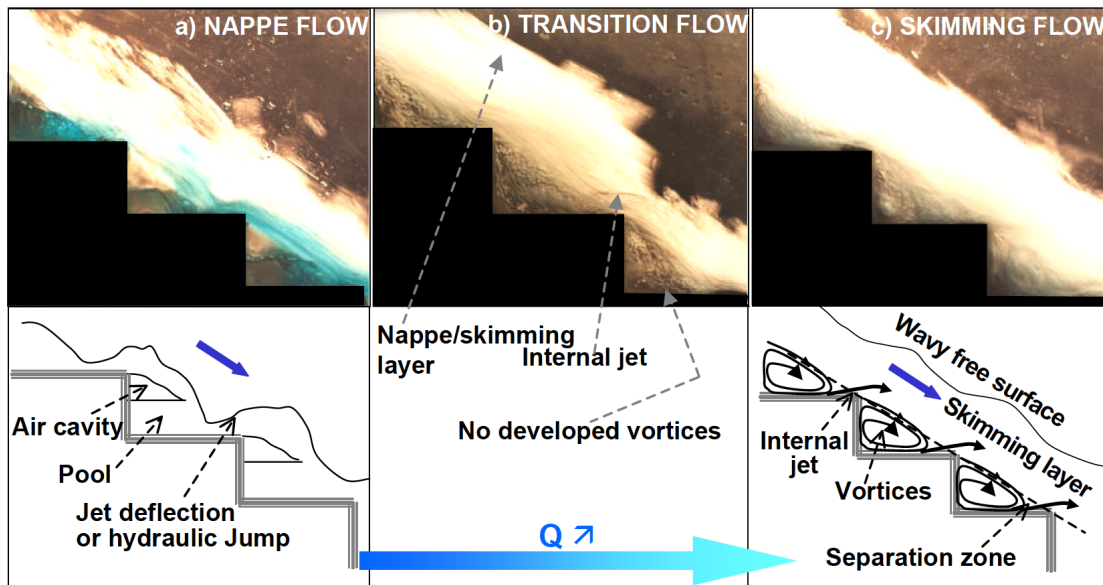


Figure 2.1.2: Physical representation of nappe flow, transition flow, and skimming flow regimes in a stepped flume (André 2004).

Nappe flow In nappe flow conditions there is a sequence of free falling jets from step to step, with a fully developed or partially developed hydraulic jump as seen in figure 2.1.2. A nappe flow regime will occur in low flow conditions, or during intermediate flow conditions in a stepped chute with modest incline.

Transitional flow In the transition between nappe flow and skimming flow, the flow conditions can be chaotic, because the pressure field changes drastically. The flow conditions in a transitional flow regime are characterized by considerable aeration, and the flow conditions can also change from one step to another.

Skimming flow In skimming flow conditions the water pool fills the entire step height, and the water stream produces a pseudo-bottom on the edges of the stepped chute. Beneath the pseudo-bottom, recirculating vortices develop and are maintained by the shear stress from water flowing past the steps.

Skimming flow is the governing flow regime for a stepped spillway, nevertheless we should also pay attention to the chaotic transitional flow regime. One challenging aspect regarding the study of the transitions between the different flow regimes, particularly the onset and termination of the transitional flow, is that they are not well defined because they are assessed individually by visual inspection and therefore somewhat subjective.

2.1.3 Transition of flow regimes

There have been carried out several investigations to estimate the onset of the transitional flow regime and the skimming flow regime, resulting in empirical relationships with parameters critical depth, step height and step length. Some of the most well known and used relations are presented in figure 2.1.3 with their corresponding valid ranges.

Chanson (2003) has defined the upper limit of the nappe flow regime as

$$\frac{h_c}{h_s} = 0.89 - 0.4 \left(\frac{h_s}{l_s} \right) \quad (2.1)$$

Chinnarasri (2002) defined the upper limit for the nappe flow regime as

$$\frac{h_c}{h_s} = 0.98(0.55)^{(h_s/l_s)} \quad (2.2)$$

The onset of the skimming flow regime was defined by Boes and Hager (2003b) as

$$\frac{h_c}{h_s} = 0.91 - 0.14 \left(\frac{h_s}{l_s} \right) \quad (2.3)$$

Chanson (1994a) defined the onset of skimming flow as

$$\frac{h_c}{h_s} = 1.057 - 0.465 \left(\frac{h_s}{l_s} \right) \quad (2.4)$$

Ohtsu et al. (2004) defined the onset of skimming flow as

$$\frac{h_s}{h_c} = \frac{7}{6} \left(\frac{h_s}{l_s} \right)^{1/6} \quad (2.5)$$

We can observe an interval between the upper limit of the nappe flow regime and the onset of the skimming flow regime in figure 2.1.3, in this zone we have the transitional flow regime.

The first studies on this topic did not consider a transitional flow regime, nor did they take the angle of the chute into account, while more recent studies define the transitional flow regime, and point out that a steeper slope requires less discharge to make the transition to a skimming flow regime. One of the early studies, by Rajaratnam (1990) defines the limit between the nappe and the skimming flow regime as approximately

$$\frac{h_c}{h_s} = 0.8 \quad (2.6)$$

Comparing this relationship to the empirical relations in figure 2.1.3 we can observe that the formula is somewhat valid for $0.4 < \frac{h_s}{l_s} < 1.4$, which corresponds to slopes of approximately $20^\circ < \theta < 55^\circ$ as we should be within the transitional flow regime for those specific criteria, if we do not include Chanson (1994a).

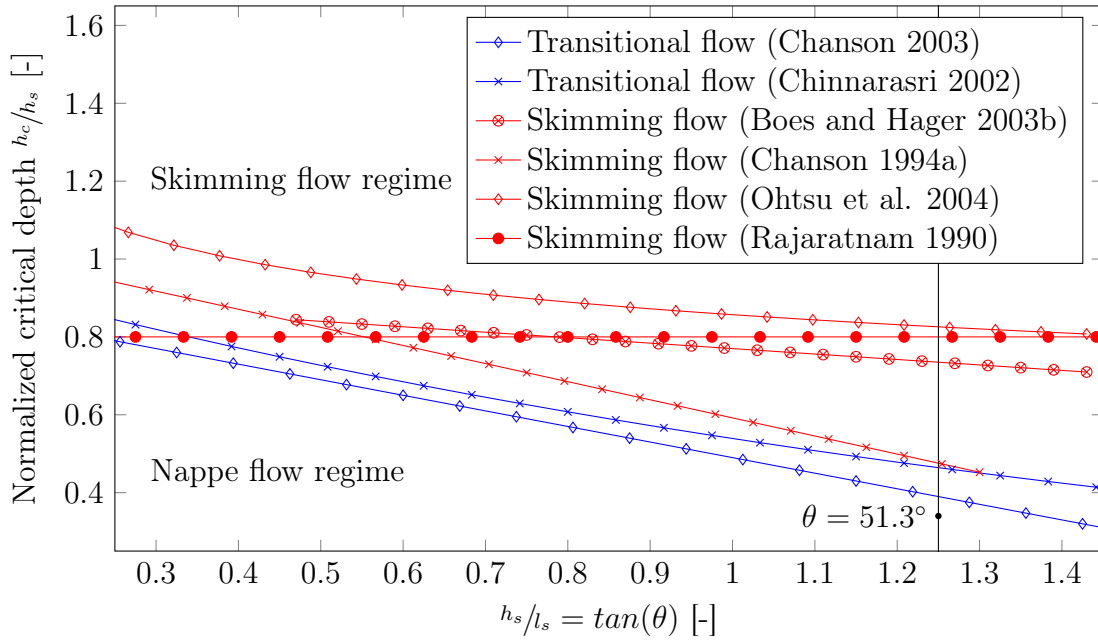


Figure 2.1.3: Empirical relations for the onset of flow regimes on stepped spillways.

2.1.4 Inception of free-surface aeration

In skimming flow conditions, the water in the triangles formed by the steps, under the pseudo-bottom observed in figure 2.1.1 is cut off from the stream. There is some exchange of water from this lower area with the upper flow due to intense turbulence (Khatsuria 2004) and energy dissipation occurs by momentum transfer. In flow conditions like this, a turbulent boundary layer develops from the crest, and along the upper steps due to the intense turbulence. The turbulent boundary layer grows until it intersects the free surface, this is called the point of inception (IP). Downstream the point of inception, the air concentration in the flow gradually increases until the quasi-uniform equilibrium flow region. In this region, the air concentration, velocity distribution and flow depth of the stream are somewhat constant.

The longitudinal distance between the critical depth position on the crest of the dam and the horizontal face where the inception point is located, L_i , is shorter on a stepped spillway than on a smooth chute. The reduction in L_i on a stepped spillway is caused by the additional turbulence generated by the substantial surface roughness, causing the turbulent boundary layer to grow faster. There have been conducted several studies to establish an empirical formulation for this distance, summarized in figure 2.1.4 for a stepped slope, where the spillway slope is $\theta = 51.3^\circ$.

The formulas presented in this section are based on the relation between a dimensionless distance to the inception point and the roughness Froude number.

The roughness Froude number is defined as

$$F_* = \frac{q_w}{\sqrt{g \sin(\theta) k_s^3}} \quad (2.7)$$

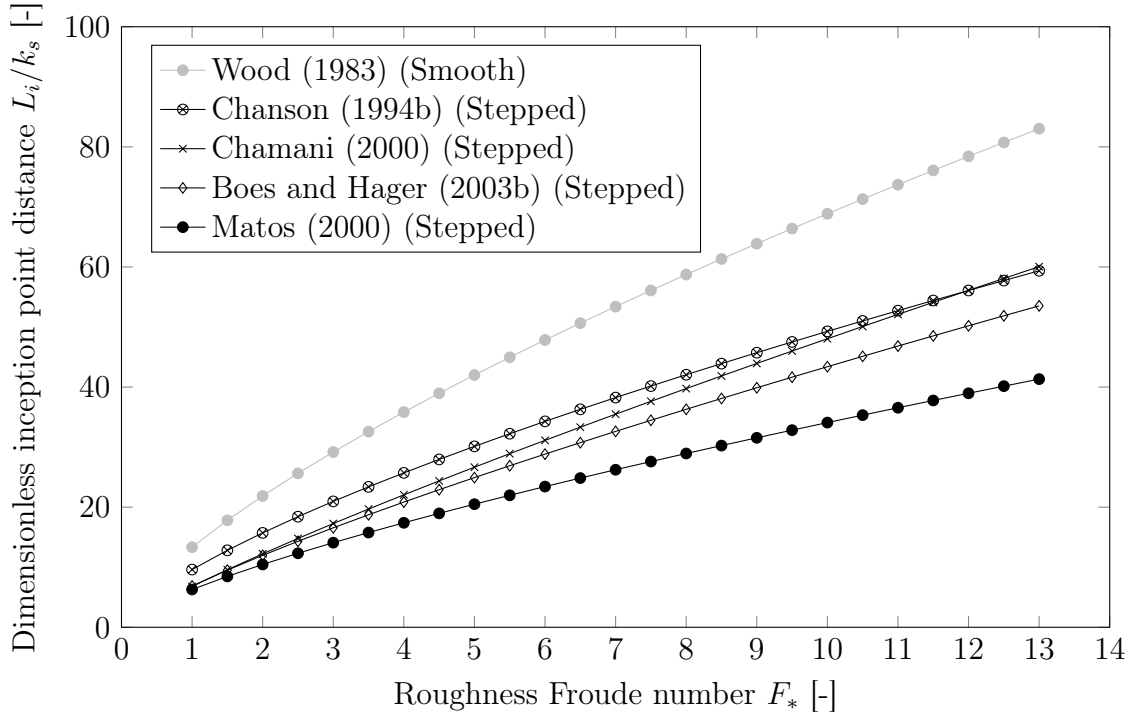


Figure 2.1.4: Comparison of empirical relations for the location of the inception point on stepped spillways.

André (2004) derived a formula for a smooth chute, based on Wood (1983):

$$\frac{L_i}{k_s} = 13.6(\sin(\theta))^{0.0796} F_*^{0.713} \quad (2.8)$$

Chanson (1994b) has established the relation for stepped spillways, also using the roughness Froude number as

$$\frac{L_i}{k_s} = 9.8(\sin(\theta))^{0.080} F_*^{0.71} \quad (2.9)$$

Chamani (2000) uses the inception Froude number to give the relation

$$\frac{L_i}{k_s} = 8.29 F_i^{0.85} \quad (2.10)$$

Where the inception Froude number is defined as

$$F_i = \frac{q_w}{\sqrt{g(h_s/l_s)k_s^3}} \quad (2.11)$$

Boes and Hager (2003b) state the following relationships

$$\frac{L_i}{k_s} = \frac{5.90(\cos(\theta))^{1/5}}{\sin(\theta)} F_*^{4/5} \quad (2.12)$$

$$\overline{C}_i = 1.2 \cdot 10^{-3}(240 - \theta) \quad (2.13)$$

Where \overline{C}_i is the depth-averaged air concentration at the point of inception. Matos (2000) gives the relationships

$$\frac{L_i}{k_s} = 6.289F_*^{0.734} \quad (2.14)$$

$$\overline{C}_i = 0.163F_*^{0.154} \quad (2.15)$$

Note that the location of the point of inception is determined by visual inspection, like the transition of the flow regimes, and therefore also subjective, but presumably less than the transition of flow regimes. From figure 2.1.4 we can see that the different empirical formulations for L_i in a stepped spillway are somewhat conclusive, but there is a significant spread, especially from the formulation of Matos (2000). As expected, the equation for the smooth slope produces a longer distance to the point of inception.

2.1.5 Air entrainment and cavitation potential

At the point of inception, the air concentration at the pseudo-bottom C_{bi} is 0.01 and the depth-averaged air concentration \overline{C}_i can be found with equation 2.13 (Boes and Hager 2003b). The $\overline{C}_i = 0.226$ with a slope of $\theta = 51.3^\circ$ is a result of the increasing non-linear relation between water depth and air concentration (Matos 2000; Boes and Hager 2003b). The air concentration C ranges from low concentration close to the invert and 100% in the atmosphere, and the surface of the air-water mixture is often defined where the air concentration is 90% (Chanson 2021a). After the point of inception where the turbulent flow entrains air from the atmosphere, the depth-averaged air concentration increases rapidly as the flow propagates downstream. As water approaches the uniform flow, the mean air concentration converges to a maximum of between 30% - 60% depending on the slope and remains somewhat constant after the quasi-uniform flow is reached (André 2004).

The air concentration at the pseudo-bottom can be calculated with

$$C_b(x_i) = 0.015x_i^{\sqrt{\tan\theta/2}} \text{ for } 26^\circ \leq \theta \leq 55^\circ \quad (2.16)$$

where $x_i = (x - L_i)/z_{m,i}$ is the non-dimensional distance from the inception point (Boes and Hager 2003b). x is the longitudinal streamwise distance from the crest of the spillway and $z_{m,i}$ is the air-water mixture depth at the point of inception.

High flow velocities in smooth and stepped chutes introduce cavitation risk. The hydrodynamic pressure can fall below the vapor pressure, causing cavitation and possibly damaging the concrete in the spillway (Boes and Hager 2003b). For stepped spillways, the lowest pressures at the concrete surface often appear at the upper part of the vertical step face (Khatsuria 2004; Amador et al. 2006; Frizell et al. 2015).

Peterka's (1958) work shows that a bottom air concentration of 5-8% is sufficient to avoid problems due to cavitation, therefore free-surface aeration in stepped chutes is a big advantage. For such air concentrations close to the invert, the impact of the collapsing vaporized bubbles that occur is absorbed by the compressible two-phase air-water mixture. This means damages to the concrete from cavitation may occur in the non-aerated black water zone and for the flow downstream of the inception point before a sufficient bottom air concentration is reached. Artificial

aeration from an aerator or other elements that affect the black water region and move the point of inception closer to the crest may be of interest in certain cases where cavitation is expected.

Damages from cavitation on stepped spillways have not been registered, and it is believed that the large uncertainty on this phenomenon has resulted in conservative design practices (Frizell et al. 2015). During the last 20 years, researchers have come up with different design recommendations to avoid cavitation damage. Among the researchers, Boes and Hager (2003b) recommend avoiding flow velocities over 20 m/s in the non-aerated zone, and limiting the specific design discharge to $25\text{ m}^2/\text{s}$. Pfister et al. (2006) state $30\text{ m}^2/\text{s}$ as the limit for unit discharge. Amador et al. (2009) propose a more conservative limit on the flow velocity of 15 m/s and unit discharges down to $11.5\text{ m}^2/\text{s}$.

Frizell et al. (2015) claim that recommendations regarding the unit discharge are rather insufficient without more information about when and if cavitation will be present. Their research on stepped spillways in a closed system with reduced ambient pressure allowed cavitation to develop in a laboratory-sized flume. Measurements from this study resulted in the recommendation

$$\sigma_c > \sigma_{cr} = 4f \quad (2.17)$$

where σ_c is the cavitation index and σ_{cr} is the critical cavitation index. The friction factor in stepped spillway f is given by several different equations. One example from Boes and Hager (2003a), gives the friction factor including sidewall correction as

$$\frac{1}{\sqrt{f}} = \frac{1}{\sqrt{0.5 - 0.42\sin(2\theta)}} \left[1 - 0.25\log\left(\frac{h_s\cos(\theta)}{D_{h,w,u}}\right) \right] \quad (2.18)$$

where $D_{h,w,u}$ corresponds to the equivalent clear water hydraulic diameter in the quasi-uniform zone of the flow.

The cavitation index

$$\sigma_c = \frac{P_0 - P_v}{\frac{1}{2}\rho_w u_0^2} \quad (2.19)$$

is a function of the pressure at flow surface P_0 , the vapor pressure P_v , the water density ρ_w and the mean velocity u_0 . This shows that the occurrence of cavitation varies with several other factors than the unit discharge and velocity. Frizell et al. (2015) also reported that larger steps are in some content more prone to cavitation than smaller steps for the same angle. The angle itself influences the relation given in equation 2.17 much more than the step height. Steps in steep chutes can experience cavitation damage to the concrete at different locations than for chutes with milder slopes. The exact conditions when cavitation will lead to damage to the concrete in stepped spillways are still not known and are a topic for further research.

2.1.6 Flow depths

Due to the acceleration, the incoming flow is decreasing in depth through the critical section, approximately on top of the crest, until the flow reaches the point of inception. From this point on, the aeration of the water causes bulking and larger depths of the air-water mixture flow (Sorensen 1985). The depth continues to increase until the quasi-uniform region or the dam toe is reached. The phenomenon of increasing depths is important when designing chute training walls (Boes 2000). Empirical formulas for the mixture air-water depth at the point of inception and in the quasi-uniform region are developed by Boes and Hager (2003a).

Measuring the flow depth over stepped spillways downstream of the point of inception is a difficult task because of the undulating surface caused by turbulence and aeration (André 2004). Defining any meaningful surface in the nappe flow regime is hardly obtainable, but for transitional and skimming flow there are some successful descriptions of the surface. As seen in section 2.1.5, the two-phase water surface is often defined where the time-averaged air concentration is 90% (Bung 2011), but this definition relies on equipment for measurements of air concentration in the flow.

2.1.7 Flow velocities

Most literature on flow velocity over stepped spillways focuses on the longitudinal streamwise velocity parallel to the chute slope measured with different equipment (André 2004). Early studies on the topic, like Frizell (1992), measured velocities with a laser Doppler anemometer over the tip of the step and up close to the surface perpendicular to the slope of 27 degrees. The velocity profile achieved in the gradually varied flow region was adjusted by a constant to fulfil the continuity if necessary.

Chanson (1994b) reanalysed the same data and found that the velocity profiles follow a power law with the exponent being approximate $n = 3.5$. Other studies (Boes 2000; Matos 2000; Boes and Hager 2003b; André 2004; Bung 2011; Bombardelli et al. 2011; Zhang 2017; Toro et al. 2017; Nina et al. 2022) also propose that the velocity distribution above the step edge in stepped spillways follows the power law. For flow in the aerated zone and in the non-aerated zone the velocity distribution is given respectively by

$$\frac{u_m(z)}{u_{90}} = D \left(\frac{z}{z_{90}} \right)^{1/n} \quad (2.20)$$

$$\frac{u(z)}{u_{FS}} = \left(\frac{z}{\delta} \right)^{1/n} \quad (2.21)$$

where $\frac{u_m(z)}{u_{90}}$ is the dimensionless mixture velocity with $u_m(z)$ being the mixture velocity in the normal distance z over the pseudo-bottom. u_{90} is the mixture flow velocity at the characteristic flow depth z_{90} with the local air concentration of 90%, often defined as the surface of the air-water mixture flow. $\frac{z}{z_{90}}$ is the dimensionless mixture flow depth. For non-aerated flows, $\frac{u(z)}{u_{FS}}$ is the dimensionless velocity, u_{FS} is the free-stream velocity and δ is the boundary layer thickness defined as the normal distance z where the velocity has reached 99% of the maximum value (Amador et al. 2006; Zhang 2017; Kramer 2023).

D and n are chosen coefficients to fit the data obtained from the experiments and n is often reported with a wider spread than the value for D which is often set to 1. n ranges from 3.0 to 5.4 in the non-aerated zone and from 6.6 to 14 in the aerated region (Amador et al. 2006; Kramer 2023). The following table 2.1.2 summarizes some of the coefficients used by other researchers. Some studies have reported for which values of $H_{90} = \frac{z}{z_{90}}$ the flow follows the power law. Above the boundary layer in non-aerated and aerated flows, the velocity is somewhat constant up to the surface.

Table 2.1.2: Summary of coefficients used to fit the power law. The data in the table without references are conducted from (André 2004). Kramer’s (2023) findings are done as a reanalysis of Amador et al.’s (2006) experiments.

Researcher(s)	D	n	θ	H_{90}
(Amador et al. 2006)	-	3.0	51.3 °	-
(Kramer 2023)	-	3.3	51.3 °	-
(Chanson 1994a)	-	3.5	27 °	-
Tozzi	-	4.0	53°	-
(Boes and Hager 2003b)	1.05	4.3	26° ≤ θ ≤ 55°	0.04 ≤ H_{90} ≤ 0.8
Chanson	1	5 to 6	-	-
Chamani and Rajaratnam	1	6.3	30°	0.04 ≤ H_{90} ≤ 0.5
Yasuda and Chanson	-	9	15.6°	0.05 ≤ H_{90} ≤ 1

An empirical relation between chute slope, normalized discharge and the power-law coefficient n has been proposed by Takahasi and Ohtsu (2012) and later used by Kramer (2023) as

$$n = 14\theta^{-0.65} \frac{h_s}{h_c} \left(\frac{100 h_s}{\theta h_c} - 1 \right) - 0.041\theta + 6.27 \text{ for } 19^\circ \leq \theta \leq 55^\circ \quad (2.22)$$

Researchers have also proposed other models for describing flow velocities over triangular cavities. Kramer (2023) combined four different models in his study, creating a multilayered velocity model that corresponded well with measurement data. The number of parameters needed for such a model is higher than for simpler models using the power law.

The model proposed for the mixing layer is

$$\bar{u}_{ML} = (\bar{u}_{if} - \bar{u}_{min}) \left(1 + \tanh \frac{z - z_{if}}{L_e} \right) + \bar{u}_{min}, \text{ if } z < \delta \quad (2.23)$$

Where \bar{u}_{ML} corresponds to the mixing layer velocity, \bar{u}_{if} is the velocity at the inflection point, \bar{u}_{min} is the minimum velocity in the mixing layer, and L_e is the characteristic length scale of the mixing layer. z_{if} is the elevation of the inflection point above the pseudo-bottom, where $\frac{\bar{u} - \bar{u}_{min}}{\bar{u}_{FS} - \bar{u}_{min}} = 0.5$.

2.2 Energy dissipation

Insufficient energy dissipation caused by inadequate energy dissipation structures is one of the leading causes of damage to dams worldwide (Lysne et al. 2003). There are several factors that govern the choice of energy dissipation structure for a given project, like hydraulic and hydrological aspects, topography, geology, and type of dam. Ultimately, we need cost-effective, feasible designs of energy dissipation structures, where it is possible to precisely document sufficient energy dissipation at an early stage of the project.

In many projects, a combination of different energy dissipators are installed at large dams, as seen in figure 2.2.1.



Figure 2.2.1: Wadi Dayqah main dam, Oman (CCC 2009).

Wadi Dayqah main dam is a 75 meter high RCC dam, located in Oman (CCC 2009), which utilizes a combination of three different energy dissipators, aerated Roberts splitters, a stepped spillway, and an embedded downstream hydraulic jump stilling basin seen in figure 2.2.1.

2.2.1 Roberts splitters

Roberts splitters is a concept where a horizontal row of projecting teeth or splitters are positioned relatively close to the crest for dissipation of energy where the unit discharge is too high for a stepped spillway or the velocities are too high for the use of stilling basin (Calitz and Basson 2018). It was first built for Loskop Dam in 1936 on the basis of laboratory experiments conducted by Roberts (1943) in South Africa. The invention has been used on more than 25 dams of different sizes since 1936 (Mikalsen 2022), seen installed at Wadi Dayqah dam in figure 2.2.1.

The projecting teeth cover typically between 50% and 40% of the spillway width. Immediately downstream of the teeth, it is a step covering the whole width causing a projection to the water that is not projected by the teeth (Calitz and Basson 2018). Considerable energy is dissipated when the jets from the teeth and the step collides in the air, causing a spray and losing energy due to air resistance.

As for other spillway structures, Roberts splitters may be prone to cavitation for specific circumstances if the pressure in the water approaches the vapour pressure. The study by Roberts (1943) limited the design spillway head up to 3.0 m which typically corresponds to a unit discharge of $q_w = 12\text{ m}^2/\text{s}$ for standard ogee crest, and recommend to conduct model test for larger design heads. Later there has been conducted research on artificial aeration of the Roberts splitters to mitigate the risk of cavitation for larger unit discharges (Calitz and Basson 2018).

2.2.2 Hydraulic jump

The hydraulic jump is a well-described phenomenon often utilized to dissipate energy in a stilling basin, which typically reduces the specific energy by 60%, depending on incoming Froude number, turbulent characteristics, and level of air-entrainment of the flow (Khatsuria 2004). Incoming flow with lower depth and higher kinetic energy develops through the hydraulic jump to higher flow depth with higher potential energy and lower kinetic energy due to lower velocities. Through the equations of continuity and conservation for mass and momentum, the upstream incoming water depth Y_1 can be calculated by measuring non-aerated tailwater Y_2 at a given discharge. The so-called Belanger formula from Belanger's (1828) work is given by

$$Y_1 = \frac{Y_2}{2} \left(\sqrt{1 + 8Fr_2^2} - 1 \right) \quad (2.24)$$

where $Fr_2^2 = \frac{q_w^2}{gY_2^3}$ is the Froude number squared at the downstream cross-section of the jump.

2.2.3 Stepped spillways

The expected rate of energy dissipation on a stepped spillway is typically 40-90% (André 2004), depending on the design and operation of the spillway. It can be difficult to precisely estimate the energy dissipation for a wide range of discharges and operating conditions in a given stepped spillway design, where the approaches typically are analytical calculations, physical modelling and numerical modelling.

The analytical methods are often general empirical relations based on physical model studies (Boes and Hager 2003a). Numerical modelling is typically based on computational fluid dynamics (CFD) models, but they require extensive experience and expertise in both hydraulics and numerical modelling, especially when dealing with complex, highly turbulent two-phase flow modelling (Olsen 2015). Hybrid modelling, a combination of physical modelling, sometimes prototype data, and numerical modelling can also be used when dealing with complex flow and geometries (Chanson 2021a).

2.3 Review of hydraulic studies

Ever since stepped spillways regained popularity with the introduction of RCC as a dam construction material, there has been conducted many hydraulic studies in several different laboratories to gain a better understanding of the behavior of the flow of stepped chutes. The highly turbulent characteristics of two-phase flow in stepped spillways cannot be modelled without significant scale effects in down-scaled physical models, mainly because of surface tension, air bubble velocity, and viscosity (Khatsuria 2004). Boes and Hager (2003b) among others have studied the scale effects in stepped spillways and recommended areas of validity for laboratory experiments and it is explained further in section 2.4.1.

There has also been conducted numerous of numerical studies on stepped spillways, both with CFD models and smoothed-particle hydrodynamics (SPH) models, but the available computational power restricts the level of accuracy that we can achieve when simulating complex, highly turbulent two-phase flows.

In this section, some stepped spillways hydraulic studies will be presented, focusing on modifications on the traditional stepped spillway invert to improve energy dissipation.

Triangular protrusions Wright (2006), inspired by the South African invention Roberts splitters, conducted a laboratory study where he added triangular protrusions on the face of the downstream slope of the stepped spillways to increase flow resistance, air entrainment and turbulence. The 1:30 scale model is shown in figure 2.3.1, one advantage of this method is that it would be easy and cost-effective to implement in a dam construction project.



Figure 2.3.1: Physical model of stepped spillways with triangular protrusions (Wright 2006), flow direction from left to right.

In addition to increasing energy dissipation, the protrusions induce more turbulence, which gives a shorter length of inception, which then leads to an increase of the maximum allowable unit discharge.

Macro-roughness elements The introduction of different roughness elements on the face of stepped chutes, both in 2D and 3D, in addition to inclined steps have been studied systematically by André (2004) at the hydraulic laboratory of EPFL in Lausanne. Based on the experimental results from the hydraulic laboratory, a quasi- 2D numerical model was also developed.

Inclined steps There have been conducted several other studies on inclined steps, both in physical (Peyras et al. 1992) and in numerical models (Ikinogullari 2023).

Pooled step cascades Another approach to acquire pooled steps is to construct some version of an end-sill on the end of the step, as demonstrated in figure 2.3.2 (c) and (d), from a numerical investigation conducted by Li et al. (2017). This configuration has been investigated in several other studies (Peyras et al. 1992; Emiroglu et al. 2003; Guenther et al. 2013), and can also be found in a wide range of existing dams.

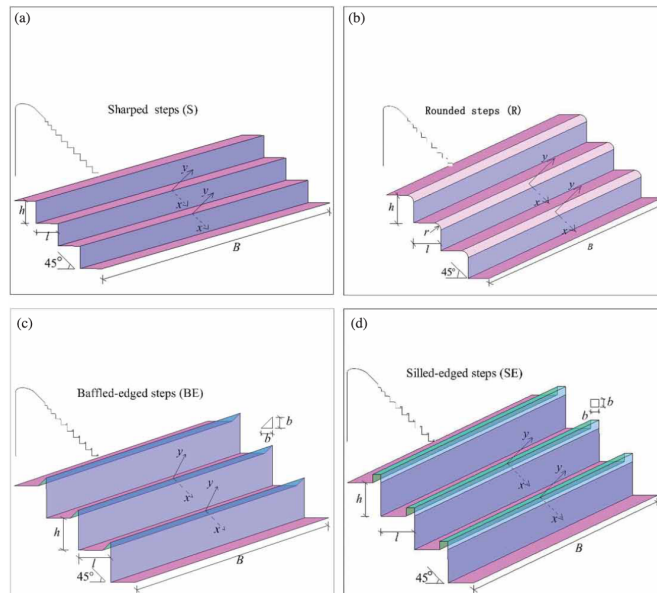


Figure 2.3.2: Sketch of a selection of different stepped spillway configurations investigated by Li et al. (2017).

Rounded steps Several studies including rounded step edges have been conducted, with the intention to accelerate the skimming flow regime and increase energy dissipation (Zare and Doering 2012; Zhang 2017). Some stepped spillway models and prototypes have implemented rounded step edges already (Zhang and Chanson 2015).

Non-uniform stepped chute A transitional crest profile, combined with steps evolving to match the standard ogee profile has been introduced in several hydraulic studies (Sorensen 1985; Christodoulou 1993; Boes and Hager 2003a; Chatila and Jurdi 2004; Bombardelli et al. 2011) and in some prototypes (Wright and Cameron-Ellis 2018; Chanson 2021c). Chanson (1994b) points out that the growth of the turbulent boundary layer on spillways with varying step heights is extremely complex.

Another approach by Felder and Chanson (2011; 2014) was to introduce a non-uniform stepped spillway. The conclusion from the comprehensive investigations was that there were small differences in important parameters like bubble count rate, turbulence levels, and air-water flow characteristics in the non-uniform configuration compared to the uniform stepped spillway configuration. Some flow instabilities were observed in the non-uniform stepped chutes, and with minimal differences in governing flow behavior in the individual configurations.

Cavitation potential In addition to the research conducted by Frizell et al. (2015) described in section 2.1.5, artificial aeration as a measure to reduce cavitation potential has been investigated in several studies (Yiguo et al. 2003; Dong et al. 2019). Because the cavitation potential restricts the maximum allowable unit discharge, measures to reduce cavitation potential may also increase the maximum unit discharge.

Instrumentation and validation Recently, with the improvement of computational power, image-based velocimetry, like the optical flow technique has become a powerful tool in the study of highly turbulent two-phase flow conditions, both in scale models and for prototype data collection. This has been a recent research topic for Chanson (2021b) and Zhang and Chanson (2018) and others (Bung and Valero 2016; Nina et al. 2022). Traditional studies combining numerical and physical models are common (Bombardelli et al. 2011; Meireles et al. 2014; Bung and Valero 2015; Toro et al. 2017; Zabaleta et al. 2020), and the idea of combining a prototype with a physical hydraulic model or a numerical model recently gained interest, often called hybrid modelling (Chanson 2021a).

PIV has also been utilized in stepped spillway research studies and is useful in the non-aerated region (Amador et al. 2006). In the aerated region, the BIV technique has recently been successfully employed by Sánchez-Juny et al. (2022). This study used PIVlab, a MATLAB toolbox, to analyse the flow velocity in a stepped chute. Comparison with Estrella et al.'s (2015) measurements with a double fibre-optical probe on the same chute, shows that BIV underestimates the surface velocity in the non-aerated zone and overestimates the surface velocity in the aerated zone for the largest discharges. They also express that light conditions and sufficient image acquisition rate are essential for achieving useful results.

Another measure of instrumentation employed in hydraulic studies is pressure sensors (Sánchez-Juny and Dolz 2003; Amador et al. 2009), often in combination with studies of cavitation potential.

Hinze dam One prototype dam studied extensively on a wide range of unit discharges is Hinze dam (Chanson 2021c; Chanson 2021b), located in Queensland, Australia. Hinze dam is equipped with a stepped spillway, with a step height of $h_s = 1.5$ meters, and a slope of $\theta = 51.3^\circ$. The optical flow method is applied (Zhang and Chanson 2018; Kramer and Felder 2021; Chanson 2021b) to collect field data, which is used to calculate surface velocities.

2.4 Physical hydraulic modelling

2.4.1 Similarity and scale effects

For hydraulic experiments on scale models, three similarity laws have to be fulfilled to represent complex two-phase flow in a stepped chute accurately (Boes and Hager 2003b; André 2004). They are the following; Froude similarity, Reynolds similarity and Weber similarity, and they represent the relationship between flow inertia and gravity forces, the role of the viscosity of the fluid, and the impact of surface tension respectively. Usually, for open channel flow where gravity forces introduce the dominant effect, Froude similitude can be sufficient without scale effects being decisive (Henderson 1966; Sorensen 1985; Boes and Hager 2003b).

Studies done on highly complex air-water phenomena show that turbulent shear forces are significant in addition to gravity forces, and this causes scale effects. Further, it is shown that it is impossible to fulfil Froude and Reynolds similarity in scaled models without changing fluid. (Chanson and Murzyn 2008; Felder and Chanson 2009). Due to the importance of viscosity and surface tension, highly turbulent air-water flow experiments need to be done on full-scale to achieve correct results (Boes and Hager 2003b; Chanson and Murzyn 2008).

Scale effects in stepped spillways are proportionally larger air bubbles, lower interfacial turbulence intensities, less air transport capacity and quicker deaeration as for a comparable prototype (Pegram et al. 1999; Boes and Hager 2003b; André 2004; Zhang 2017). This means that the air concentration close to the surface of the steps is larger in prototypes, which is beneficial for cavitation problems. Felder and Chanson (2009) also refer to lower turbulence levels causing lower aeration efficiency and underestimation of energy dissipation. Their study also shows larger scale effects on the model with a height of steps being $h_s = 0.05\text{ m}$ compared to $h_s = 0.10\text{ m}$. In addition, they tested the experiment with the alternative Reynolds similitude but concluded that it was not valid for this complicated air-water mixture flow.

Boes and Hager (2003b) have studied the scale effects in stepped spillways in their experiments and compared results with earlier studies. They state a minimum scale of 1:15 for minimizing scale effects in a typical stepped spillway with a unit discharge of $20\text{ m}^2/\text{s}$ and a step height of 0.6 m , based on a Reynolds number higher than 10^5 and a Weber number higher than 100. This is in agreement with the recommendations from Kobus (1984) and Pegram et al. (1999) along with other research from the 80s and 90s. Boes and Hager's recommendations are summarized in table 2.4.1.

Table 2.4.1: Recommended criteria by Boes and Hager (2003b) for stepped spillways model scaling.

Criterion	Limit
λ_F	≤ 15
W	≥ 100
Re_e	$\geq 10^5$

Reynolds number corresponds to $Re = uz_w/\nu = q_w/\nu$ and Weber number is $W = \overline{u_m}/\sqrt{\sigma_{sur}/(\rho_w x_s)}$, where z_w =equivalent clear water depth; ν =kinematic viscosity; $\overline{u_m}$ =time-averaged mixture velocity; σ_{sur} =surface tension between water and air; ρ_w =density of water; and x_s =longitudinal distance between two step edges. André (2004) adds that a flow depth of more than 2 to 3 *cm* may also be necessary.

In research on other hydraulic structures and phenomena than stepped chutes, Chanson and Murzyn (2008) show that drastic scale effects are expected when modelling hydraulic jumps in Froude similitude. The main issue with scaling hydraulic jumps in Froude similitude is scaling two-phase flow, where substantial deviations in terms of bubble count rate and void fraction are observed. Recently, studies on novel scaling laws that avoid scale effects on air-water flow in dam break and plunging water jet experiments were published (Catucci et al. 2021). This proposed method governs both the scale effects due to viscosity and surface tension by using so-called Lie group transformations. However, this new method is validated by numerical models only, and validation with physical models still requires another fluid than normal water to satisfy the proposed scaling laws.

2.4.2 Physical measuring methods

The local energy head at a chosen location in a stepped spillway is typically described as (Christodoulou 1993)

$$H = y_x + z_w + \alpha \frac{u_0^2}{2g} \quad (2.25)$$

where y_x corresponds to the vertical distance from the downstream dam toe to the pseudo-bottom, z_w is the equivalent clear water flow depth, u_0 the mean streamwise water velocity, and α is the kinetic energy correction coefficient due to non-uniform velocity.

From equation 2.25, we can recognise that velocities, air concentration, and water flow depths are important parameters to determine in order to calculate the local energy head. Some parameters, such as water depth in clear water flow are often easier to measure than others such as velocities and air-water mixture depth. The availability of measurement technology is continuously improving due to the advancement and access to computational power among others (Zhang and Chanson 2018).

Physical measuring methods applied in stepped spillway research are often split up into intrusive and non-intrusive methods (Nina et al. 2022). Flow velocities are typically measured with intrusive methods, where a probe is placed within the flow. These probes cause perturbation of the flow and their measurement is limited to a single point, which is disadvantageous for this method. Non-intrusive imaging techniques deal with both of these drawbacks and have been reported to be used since the middle of the 2000s (Bung and Valero 2016). An overview of some of the most used methods is presented in this section, starting with intrusive methods.

Direct measurements Directly measuring the water depth with a ruler is straightforward, however, it can be challenging to get a stable read in a turbulent flow, especially in an aerated flow.

Pitot tube A back-flushing Prandtl-Pitot tube is a Pitot tube type that takes the air bubbles into account through a flushing system (André 2004). However, this system is reported to underestimate the velocity considerably in two-phase air-water flows with air concentration $\bar{C} > 0.7$ which commonly occurs in stepped spillways and is thereby not recommended.

Acoustic Doppler velocimetry ADV is a method to record velocities in 3D using the Doppler effect. This is when the frequency of a wave changes because of the movement of the wave source itself, the receiver or the medium the wave propagates through. The ADV sends acoustic waves out from one part of the probe and receives the wave in another part with a given distance in between. By knowing the speed of sound through water, it computes the flow velocity. Changing the medium to a two-phase air-water mixture introduces problems because the speed of sound through this medium is different. Therefore ADV is only applicable for low air concentration $\bar{C} < 0.08$ (André 2004).

Conductivity probes CP exist with single or double-tip and the technology behind these probes was first developed by the United States Bureau of Reclamation (USBR) (André 2004). Chanson has developed a similar method and used it considerably in research on air-water mixture flows in stepped spillways (Chanson et al. 2002). When air voids in the two-phase flow reach the probe, the air discontinues the electrical current between the two conductors and time-averaged air concentration can be measured. Velocities along the streamline can also be measured with the double-tip conductivity probe. To date, this technology is mainly used on a laboratory scale, but recently the technology was successfully used by Hohermuth et al. (2021) in prototype experiments with flow velocity and Reynolds numbers up to 38 m/s and 2.4×10^7 respectively. Though with some challenges with sensitive probes in the violent flow.

Dual-tip fibre-optical probes Two-tip fibre-optical probes developed by RBI Instrumentation in France are used in the PhD research works by Boes (2000) and André (2004) among others. This technology makes use of the difference in optical refraction indices of the water and air and is used for measuring local air concentration and flow velocity (Boes and Hager 2003b). This type of instrumentation together with conductivity probes is called for phase-detection needle probes (Nina et al. 2022).

Pressure sensors Dynamic pressure sensors are often installed in hydraulic models when the research is concerning cavitation (Sánchez-Juny and Dolz 2003; Amador et al. 2009; Calitz and Basson 2018). The pressure is typically logged to a file at a sampling rate of at least 100 Hz .

Some non-intrusive methods include, but are not limited to

Ultrasonic distance sensors Ultrasonic sensors are often placed over the flow, and make use of sound waves to measure the distance to the water surface, within a certain range. Measurements can be logged to a file over a period to get an average depth.

Particle image velocimetry PIV is a non-intrusive technique that uses high-speed cameras to capture the movements and velocities of particles in a fluid (Thielicke and Sonntag 2021). Special reflective particles are added to the fluid and a laser sheet illuminates the particles which makes them easier to capture for the camera. The displacement of the particles between two pictures in a series with a given time resolution is used to calculate the velocities of the particles. There are several commercial and free PIV software packages available.

Bubble image velocimetry A modified PIV method, called BIV, uses air bubbles in two-phase flow as tracers (Bung and Valero 2016; Sánchez-Juny et al. 2022). White light is commonly used to illuminate the bubbles, and traditional PIV techniques can then be applied to process the videos.

Optical flow OF tracks brightness patterns from one frame to another in a series of images and is used for self-aerated flows since 2008 (Bung and Valero 2016; Chanson 2021c). Chanson has also used OF in prototype experiments with meaningful surface velocities results in the blackwater region upstream of the point of self-aeration. A drawback of the OF method is the requirement of an extremely high frame rate, in addition to specialized camera equipment.

One drawback of velocimetry methods based on high-speed videos is sidewall effects for side-view analysis. Research on laboratory experiments shows that the velocity measured through the glass wall with velocimetry techniques like optical flow shows an underestimation of 10% to 30% compared to measurements done on the centreline of the flume (Chanson 2021a; Nina et al. 2022). In addition to an underestimation of velocity, a reduction in air concentration and bubble count rate is also found compared to the centreline flow.

Due to the difficulty of defining the depth of the turbulent aerated flow over stepped spillways to calculate energy, a hydraulic jump just downstream of the chute toe is found to be an acceptable alternative for measuring residual energy indirectly (André 2004). This method for measuring energy dissipation over stepped spillways is used by Pegram et al. (1999), Boes (2000), Ohtsu et al. (2004) and André (2004) among others. Even though this method avoids the difficulty of measuring the aerated water depth, it introduces other challenges. Pegram et al. (1999) stress that the specific energy at the incoming cross-section varies approximately with the fourth power of Y_2 , meaning that precise measurements of the sequent depth are crucial for obtaining useful results. The position of the hydraulic jump must be as close to the toe as possible without drowning the last step. It is typically controlled by adjusting the tailwater depth with a gate downstream of the necessary length for an undisturbed development of a hydraulic jump. André (2004) investigated the effect of the position of the hydraulic jump. The results

showed significant differences in residual energy after the stepped chute if the last steps were submerged and minor differences when the jump was further downstream compared to the optimum position shown in figure 2.4.1.

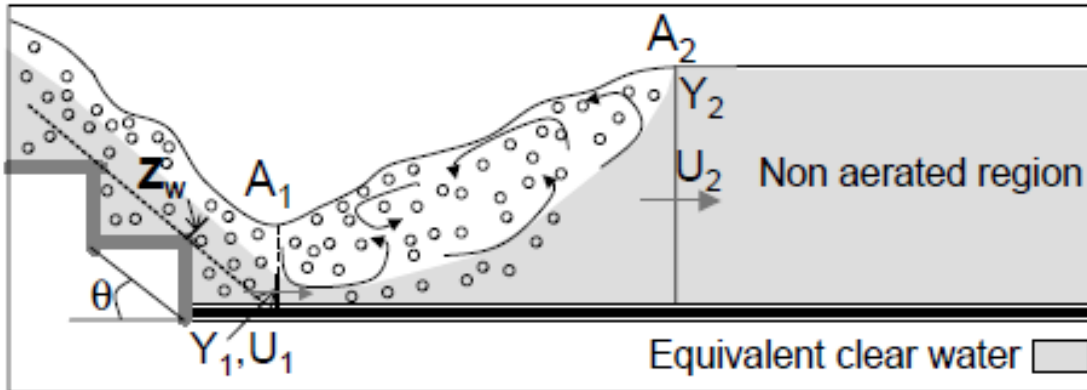


Figure 2.4.1: Characteristics of the optimum position of the hydraulic jump immediately downstream of the stepped chute. Figure from (André 2004).

Figure 2.4.1 shows the position of both Y_1 and Y_2 and the process of deaeration in the hydraulic jump. It can also be seen that Y_1 is an equivalent clear water depth often referred to as z_w in the context of stepped spillways. U_1 and U_2 in the figure correspond to the incoming and outgoing velocities of the hydraulic jump. Using formula 2.24 for further calculations of residual energy requires several assumptions of the quite complex hydraulic situation (André 2004):

- Incoming hydrostatic pressure distribution
- Negligible wall friction
- Neglecting the effect of differences in density for the incoming air-water mixture flow and the outgoing deaerated water flow in the hydraulic jump
- The velocity in the upstream and downstream cross-section is uniformly distributed. If not, one can use a kinetic energy correction coefficient α to avoid under-estimation of the residual energy downstream from the stepped chute. Typically $\alpha = 1.1$ for turbulent flow.
- Factor to account for singular energy loss where the flow over the inclined steps collides with the horizontal basin bed. This factor is recommended to be $\eta = 1.15$

Regarding the latter bullet point, the aerated flow downstream of the stepped spillway the density of the mixture flow can vary much from $\rho_w = 1000 \text{ kg/m}^3$. In a situation with mean air concentration $\bar{C} = 30\%$ the air-water mixture density will be $\rho_m = 700 \text{ kg/m}^3$ in the inflow to the hydraulic jump. In this case, the assumption of constant density used in the momentum and mass conservation equations is not correct and the Belanger equation (2.24) needs to be adjusted. However, André (2004) investigated this problem by doing calculations on the relative energy loss with both constant density and varying density of the flow. She concluded that the assumption of constant density could be maintained due to negligible effects from the variation in density if mean air concentration $\bar{C} \leq 65\%$. This investigation proved the effects on a spillway with angle $\theta = 30^\circ$ with and without alternate blocks in the steps for unit discharges q_w up to $0.27 \text{ m}^2/\text{s}$.

2.5 Resulting research method

Considering the time schedule, available resources, experience in numerical and physical modelling, combined with the theoretical framework explained in this chapter, it was decided that the most feasible research method to proceed with is an extensive physical model study.

A numerical CFD model was also considered, but after a feasibility study and discussion with advisors, it was decided not to go forward with this method, because of the severe complexity of modelling highly turbulent two-phase flow numerically. Maybe it would have been possible to engineer a CFD model that replicates a physical model in regards to air entrainment and other two-phase flow characteristics, but making use of a CFD model like this in a practical application seemed far-fetched for this study. The scale effects you experience in the physical model will also be present in a numerical model that is calibrated with a physical scale model. In regards to hybrid modelling, combining a physical scale model with prototype data seemed more credible and applicable.

As research on the transition of flow regimes seems adequate, and the characteristics of a nappe flow regime differ a lot from the skimming flow regime, it was decided to focus on the skimming flow regime on a steep stepped spillway in this study.

It should also be noted that the experiments are conducted in a generalized two-dimensional setup, while the resulting design can be applied for any length of a dam.

Regarding the characteristics of the prototype, typical dimensions of a RCC dam equipped with a stepped spillway is selected, also corresponding to Hinze dam, where full-scale field data is available for validation of results. The recommended minimum scale, summarized in table 2.4.1, along with the facilities at hand is used as framework to decide on the scale for the experiments. In addition to one model in the range of recommended scaling criteria, another model outside of the range was proposed to look at scale effects of stepped spillway hydraulic modelling. Due to limitations in instruments at our disposal, it was not within reach to determine air concentrations in two-phase flows for this study. However, the possibility of using image-based velocimetry methods to determine velocities seemed to have great potential. It was decided to utilize BIV, because it seemed most feasible, with regard to equipment, experience, and computational capacity.

EXPERIMENTAL SETUP

3.1 Experimental facilities

Hydraulic model experiments were conducted in the Norwegian Hydrotechnical Laboratory at the Norwegian University of Science and Technology in Trondheim.

3.1.1 Flume system layout

The layout of the D-flume can be seen in figure 3.1.1. The layout of the C-flume can be seen in figure 3.1.2. Note that some of the flume lengths are removed from the drawings in both flumes, indicated by break-line symbols.

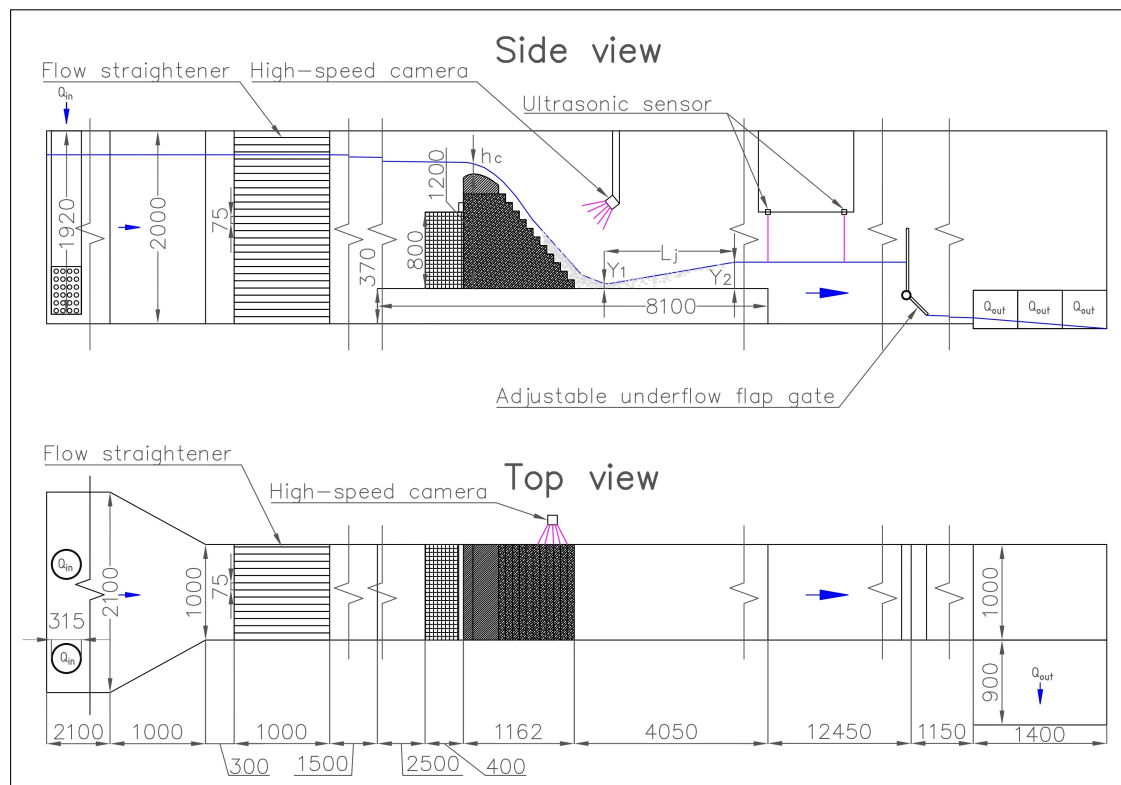


Figure 3.1.1: D-flume experimental setup, flow direction from left to right and dimensions in millimetres.

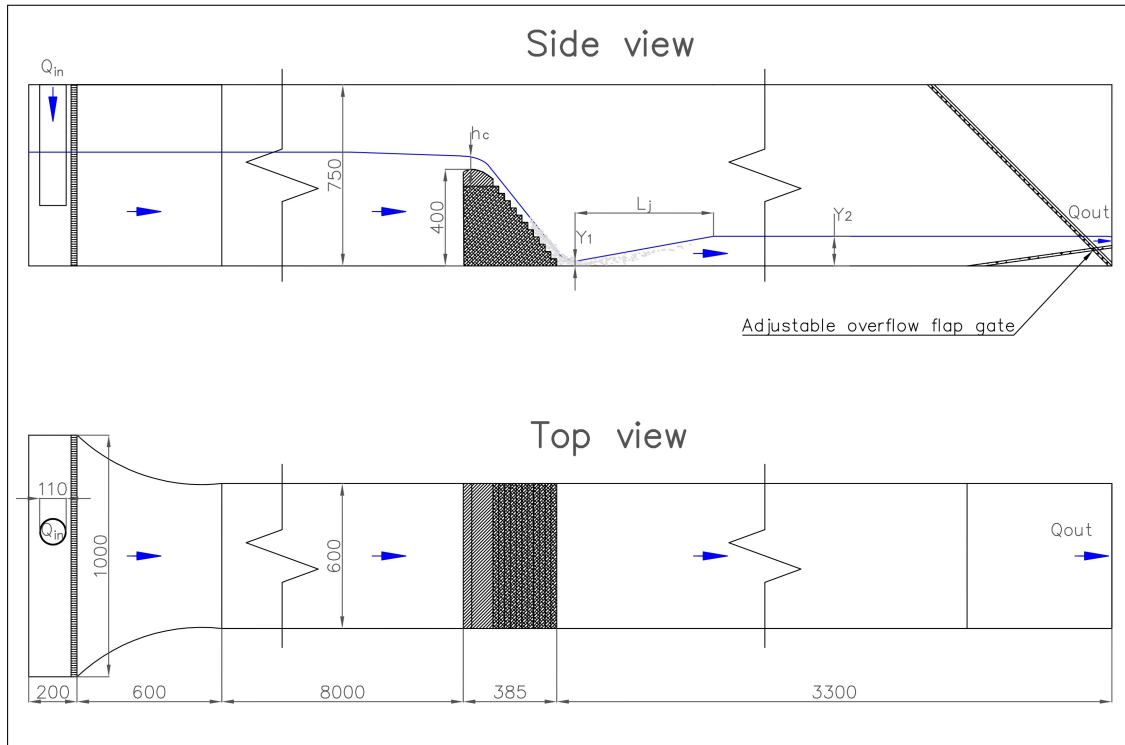


Figure 3.1.2: C-flume experimental setup, flow direction from left to right and dimensions in millimetres.

Apart from removing some of the flume lengths, the drawings are to scale.

3.1.2 Entrance conditions

Flow straighteners are used to reduce turbulence and create a calm water surface with little transverse flows in the flumes. The D-flume is equipped with a one meter long tube-type flow straightener, while the C-flume is equipped with a permeable barrier next to the inflow. Preliminary experiments by adding dye to the stream flow were conducted to control the incoming flow conditions and adjustments on the flow straighteners were performed.

A standard ogee crest is designed according to USBR (1987) with two upstream radii being $0.5H_0$ and $0.2H_0$ for R_1 and R_2 respectively with $H_0 = 4.89\text{ m}$ in prototype which corresponds to a unit discharge of $q_w = 23.8\text{ m}^2/\text{s}$. The downstream curvature of $y = -0.5H_0(x/H_0)^{1.87}$ is used for the design. y is the vertical distance from the top of the weir and x is the horizontal distance. The height of the curved crest is 2 meters which means that the slope reaches an angle of approximately 40° before the first step starts. If the curvature was allowed to evolve to the angle of $\theta = 51.3^\circ$, the number of steps would have been reduced and this was not desirable for the research aim.

3.1.3 Standard stepped spillway models

A fictional prototype RCC dam of 20 meters in height with a vertical water side and a downstream slope (V:H) of 1:0.8, corresponding to an angle θ of 51.3° is the basis of the models constructed in this hydraulic study. This represents a typical design on existing gravity dams with stepped spillway in the lower region regarding dam height (Wright and Cameron-Ellis 2018; Chanson 2021a). Hinze Dam Stage 3 at the Gold Coast in Australia, with equal slope and step heights, and the height of the stepped spillway being approximately 35 meters is used for comparison. The number of steps N_s in the prototype is 11 and the step height h_s is 1.5 meters. Physical geometrically similar models using the Froude similitude in two different scales have been built in prismatic rectangular flumes in such a way that the desired flow regime, skimming flow, is reached within the limitations of the flume size and available discharges.

The D-model scaled 1:16.67 (figure 3.1.3), is built with planks and marine plywood with a crest of extruded polystyrene (XPS). This model is located in the D-flume. Originally it was a step of 37 cm approximately 1.2 meters downstream from the toe, but this plateau was extended to be 4.05 meters for a hydraulic jump to evolve undisturbed from the bed level difference. The smaller C-model scaled 1:50 (figure 3.1.4) located in the C-flume is built with horizontal layers of marine plywood, which is comparable to the RCC construction method with a crest of XPS. The two different scales give the possibility of investigating scale effects. The size of the D-model is close to the recommendation from Boes and Hager (2003b), but due to limitations in the existing flume, it is slightly smaller. An overview of the different models is summarised in table 3.1.1. The D-model is fixed to an aluminium construction of 0.8 meters height upstream and this construction might alter the flow to some extent. Still, it is assumed not to impact the flow behavior over the steps.

Table 3.1.1: Overview of model and prototype dimensions.

Name	Scale	$H[m]$	$h_s[m]$	$H_f[m]$	$B_f[m]$	Q_{max} [m^3/s]
Prototype	1:1	20	1.50	-	-	-
D-model	1:16.67	1.20	0.09	2.0	1.0	0.510
C-model	1:50	0.40	0.03	0.75	0.6	0.058

Both of the models' steps are labelled with Roman symbols. For steps 6 to 9 on the D-model, the symbols I, II, III, IV and V with an "underline" tape are used (figure 3.1.3). The side view glass on the C-model does not start at the bed of the flume, so steps X and XI are not labelled (figure 3.1.4). The last step, XI, is not labelled for the D-model.

It should be noted that the models were designed and constructed single handedly by the authors, and this was undoubtedly the most comprehensive part of the project. Preliminary experiments were also conducted to validate the models.



Figure 3.1.3: D-model scaled 1:16.67 with a total height of 1.20 meters seen from the side through the glass wall of the D-flume.



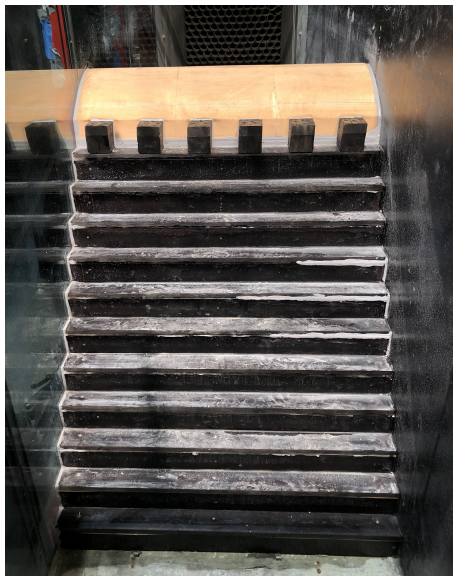
Figure 3.1.4: C-model scaled 1:50 with a total height of 0.40 meters seen from the side through the glass wall of the C-flume.

3.1.4 Stepped spillway models with crest splitters

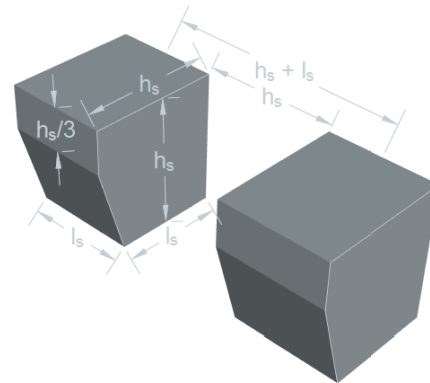
The modification to the stepped spillway models is inspired by the Roberts splitters introduced in section 2.2.1. Roberts' (1943) design criteria are used with some adjustments so the modification easily can be implemented in new and existing stepped spillways. The splitters are made of wood and the design can be seen in table 3.1.2 and figure 3.1.5. More pictures of the models with water flowing over the stepped spillway with and without splitters are shown in chapter 4.

Table 3.1.2: Crest splitters design parameters.

Dimension	Length [m]	Relative size
Height	1.5	h_s
Top length	1.5	h_s
Bottom length	1.2	l_s
Width	1.2	l_s
Gap	1.5	h_s
Vertical face	0.5	$h_s/3$



(a) Downstream face of the D-model with crest splitters installed.



(b) Design of crest splitters with dimension given relative to the size of the steps.

Figure 3.1.5: Crest splitters positioning and design.

3.1.5 Tailwater adjustment and outflow conditions

For measuring the residual energy at the spillway toe, it is desired to create a hydraulic jump immediately after the water flow reaches the horizontal part of the flume, as explained in section 2.4.2. This is achieved by adjusting the tailwater with an adjustable gate. In the C-flume, this is controlled by a manual adjustable overflow flap gate probably similar to the ones used by Boes (2000) and André (2004). The gate used in the D-flume is an electric adjustable underflow flap gate. It is challenging to adjust the tailwater precisely with the latter type, but it was still used because it was already installed in the D-flume. As shown in section 2.4.2 regarding the hydraulic jump, the position of the jump influences the sequent water depth Y_2 a great deal. This is a sensitive value for the calculations of residual energy and it was therefore a good routine for measuring the sequent depth precisely was crucial.

3.2 Measuring instrumentation

A picture of the D-model running, as well as some of the instrumentation used in the research can be seen in figure 3.2.1.

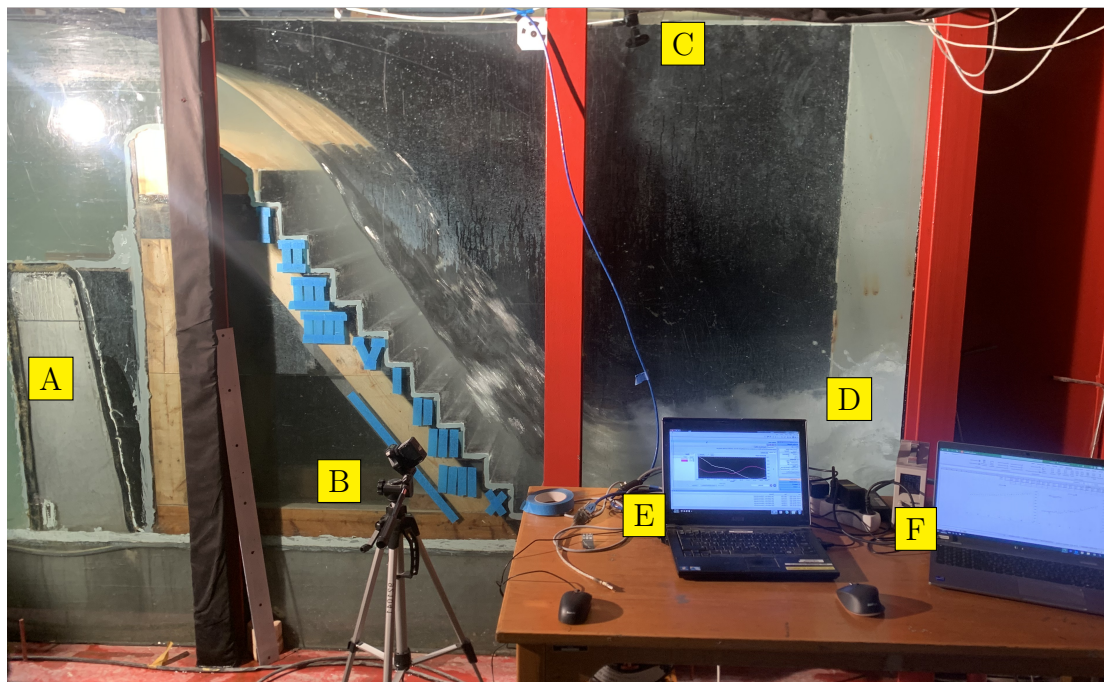


Figure 3.2.1: Experimental setup for the D-model in the D-flume.

A corresponds to the metal box, B is the camera position from the side view, C is the camera position from the top view, D is the hydraulic jump at the toe but not at the optimal position, E is the computer logging measurements from the ultrasonic sensors and F is the computer used for saving and analysing data.

3.2.1 Discharges

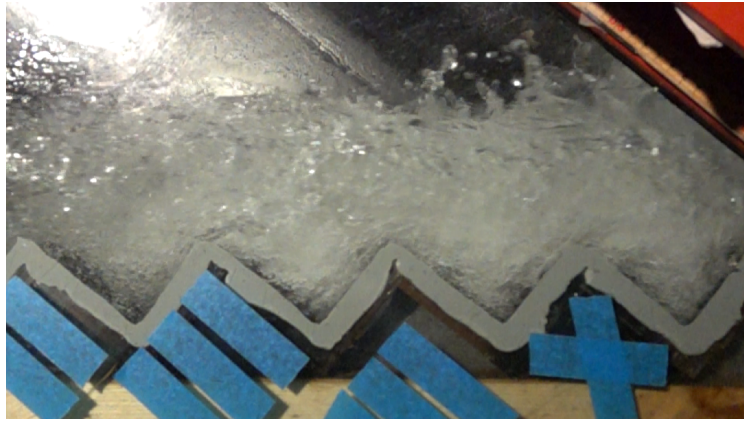
An electromagnetic flow measurement system mounted on the inlet pipes with a constant pressure head was used to measure the discharge in the experiments. The sensor used is Siemens Sitrans FM MAG 5100 W and the transmitter is a Siemens Sitrans FM MAG 5000. The system has a measuring range from 0 to 10 m/s with an accuracy of 0.2% $\pm 2.5 mm/s$ (Siemens 2023a; Siemens 2023b).

3.2.2 Image-based velocimetry

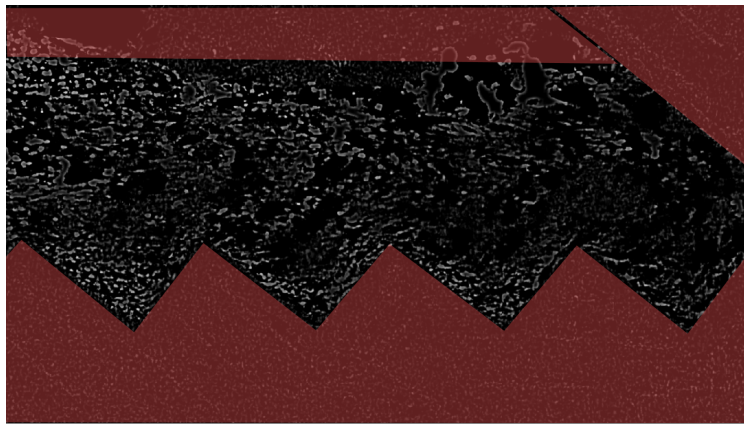
In this study, the open-source toolbox in MATLAB, PIVlab, is used to track white light-illuminated bubbles captured with a Sony DSC-RX0M2G camera. The videos were captured in 1920×1080 pixels, with a 16:9 aspect ratio and 1000 frames per second (FPS). There are several methods of doing pre-processing, image evaluation, post-processing and data exploration in PIVlab, and it is explained thoroughly by Thielicke and Stamhuis (2014).

The videos used in PIVlab were recorded with the above-mentioned high-speed camera located in position B and C in figure 3.2.1 for the side view and the top view respectively. Several videos were recorded from the side view in a way that all steps were captured with some overlap from video to video. Dimensionless discharges h_c/h_s of 1.2 and 1.6 in both flumes were chosen to analyze. High-speed settings recording at 1000 FPS over a 2 seconds period were used in the analysis. It was discovered that the video files consisted of 2064 frames, but there was no movement in the last 22 frames, which lead to a choice of analysing the first 2042 frames.

The settings used in PIVlab for the analysis are shown in table B.0.1 in the appendix, and the result of the pre-processing is shown in figure 3.2.2. The red areas are masked out and particle movements in these regions were not analysed to save processing time. The picture processing makes it easier for the program to track air bubbles, seen as white particles on black background, from frame to frame. The results from every particle movement from frame to frame are time averaged over the 2042 ms analysed and default settings are used for post-processing. A known measured reference length is used for calibration and this is crucial for extracting correct velocities.



(a) Original frame.



(b) Pre-processed and masked frame.

Figure 3.2.2: One representative frame from the video recordings before and after pre-processing and masking in PIVlab - flow direction from left to right.

3.2.3 Flow depths

Over the crest in the non-aerated region, the water depth can be measured along the glass with a ruler because of the flow's relative steady state. Sidewall effects may occur and must be taken into account. Depth over the pseudo-bottom or the mixture depth is difficult to determine accurately due to the turbulence and aeration that creates a rough and fluctuating surface (André 2004). As mentioned in section 2.1.6, the air-water surface is often defined where the air concentration is 90%, but because this study does not have a conductivity probe or fibre-optical probe available it is nearly impossible to determine the depth over the pseudo-bottom in the two-phase flow in an accurate way.

In the D-flume, two ultrasonic sensors of the type Microsonic mic+130/iu/tc with a stated accuracy of $\pm 1\%$ (Microsonic 2023), are used to measure the downstream sequent depth of the hydraulic jump. Due to the uncalm water surface, it is preferable with a time-averaged depth measurement rather than a point measurement with a ruler. The sensors are located in the centre of the flume with an internal distance of 0.8 meters and the upstream sensor is 4.05 meters from the spillway toe. A hydraulic jump creates wavy tailwater and the measurements will therefore be attempted to last over at least 10 seconds period with a frequency of 100 Hz. André (2004) used a measuring series over 120 seconds, but it was found to be too difficult to achieve in this setup with the tailwater controlled by an underflow gate at the flume's end. The sequent depth of the hydraulic jump was measured with a ruler in the C-flume.

The ultrasonic sensors measure depths in a given range, and preliminary experiments were conducted to determine the relevant range of depths for the different discharges used.



Figure 3.2.3: Looking upstream in the D-flume, ultrasonic sensors for measuring the sequent depth of the hydraulic jump are seen in the front. The wood construction on the bed downstream of the toe is to ensure an undisturbed development of the hydraulic jump. The D-model with splitters can be seen in the background.

3.3 Experimental program

The experiments in the C- and D-flume were conducted with an initial normalized critical depth $h_c/h_s = 0.8$. Manual valves controlled the discharge and this was measured by the earlier-mentioned flow meters. All models were run with increased discharges from $h_c/h_s = 0.8$ to approximately $h_c/h_s = 3.3$ with intervals of $h_c/h_s = 0.1$. This corresponds to prototype unit discharges range of $4 m^2/s$ to $34 m^2/s$.

The range of the Reynolds numbers and the Weber numbers together with the range of discharges for the experiments are given in table 3.3.1. As shown in section 2.4.1 the Reynolds number is $Re = uz_w/\nu = q_w/\nu$ and the Weber number is $W = \overline{u_m}/\sqrt{\sigma_{sur}/(\rho_w x_s)}$. The Weber number in the present study is calculated in the upstream cross-section of the hydraulic jump at the dam toe because measuring the depth-averaged mixture velocity $\overline{u_m}$ is not possible without intrusive probes. Therefore $\overline{u_m}$ is replaced with u_1 in the equation for Weber number and it results in $W = u_1/\sqrt{\sigma_{sur}/(\rho_w x_s)}$. The kinematic viscosity $\nu = 1.0 \times 10^{-6} m^2/s$, the surface tension between water and air $\sigma_{sur} = 0.0728 N/m$ and the density of water $\rho_w = 1000 kg/m^3$ is used.

Table 3.3.1: Summary of parameters and ranges in the experimental scheme.

Model	$\lambda_F[-]$	$Q[m^3/s]$	$h_c/h_s[-]$	$Re[-]$	$W[-]$
D-model	16.67	0.0605 –	0.80 –	6.05×10^4 –	106 –
		0.5070	3.30	5.07×10^5	179
C-model	50	0.0072 –	0.80 –	1.17×10^4 –	32 –
		0.0580	3.24	9.51×10^4	62

The experimental program was repeated three times for each of the four models to reduce uncertainty in the results, as outlines can be identified in a series of three runs for each discharge. The two students who conducted these experiments (the authors) also changed roles during the experiments to reduce subjectivity, and pictures were also taken for every discharge.

RESULTS

In this chapter, the key results and observations from the hydraulic model study are summarized and presented.

4.1 Flow characteristics

Figure 4.1.1 displays skimming flow conditions in the stepped spillway models.

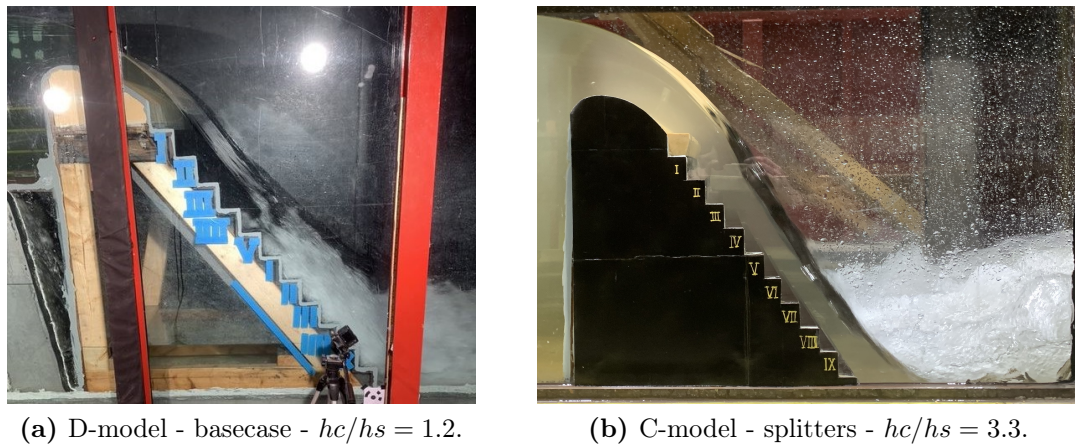


Figure 4.1.1: Side view of skimming flow in the stepped spillway models.

The point of inception is observed at $L_x/x_s = 5$ in the D-model, the high-speed camera can also be seen fixed at the lower steps. The C-model is running at maximum capacity, configured with the crest splitters, but no free surface aeration is observed at this discharge.

For very low discharges up to approximately $h_c/h_s = 0.6$ in the C-flume and slightly less for the D-flume, the water formed a deflection nappe from the first step which fell downward as a free-falling nappe before it landed on the spillway further downstream. Figure 4.1.2 shows the nappe deflecting out from step I and lands on the stepped chute further downstream at step IV. For even smaller discharges, outside the experimental range, the nappe was observed hitting step VIII/IX.



Figure 4.1.2: A nappe from the first step is formed for very low discharges, here shown in the C-model basecase - $h_c/h_s = 0.6$.

In figure 4.1.3, velocity vectors from the BIV analysis can be observed at the maximum discharge of the D-model basecase, which correspond to the flow conditions of the C-model seen in figure 4.1.1 above.

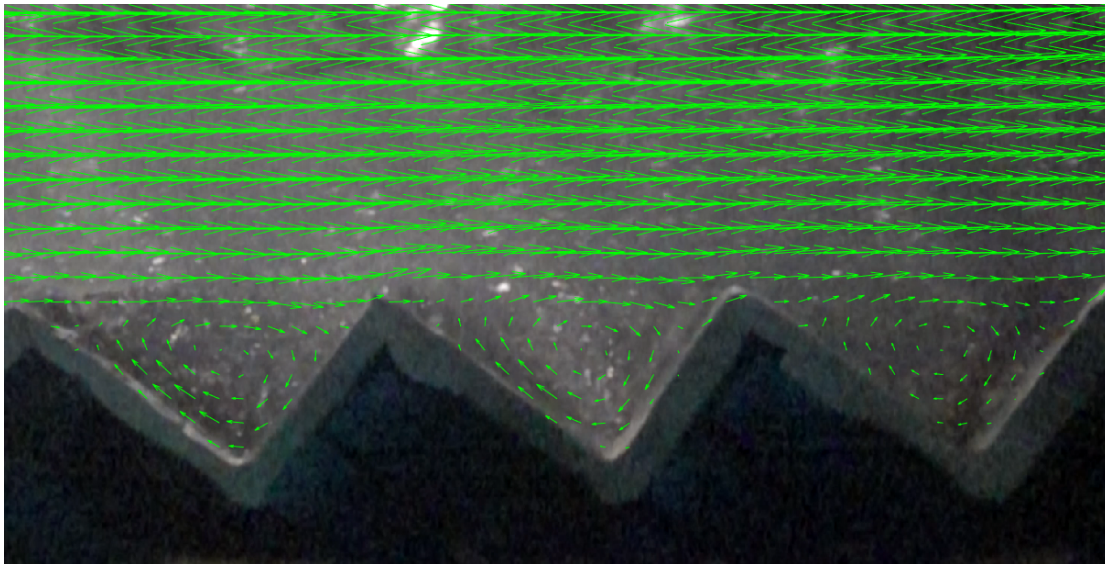


Figure 4.1.3: Velocity vectors in D-model obtained from BIV analysis - $h_c/h_s = 3.3$, $6 < L_x/x_s < 9$, $L_x < L_i$ - basecase, flow direction from left to right.

The phenomenon of circulating vortices in the step cavities can be observed. As in the C-model, no free-surface aeration is occurring at this discharge. The density of vectors does not represent the density of information in the velocity field, but the length of the vector represents the magnitude of the velocity. Since no natural aeration is occurring, bubbles are introduced at the first step to use as BIV tracers.

Figure 4.1.4 displays the velocity magnitude from the same BIV analysis as in figure 4.1.3. The analysis is zoomed out to present the whole velocity field.

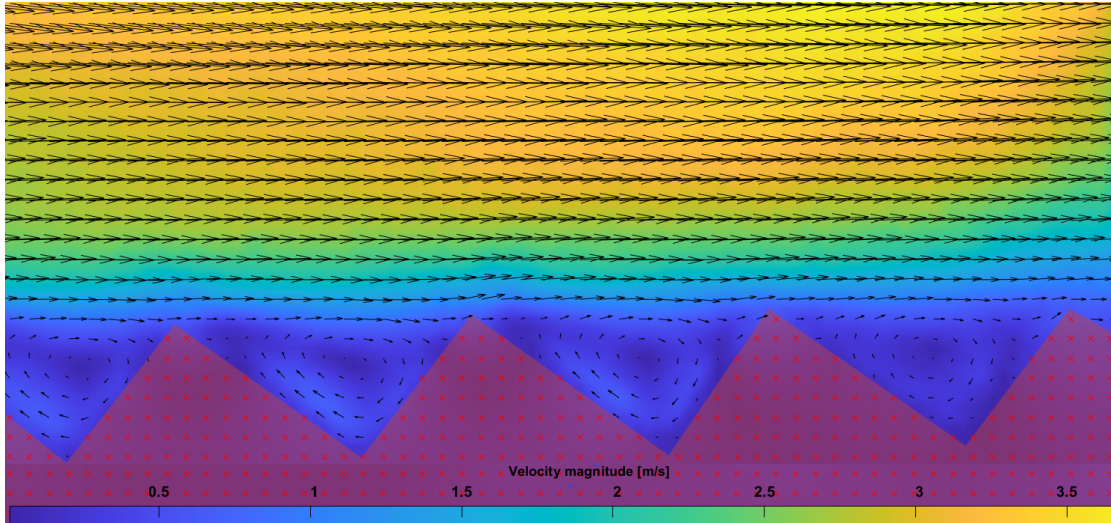


Figure 4.1.4: Velocity magnitude in D-model obtained from BIV analysis - $hc/hs = 3.3$, $5.5 < L_x/x_s < 9.2$, $L_x < L_i$ - basecase, flow direction from left to right.

Figure 4.1.4 show the same information as figure 4.1.3, along with the velocity magnitude in meters per second. Note that the velocities of the far-right area in the velocity field seem to be decreasing, this is not the case, but is an effect caused by insufficient lightning for the BIV analysis in this area. This region downstream $L_x/x_s = 8$ is only included for illustration and is not used for any calculations.

Figure 4.1.5 shows streamlines from the same BIV analysis as in figure 4.1.3 and figure 4.1.4. Note that the density of the streamlines is not related to the density of particles in the flow.

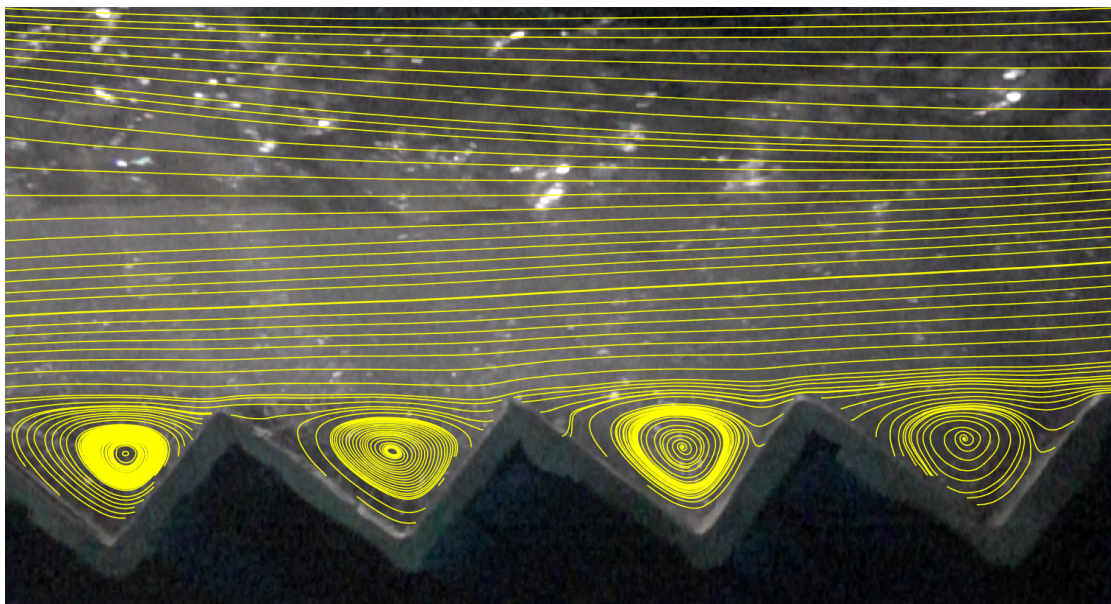


Figure 4.1.5: Streamlines in D-model obtained from BIV analysis - $hc/hs = 3.3$, $5.3 < L_x/x_s < 9$, $L_x < L_i$ - basecase, flow direction from left to right.

Transition of flow regimes

The transition of flow regimes in the models with the basecase configuration, although rather subjective, seem to coincide with established theory summarized in figure 2.1.3. The research domain is in the skimming flow regime, but as we can observe in figure 4.1.6, the splitters alter the skimming flow regime at intermediate discharges.



(a) Basecase configuration.



(b) Splitters configuration.

D-model - $h_c/h_s = 1.2$.



(c) Basecase configuration.



(d) Splitters configuration.

C-model - $h_c/h_s = 1.2$.

Figure 4.1.6: Comparison of flow regimes in the D-model and the C-model at the same normalized critical depth - basecase and splitters - $h_c/h_s = 1.2$.

For discharges up to $h_c/h_s = 1.8$ in the D-model and up to $h_c/h_s = 1.5$ in the C-model, the splitters lead to a water jet deflecting the spillway, jumping as a free-falling jet down to a lower level of the stepped spillway invert, as observed in figure 4.1.6. In addition to this deflecting jet, we can observe air-pockets inside of the cavities, reducing the traditional step-cavity circulation of the skimming flow regime, as observed in figure 4.1.7. The region drowning of the splitters occur is a bit unstable (observed in figure 4.1.8), and seems to be influenced by upstream turbulence and transverse flow. Drowned splitters can be observed in figure 4.1.1.

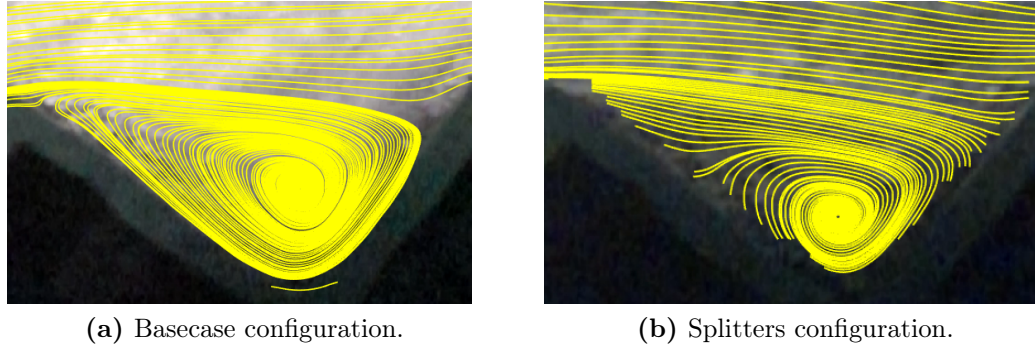
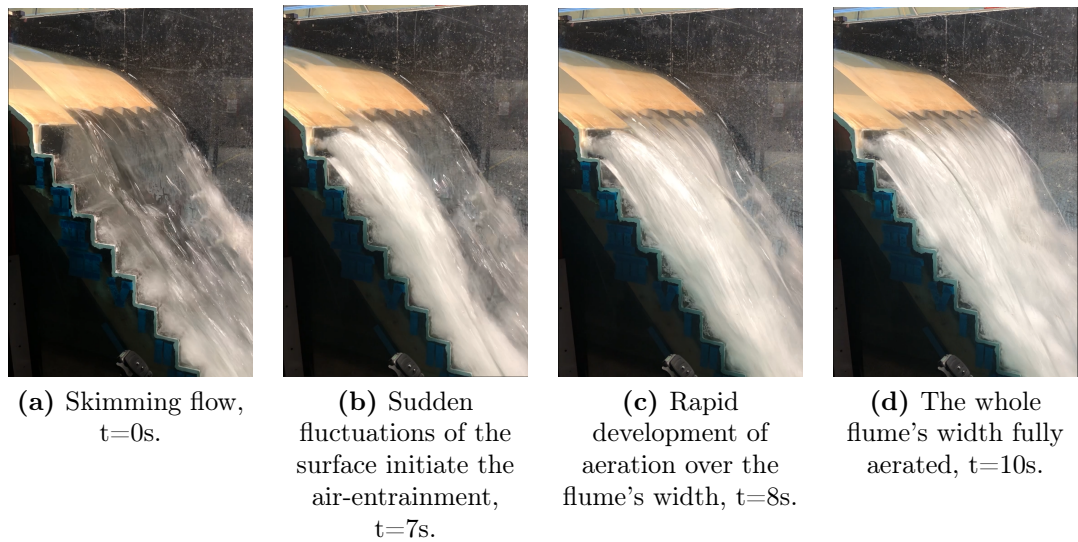
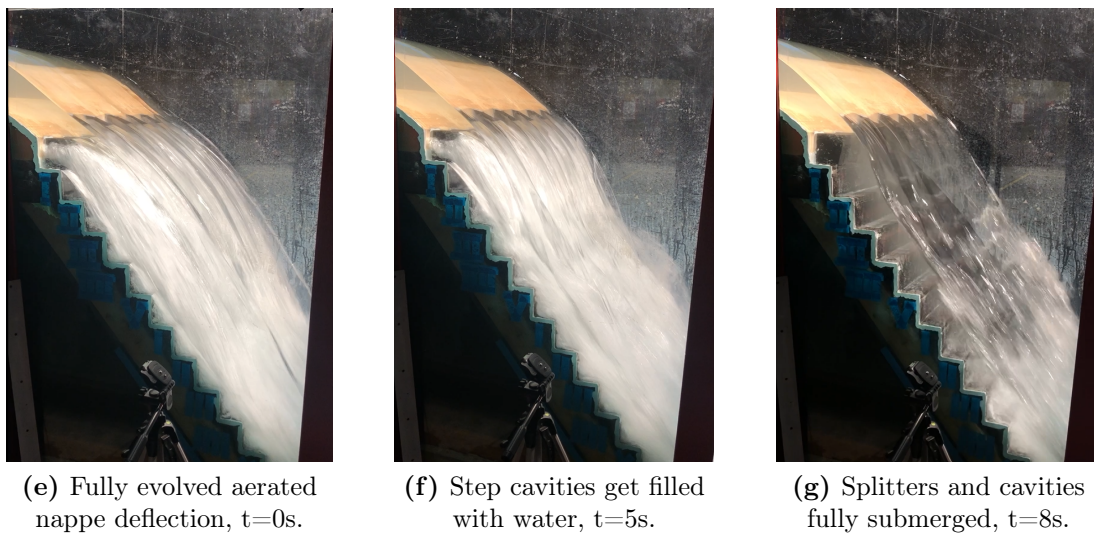


Figure 4.1.7: Comparison of streamlines obtained from BIV analysis of basecase and with splitters in D-model - $h_c/h_s = 1.2$, $7 < L_x/x_s < 8$ - flow direction from left to right.

This new flow regime observed at low to intermediate discharges along with the splitters configuration can with its considerable aeration and no distinct pseudo-bottom resemble a transitional flow regime, although it seems to be a bit more stable than a traditional transitional flow regime. Figure 4.1.8 displays the unstable transitions occurring at flow rates of about $1.8 \leq h_c/h_s \leq 2.0$ in the D-flume.



Transition from a skimming regime to a deflecting nappe regime.



Transition from a deflecting nappe regime to a skimming regime.

Figure 4.1.8: Video frames displaying unstable transitions between a skimming regime and a deflecting nappe regime over approximately 10 seconds - $h_c/h_s = 1.8$.

4.2 Onset of air entrainment

The location of the inception of free-surface aeration is, similar to the transition of flow regimes, somewhat subjective. In figure 4.2.1 we can see a comparison of experimental data, prototype data of Hinze dam (Chanson 2021b), and empirical relations for the location of the inception point.

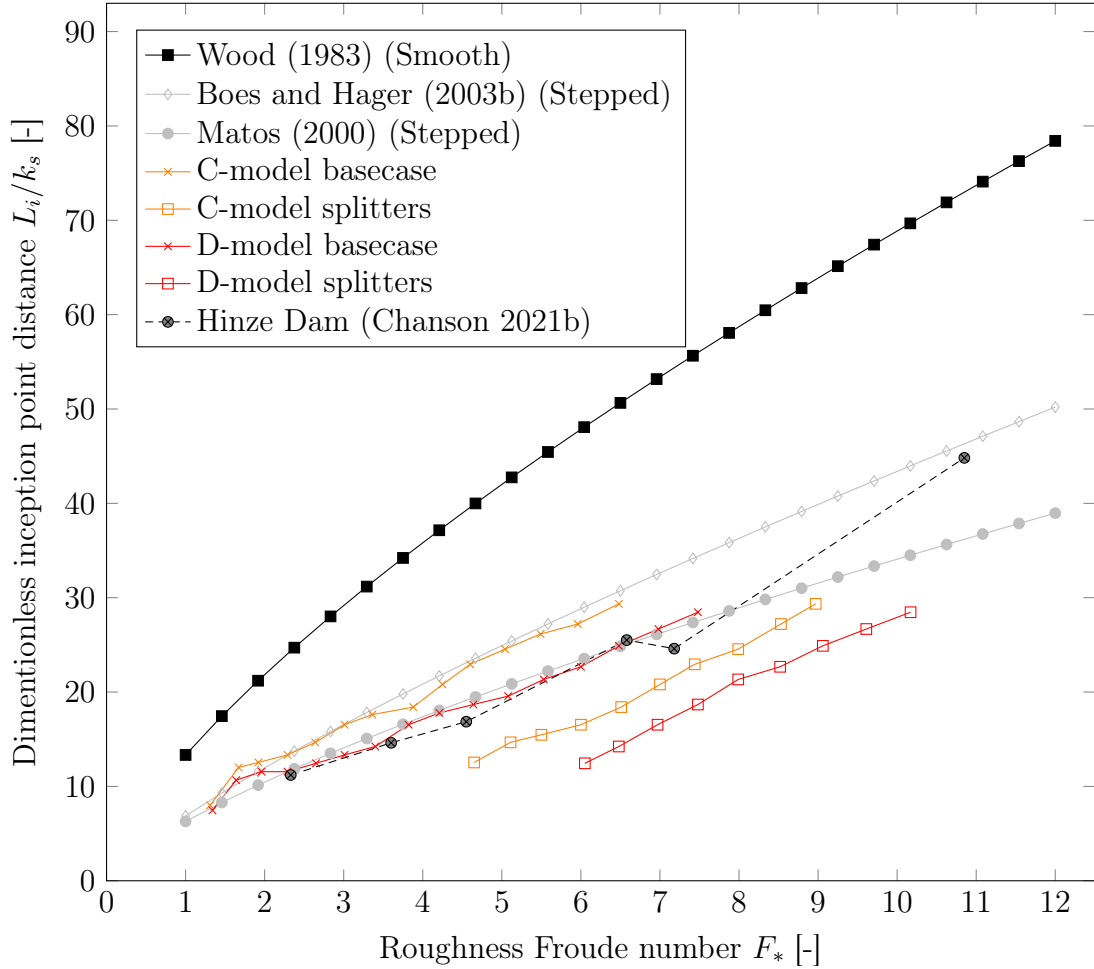


Figure 4.2.1: Comparison of experimental data, prototype data and empirical relations for the location of the inception point.

We can observe that the basecase data corresponds well to both empirical relations based on other hydraulic models, along with prototype data from Hinze dam. With the splitters configuration added to the models, we experience a reduction or a shift of the inception point distance.

4.3 Energy dissipation

Experimental data of relative energy dissipation in the D-model is estimated using the hydraulic jump method and presented in figure 4.3.1.

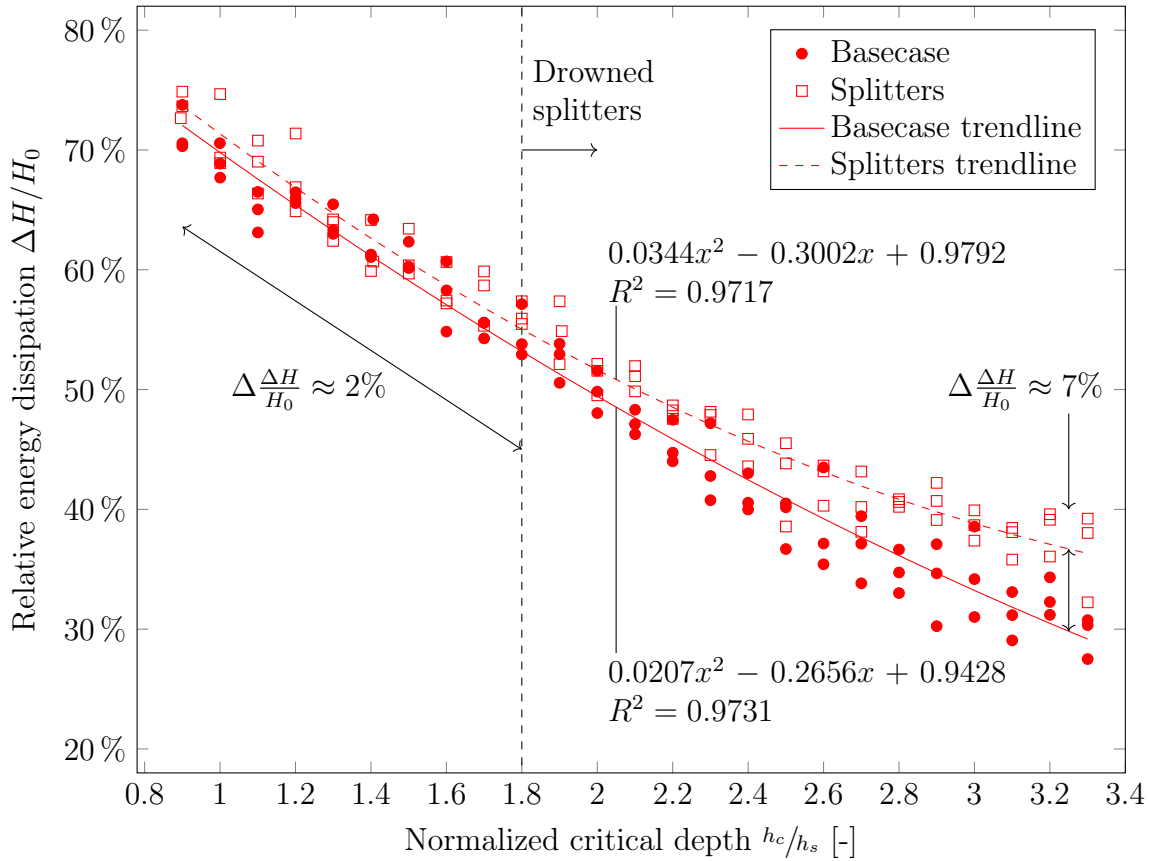


Figure 4.3.1: Experimental data of relative energy dissipation compared to normalized critical depth in D-model.

There is a difference of 2 percentage points in relative energy dissipation in the region before the splitters are drowned ($h_c/h_s < 1.8$). After the splitters are drowned, the difference in relative energy dissipation starts to increase, up to about 7 percentage points at the standard design discharges of stepped spillways.

Experimental data of relative energy dissipation in the C-model is estimated using the hydraulic jump method and presented in figure 4.3.2.

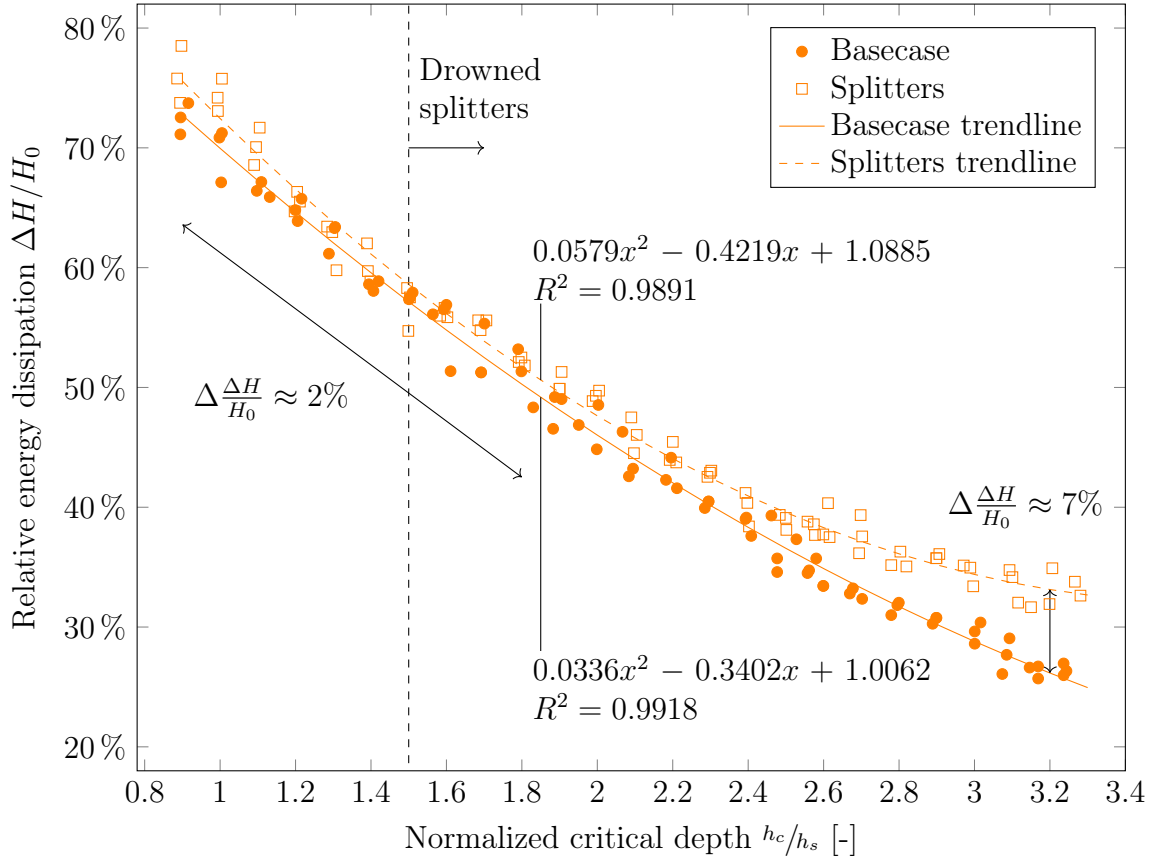


Figure 4.3.2: Experimental data of relative energy dissipation compared to normalized critical depth in C-model.

There is a difference of 2 percentage points in relative energy dissipation in the same region as in the D-model ($h_c/h_s < 1.8$), but the splitters drown at a reduced discharge. Similarly to the D-model, the difference in relative energy dissipation then starts to increase, up to about 7 percentage points at the standard design discharges of stepped spillways. We can also observe that the measurements in the C-model are more stable with less scatter than for the D-model.

Energy grade line

The calculated energy grade line in the D-model (basecase) at $h_c/h_s = 1.2$ compared with empirical residual energy level is presented in figure 4.3.3.

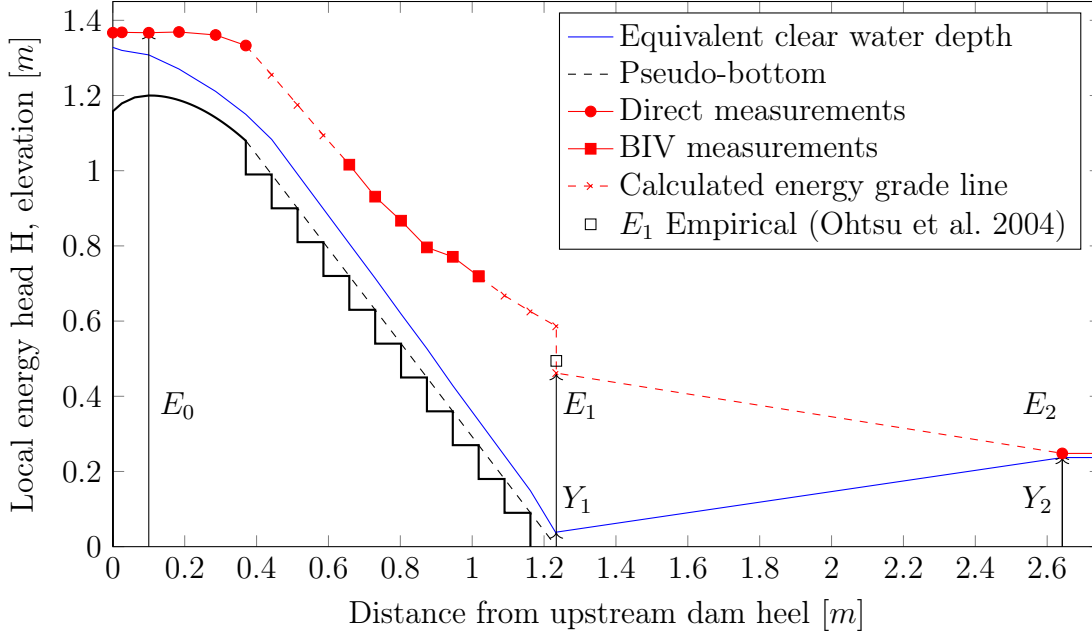


Figure 4.3.3: Calculated energy grade line in D-model compared with empirical residual energy level - $h_c/h_s = 1.2$.

The water depth is the corresponding water surface of the non-aerated flow, although in the experiment the inception of free-surface aeration is occurring around $L_x/x_s = 5$. The direct measurements are carried out by measuring the clear-water water depths, calculating the average velocities, and applying an α -value corresponding to the flow regime in the successive energy calculations.

The BIV measured velocities are corrected by a factor of 1.25 so that the sum of velocities times the area corresponds to the discharge. This correction is applied to combat the wall-effects. A difference in the E_1 calculated from interpolating the upstream BIV measurements and the E_1 corresponding to the Y_1 calculated from the hydraulic jump method can be observed.

4.4 Velocity profiles

The velocity profiles are all computed from time-averaged BIV measurements, without validation. As a result of the lack of instrumentation to carry out air-concentration measurements, the equation for velocity distribution of the non-aerated zone is used in both the aerated and non-aerated zone.

The velocity profiles measured with BIV over step edges at locations $L_x/x_s = 4, 5, 6, 7, 8, 9$ with $h_c/h_s = 1.2$ in the D-model (basecase) compared with a theoretical power-law velocity distribution are presented in figure 4.4.1.

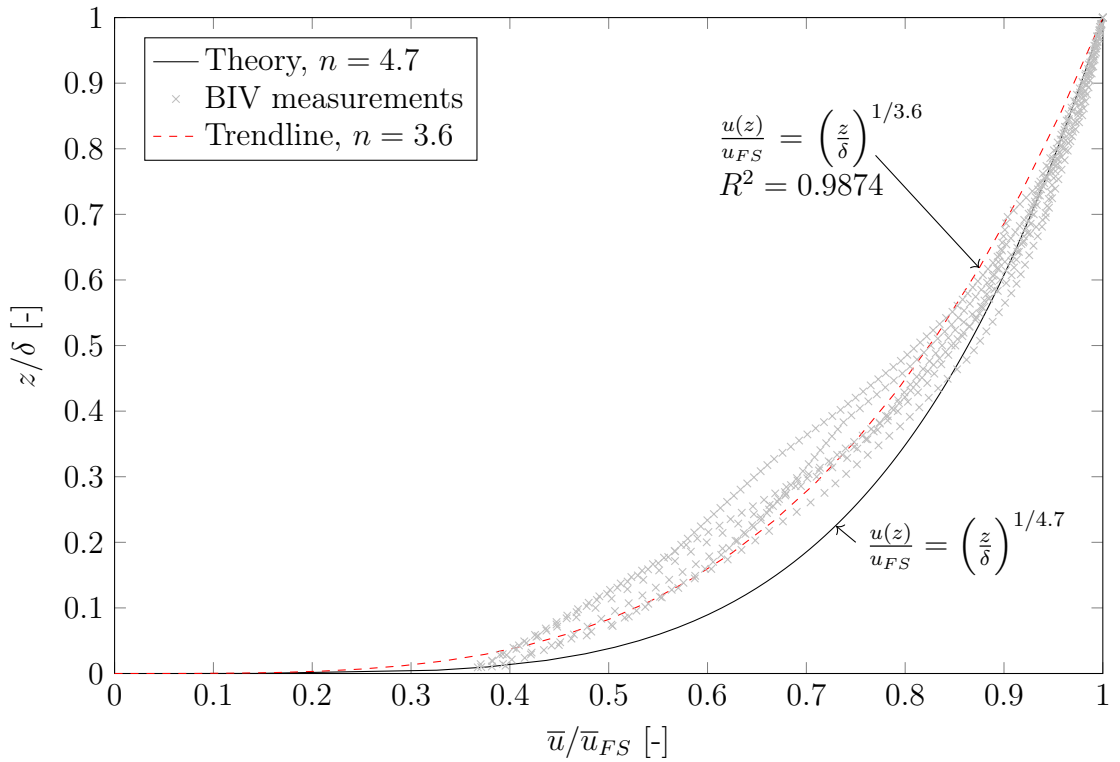


Figure 4.4.1: Dimensionless velocity profiles measured with BIV over step edges in D-model basecase compared with power-law approach - $h_c/h_s = 1.2$, $z < \delta$, $L_x/x_s = 4, 5, 6, 7, 8, 9$.

Comparison of velocity profiles measured with BIV at locations $L_x/x_s = 5.5$ and $L_x/x_s = 6.5$ with $h_c/h_s = 1.2$ in D-model for the basecase and with the splitters configuration is presented in figure 4.4.2.

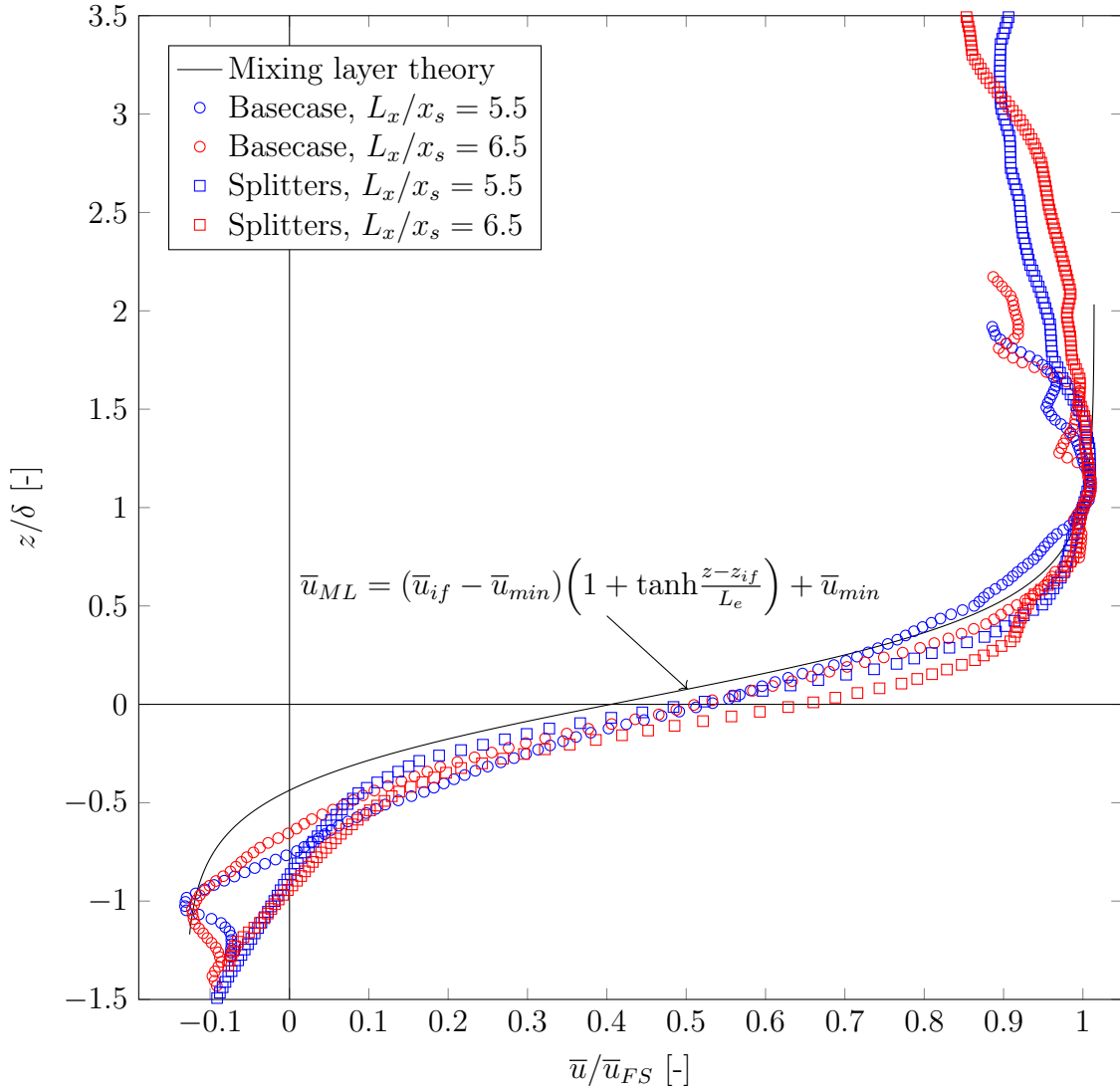


Figure 4.4.2: Velocity profiles in D-model measured with BIV compared with mixing layer theory - $h_c/h_s = 1.2$, $z < \delta$, $L_x/x_s = 5.5, 6.5$.

The velocity profiles measured with BIV seem to correspond well with established mixing layer theory in the mixing zone. The velocities seem to decrease after the end of the boundary layer, but this is most likely an effect due to air concentration increasing in this zone, reducing the number of bubbles to track for the BIV algorithm. Note that the apparent water level is higher in the splitters configuration due to the deflecting nappe in the video frames.

Comparison of surface velocities measured with BIV from a top-view at $h_c/h_s = 1.2$ and 1.6 in D-model and C-model for basecase configuration is presented in figure 4.4.3. IP corresponds to the inception point, or the location of the inception of free-surface aeration.

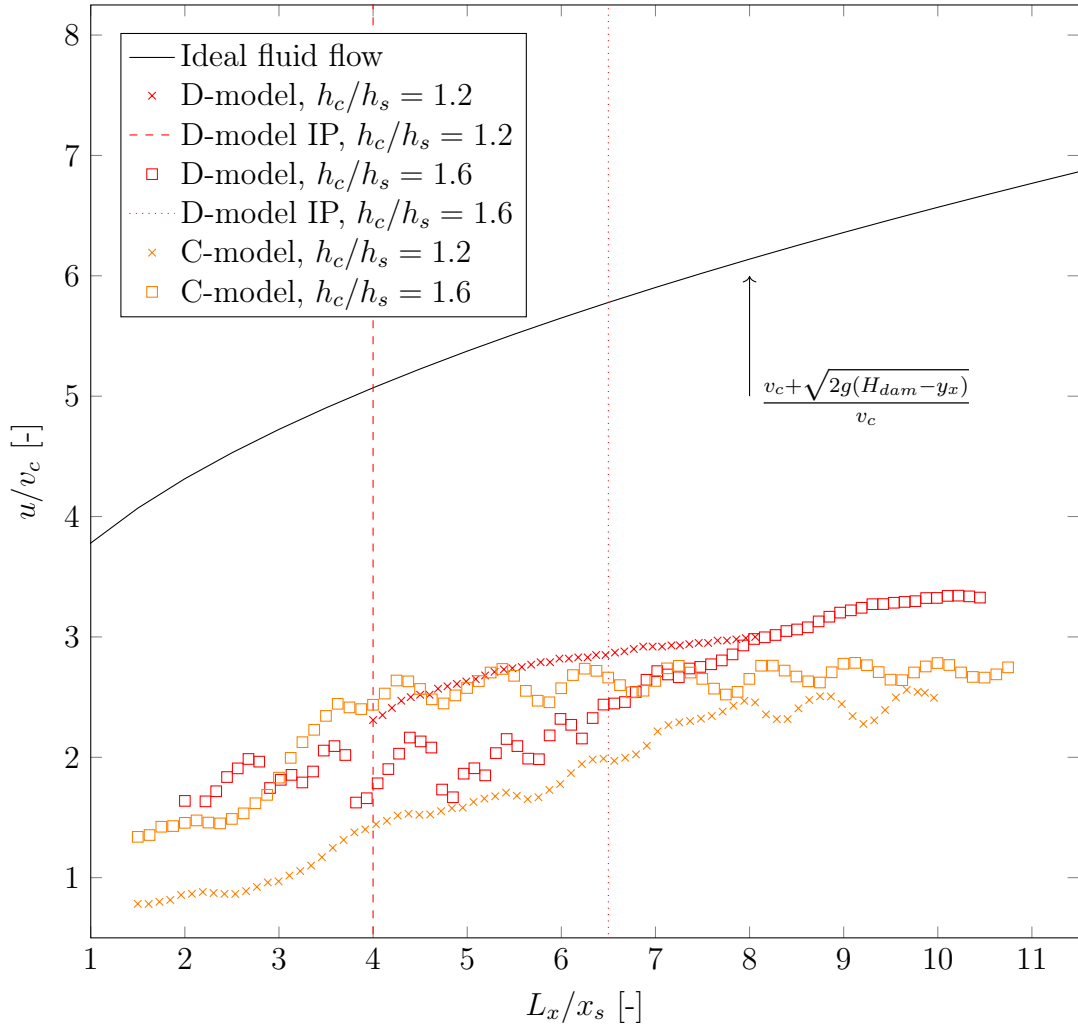


Figure 4.4.3: Surface velocities in D-model and C-model (basecase) measured with BIV from top-view compared with ideal fluid flow.

Notice that downstream the point of inception, the corresponding raw data points seem to stabilize. Surface velocities are higher compared to maximum velocities at corresponding steps from raw side-view data. Velocities lower than critical velocity can also be observed at the beginning of one of the C-model data sets, which seems unreasonable at the specified location. Oscillating patterns in raw data can be observed, especially in the non-aerated region, which most likely originates from light reflecting from surface waves in flow.

4.5 Qualitative visual observations

Early in the series of preliminary experiments, it was observed an asymmetrical incoming flow to the crest to the stepped spillway in the D-flume. With injection dye, it was confirmed an incoming turbulent flow caused a transverse flow pattern to the right in the streamwise direction. A longitudinal pattern with a lower depth located on the crest approximately 10 *cm* from the left wall was a result of this skewed flow. This caused a shorter length of inception at the section with lower flow depth. Unlike the D-flume, the C-flume had close to laminar inflow condition, causing a nearly horizontal point of inception line. An example of this can be seen in figure 4.1.6(c). After implementing measures to reduce the incoming turbulence in the D-flume, a nearly horizontal point of inception line appeared here as well.

The D-model was built with an empty air volume inside of the spillway body as seen in figure 3.1.3. During the preliminary experiments, it was minor leaks between the underlying air volume and the water flow above the stepped chute. Sometimes water was pressed from the upper side into the empty room below, while other times air was sucked out and into the water flow above. Often, low discharges pressed water downwards, and high discharges sucked air upwards. This phenomenon was suggested to be caused by pressure fluctuations in the cavities due to the unsteady turbulent flow but was not confirmed by e.g. pressure sensor measurements.

Air structures appearing from time to time immediately downstream of the step edges, as exemplified in figure 4.5.1 with the crest edge, were also observed. Air bubbles circulating in the cavity, clustered into an air body that moved towards the tip of the crest edge. This air structure could be seen in this position for up to approximately 3 seconds before the air was dragged into the vortex in the cavity below or joined the mainstream above the pseudo-bottom. This position is, as mentioned in section 2.1.5, the area with the lowest pressure close to the spillway surface, which is a possible explanation of this phenomenon. However, this observation must not be confused with the occurrence of cavitation, because the present velocities are far too low for this to happen.



Figure 4.5.1: Region of low pressure on spillway surface in D-model.

DISCUSSION

5.1 Effect of crest splitters

The intention of adding crest splitters was to trigger additional turbulence close to the crest without reducing the capacity of the spillway. Measures on the dam influence only the downstream region, therefore initiating more turbulence at the crest affects the whole dam. In addition to being able to influence the whole dam, turbulence has a self-reinforcing effect on the energy dissipation rate on a stepped spillway, favouring early disturbance of the flow. Furthermore, the velocity magnitudes in this region are too low for cavitation to occur, a major issue for hydraulic structures in high-velocity flow.

Crest splitters are also a buildable, simple hydraulic structure, that is easy to implement, and also possible to install at existing dams. Reviewing hydraulic research on the topic of improving energy dissipation in stepped spillways, there seems to be a discrepancy between research topics and measures that are implemented by dam owners. The reason for this discrepancy could be that unrealistic solutions and geometries are being researched, where the sole objective of the hydraulic study is to optimize energy dissipation, but not take the feasibility and the construction cost of the measure into account.

5.1.1 Energy dissipation

The implementation of crest splitters as a feasible, cost-effective measure to improve the energy dissipation of stepped spillways seems to be successful. At traditional design discharges for stepped spillways, the relative energy dissipation is increased by approximately 7 percentage points. The increase in energy dissipation will reduce the residual energy at the dam toe, and therefore reduce the potential for scour and bedrock erosion.

A stepped spillway is seldom the sole energy dissipator at a dam, but is often accompanied by a stilling basin, or a roller bucket downstream the dam toe. If the energy dissipation rate is increased upstream of the dam toe, we can reduce the proportions of the downstream energy dissipator. Even a slight reduction in the length of a stilling basin can greatly reduce overall cost, particularly in projects involving long dams, and in projects where a great deal of rock blasting is required to secure a firm foundation.

The interaction between the individual energy dissipating hydraulic structures is also of great importance, increasing incoming turbulence to the downstream energy dissipator can help improve the energy dissipation and decrease the length of the hydraulic jump.

Another advantage of the stepped spillway is the continuous energy dissipation happening along the spillway chute, as we can observe in the energy grade line in section 4.3. This means that we have a large area where the energy is being dissipated, reducing the stresses on the concrete and bedrock.

5.1.2 Length of inception

As observed in section 4.2, the basecase hydraulic models correlate well with the established empirical relations for the growth of the turbulent boundary layer towards the water surface, and the ensuing free-surface aeration. The prototype data from Hinze dam also seem to correspond well, especially with the primary D-model. When the splitters are introduced in the hydraulic models, the inception point distance is reduced by approximately the dimensionless distance $L_i/k_s = 10$ lower, indicating that the turbulent boundary layer is growing faster by adding the splitters.

As mentioned in section 2.1.5, the problems related to cavitation are decreasing along with increasing air concentration, and ceases at a relatively low air concentration of 5-8%. Since having a certain air concentration can eliminate problems caused by cavitation in the flow, and the cavitation potential is limiting the maximum unit discharge of stepped spillways, a shorter length of inception may lead to a higher maximum unit discharge and therefore capacity of a stepped spillway. One of the main constraints of traditional stepped spillways is the maximum unit discharge of about $30 \text{ m}^2/\text{s}$, therefore extending the maximum discharge limit would be of great importance.

As stated earlier, installing the splitters in current stepped spillways is feasible, so this could be a course of action to combat increasing design floods. One issue with this is that the relative energy dissipation drops as the unit discharge increases.

5.1.3 Flow regimes

Concerning the new deflecting nappe flow regime observed at intermediate flow rates (figure 4.1.6), the intense spray and unstable transitions are drawbacks for the splitter configuration. Optimizing the splitter geometry could potentially reduce or combat those issues, and should be investigated further. Another observation in the deflecting nappe regime is a less substantial increase in relative energy dissipation compared to the increase of relative energy dissipation in the skimming flow region as a result of implementing splitters.

5.2 Application of BIV

The application of state of the art BIV to investigate the flow characteristics of scaled stepped spillway hydraulic models is considered very useful and PIVlab, with its simple user interface, enabled the use of BIV even without any prior knowledge of the topic. Using air bubbles as tracers with white lighting appears sufficient for PIVlab to produce great data and visualizations of the flow characteristics. Such remarkable levels of detail in the cavity recirculation and visualization of the pseudo-bottom are difficult to display besides video but are attainable with BIV. This method does not require any expensive cameras, lasers or lamps, nor the need for extreme processing capacity or commercial software.

A major drawback of the present study is the lack of validation of the velocity data resulting from PIVlab. ADV was initially considered for validation measurements, but was early discarded because of its limitation for air concentrations. As seen in section 2.4.2 the flow velocity measured with velocimetry techniques through the flumes glass wall shows an underestimation of 10% to 30% compared to velocity measured in the centre line with phase detection needle probes due to wall effects (Chanson 2021a; Nina et al. 2022). Some of the same effects are observed in the present study, but it has been difficult to quantify the magnitude of this wall effect. In addition to a lack of validation of BIV, the lack of air concentration measurements resulted in difficulty apply formulas including air concentration characteristics, as seen in the velocity profiles results.

5.2.1 Velocity profiles

The development of streamwise velocity above the pseudo-bottom seen in figure 4.4.1 has the best fit to the power law when $n = 3.6$. This is intuitively in agreement with several other studies for similar chute slopes as seen in table 2.1.2, but it must be duly noted that these power-law coefficients are calculated from the non-aerated blackwater region. The analytic solution using equation 2.22 gives $n = 4.7$ which gives a shift of the graph to the right and in general larger dimensionless velocities for all values of z/δ .

The velocity profiles for the basecase from the inner corner of the steps shown in figure 4.4.2 are almost identical to the ones reported by Sánchez-Juny et al. (2022). Amador et al.'s (2006) results and Kramer's (2023) mixing layer theory (equation 2.23) are also very similar, though with minor differences especially below the pseudo-bottom. From the bottom of the graph, there are negative streamwise velocity values, with a minimum where $z/\delta \approx -1$. From this point on, the velocities evolve towards positive values through the zero point which is presumably in the centre of the cavity vortex.

Above the boundary layer δ , the velocity seems to decrease. This is also reported by Sánchez-Juny et al. (2022) who proposed that it is not a correct presentation of the actual flow velocities, but possibly due to insufficient lighting. Observations from the present study indicate that the reduction of surface velocities is a consequence of the challenge of defining the free surface rather than lighting-related

problems. It is believed that PIVlab tracks sporadic drops in the air above the surface, rather than air bubbles in the air-water volume. When the upper region of the frames including sporadic drops and stationary air are time-averaged, the velocity decreases.

The streamwise velocity distribution resulting from the deflecting nappe regime with splitters configuration shows somewhat different characteristics. The greatest negative values are seen at the lowest part of the graphs, and the zero point is further down which means that the cavity vortex is located closer to the inner corner of the step than for the basecase. This corresponds very well to visual observations shown in figure 4.1.7. Due to the free-falling nappe deflecting from the splitters (figure 4.1.6), the graphs are extended in the upwards direction.

Surface velocities captured from the top view (figure 4.4.3) show a tendency of oscillations until the inception point is reached. This might be caused by light glares in the glossy blackwater region. Sánchez-Juny et al. (2022) reports much larger differences in velocity magnitude before and after the inception point and proposes that it is caused by poor lighting. Such considerable differences are not observed in the present study.

5.2.2 Uncertainty and error sources

When working with video recordings and BIV analysis, several sources of uncertainty and errors are present. Distortion, a deformation of angles and distances in images due to the camera lens and the perspective may occur in studies like this. There is also some uncertainty related to the distance between the camera and the bubbles used as tracers because the experiments were not conducted with a light sheet as typically used for PIV. Both these effects can lead to errors in both direction and magnitude on the velocity vectors produced in PIVlab. There are methods to overcome some of these errors, but not as a built-in tool in PIVlab as the researchers of this study are aware of.

Another reasonable question to be raised is whether or not air bubbles can be used as tracers due to the upwards vertical rising velocity component. Sánchez-Juny et al. (2022) who carried out similar experiments did not seem to discuss this aspect but still concluded that air bubbles as tracers can be used. It was discovered that the results from PIVlab are very sensitive to the lighting condition of the air bubbles as seen in figure 4.1.4. These findings of lower velocities in dark regions are similar to the findings reported by Sánchez-Juny et al. (2022). A possible solution to quantify the effects of rising velocity and lighting conditions as well as for wall effects and varying distance to the traced bubbles is to conduct parallel experiments with PIV including seeding particles and laser-illuminated sheet as shown in the study by Amador et al. (2006).

Using video recordings with 1000 FPS was experienced to be sufficient for the use of PIVlab. Sánchez-Juny et al. (2022) successfully used PIVlab with 400 FPS, and reducing the frame rate in this study would have saved processing time. Additionally, optimisation of lighting conditions, choice of preprocessing and other settings in PIVlab is recommended for further research and can be conducted with a sensitivity analysis of the different parameters.

5.2.3 Other observations

There is also a deviation in velocities attained from BIV side-view, BIV top-view, and the average velocities used in the energy calculations, because of wall effects and energy correction coefficients. Methods used to combat those differences include comparing side-view and top-view maximum velocities, and including a correction factor, in addition to comparing the discharges to the sum of velocities times distance and applying a factor to minimize the difference.

Some deviation between the E_1 calculated from upstream with BIV and downstream with the hydraulic jump method seen in figure 4.3.3 is expected, because there is a local energy loss at the toe of the dam where the flow changes direction, in addition to turbulent dissipation of the flow when it plunges into the stilling basin, assumed to be approximately 15% for $\theta = 30^\circ$ by André (2004). This extra energy dissipation could be subtracted when looking at energy dissipation in the stepped spillways, however this would further complicate the calculations and add uncertainty, nevertheless, we will also benefit from this effect in a prototype.

5.3 Scale effects

Scale effects is, like explained in section 2.4.1, inevitable when down-scaling highly turbulent two-phase flow. Reduced energy dissipation and lower aeration efficiency were observed in the C-model, as anticipated.

The most visual differences between the two different scale models were the more apparent turbulent regime of the D-model, and the proportional less stable transitions and measurements.

Regarding the transitions, the deflecting water jet over the splitters is observed for a wider range of normalized critical depths in the D-flume. One explanation for this phenomenon could be that the surface tension forces are more evident in the smaller C-model, as seen in the Weber number in section 3.3, which results in more resistance for the nappe in order to deflect from the main flow.

5.3.1 Air-water flow

The size of air bubbles in the two different scale models is observed to be of similar size, which leads to proportionally larger and fewer air bubbles in the C-model in regards to the prototype it represents. One practical issue arising from this situation is that the BIV algorithm has fewer bubbles to track, which leads the C-model less fit for BIV analysis.

Less turbulence, higher relative surface tension, and proportionally larger air bubbles experienced in the C-model could all contribute to reduced aeration, and to some extent lower energy dissipation, as seen in figure 4.2.1 and figures 4.3.1, 4.3.2. The D-model basecase seems to correspond well with Hinze dam in regards to the length of inception, and the length of inception in the C-model seems to be extended compared to the D-model both in the basecase and with the splitters configuration.

The relative energy dissipation in the different scale models deviate more at larger dimensionless discharges, and the deviation for the design discharges can be observed to be substantial. At design discharges, the flow in the stepped spillway is not aerated, as seen for $h_c/h_s = 3.3$ in figure 4.1.1, which means that the two-phase characteristics in the spillway are not the issue at hand. However, the hydraulic jump at the dam toe is highly turbulent and aerated, and therefore subject to drastic scale effects, which could explain the deviation in energy dissipation for higher flow rates in the two different models.

5.3.2 Length scale magnitude

The findings in this research correspond well to the established theory regarding the valid length scales for studying highly turbulent two-phase flow in Froude similitude. It would also have been interesting to investigate a wider range of different scales for the splitters configuration, like others have done before for stepped spillways (Pegram et al. 1999).

While it seems like the C-model is unfit for the study of two-phase flow, the change in relative energy dissipation from the basecase to the splitters configuration is nearly identical for the two different scale models. This supports the findings in the main D-model.

5.3.3 Other error sources

The minor leaks described in section 4.5 could impact the pressure field in the stepped spillways, however, they seem insignificant, as the volume of air coming into the flow or water leaking out of the flow correspond to a tiny fraction of the flow rate.

The effects of the straightening of the flow in the D-flume demonstrate that in-going turbulence at the crest also impacts the characteristics of the growing boundary layer, in addition to the location of the inception point being subjective, adding to the possible sources of error.

Even though the asymmetrical incoming flow discussed in section 4.5 was taken care of, some of the same patterns close to the wall were observed for several different discharges probably caused by wall effects. It was noticed that the water forms a concave meniscus along the glass, caused by the surface tension. This was seen as a slightly increased flow depth along the wall and glass, and this was taken into account when measuring flow depths in the non-aerated blackwater region.

Visually, the flow over the stepped spillway in the C-flume had a calm behaviour compared to the D-flume. Less turbulence and uncertainty can be confirmed by looking at calculations and the spread in the energy dissipation results. This means that the flow characteristics vary little over time and few or no differences in the cross-section were observed. Longitudinal patterns moving over the cross-section over time are seen in the D-flume, especially for larger discharges. Similar behaviour and patterns of "elongated air-water surface features" are seen in prototype conditions on Hinze dam by Chanson (2021b). Sudden ruptures of the surface, causing a spray jumping out from the air-water mixture are also observed in the D-flume for certain discharges. This is not appearing in the same magnitude in the C-flume.

In addition to having a calmer flow, it was easier to accurately adjust the tailwater level with the flap gate in the C-flume, as the discharge in the overflow gate is dependent on the water level to the power of $\frac{3}{2}$. In the D-flume however, where the tailwater is controlled by an underflow flap gate, the discharge is dependent on the water level to the power of $\frac{2}{3}$, and keeping a stable tailwater level for the hydraulic jump to be in its optimum position for a long time period was difficult. This issue lead to the measuring series being shorter than ideal, which again can lead to a larger spread and uncertainty in the measured Y_2 , and ensuing energy dissipation results. Utilising a V-notch weir, which would work as a stable overflow gate for most of the flow, in combination with the electric adjustable underflow flap for smaller adjustments in the D-flume could have made the tailwater conditions more stable.

Regarding the deflecting water jet occurring at smaller discharges seen in section 4.1, this phenomenon has, as mentioned earlier, been described in the literature by Sorensen (1985), Ohtsu et al. (2004) and Zhang (2017) among others. Non-uniform steps can be added to combat this issue, which is often the case in prototypes, however, this adds complexity to the hydraulic model study. In generalized stepped spillways hydraulic research, it might be advantageous to keep a simple geometry, depending on the scope of the study.

CONCLUSIONS

6.1 Key findings

This study finds crest splitters to be a practical, feasible, and cost-effective measure to improve energy dissipation in stepped spillways, applicable both for existing dams and in new projects. An increase of 7 percentage points in relative energy dissipation was achieved for design discharges, prior to the optimization of splitter geometry. In addition to increasing energy dissipation, a reduction in the length of inception and the following cavitation potential was attained, which results in an increased maximum allowable unit discharge.

Potential drawbacks for the splitter configuration include extra spray and less stable transitions of flow regimes. Modification of splitter geometry can probably reduce those issues.

The application of BIV for accurately measuring and determining flow characteristics in aerated flow conditions is found to be rather straightforward, extremely powerful, and probably the best practice. BIV makes it possible to gather large quantities of high quality data with regular camera equipment, in addition to extracting information and producing plots dense in information without the need for commercial software or major processing capacities.

Validation should be included when employing BIV in studies, and furthermore, a large scale is essential in order to utilize the full potential of BIV in hydraulic scale models.

Scale effects observed in this study correspond well with established theory, where severe scale effects were present in the air-water flow in the smaller-scaled model. It must be emphasized that a large scale is crucial in order to accurately study highly turbulent two-phase flow conditions. This corresponds to, and amplifies, the findings from the application of BIV.

6.2 Recommendations for future research

Based on the experiences made during this research, the following recommendations are made for future research:

- Increase the upper range of prototype unit discharges in the hydraulic model study to investigate flow conditions, cavitation potential, and energy dissipation at new design discharges. Determine new maximum unit discharge with splitters configuration. Due to the hydraulic models in this study being limited to a prototype unit discharge of roughly $30 \text{ m}^2/\text{s}$, the traditional maximum unit discharge of stepped spillways, this study did not investigate the hydraulics and energy dissipation at discharges exceeding this limit.
- Optimize splitter geometry to further increase the energy dissipation, shorten the length of inception, reduce cavitation potential, increase maximum unit discharge, reduce unstable transitions, and reduce spray. The splitter geometry in this research was partly inspired by Roberts splitters, and partly based on a simple design that corresponded to step geometry. Consequently, the geometry certainly has potential for improvement.
- Investigate the potential to install internal aeration ducts in order to aerate the splitters. Based on observed low pressure zones and the behavior of the flow, air vents placed at the splitter faces could reduce cavitation potential and improve maximum unit discharge substantially.
- Validate BIV measurements with probes and include air-concentrations in the field of study. Measuring air concentration is fundamental to the study of two-phase flows. The utilization of BIV seems to have great potential for the study of two-phase flow, but the results must be validated in order to verify the success.
- Obtain more prototype data to compare with the hydraulic scale models. Nature is the final jury, therefore combining prototype data with laboratory data will determine the applicability of the hydraulic scale model results.
- In combination with including more prototype data, a more comprehensive study of different scales should be carried out to further investigate scale effects in two-phase flows and in the inception of free-surface aeration.
- There seems to be a humongous advantage in being a two-person team when undergoing such extensive hydraulic model studies, and therefore this is the most important recommendation we conclude with.

REFERENCES

- Amador, António, Martí Sánchez-Juny, and Josep Dolz (2006). “Characterization of the Nonaerated Flow Region in a Stepped Spillway by PIV”. In: *Journal of Fluids Engineering* 128.6, pp. 1266–1273. ISSN: 0098-2202. DOI: 10.1115/1.2354529.
- (2009). “Developing Flow Region and Pressure Fluctuations on Steeply Sloping Stepped Spillways”. In: *Journal of Hydraulic Engineering* 135.12. Publisher: American Society of Civil Engineers, pp. 1092–1100. ISSN: 0733-9429. DOI: 10.1061/(ASCE)HY.1943-7900.0000118.
- André, Stéphanie (2004). “High velocity aerated flows on stepped chutes with macro-roughness elements”. In: in collab. with Anton Schleiss. DOI: 10.5075/epfl-thesis-2993.
- Belanger, Jean Baptiste (1828). *Essai sur la solution numerique de quelques problemes relatifs au mouvement permanent des eaux courantes; par m. J.-B. Belanger ..* Google-Books-ID: AZ111SILXbcC. chez Carilian-Goeury, libraire, des corps royaux des ponts et chaussees et des mines. 46 pp.
- Boes, Robert Michael (2000). “Zweiphasenströmung und Energieumsetzung an Grosskaskaden”. Doctoral Thesis. ETH Zurich. URL: www.research-collection.ethz.ch/handle/20.500.11850/144585.
- Boes, Robert Michael and Willi Hager (2003a). “Hydraulic Design of Stepped Spillways”. In: *Journal of Hydraulic Engineering* 129.9. Publisher: American Society of Civil Engineers, pp. 671–679. ISSN: 0733-9429. DOI: 10.1061/(ASCE)0733-9429(2003)129:9(671).
- (2003b). “Two-Phase Flow Characteristics of Stepped Spillways”. In: *Journal of Hydraulic Engineering* 129.9, pp. 661–670. DOI: 10.1061/(ASCE)0733-9429(2003)129:9(661).
- Bombardelli, Fabián A., Inês Meireles, and Jorge Matos (2011). “Laboratory measurements and multi-block numerical simulations of the mean flow and turbulence in the non-aerated skimming flow region of steep stepped spillways”. In: *Environmental Fluid Mechanics* 11.3, pp. 263–288. ISSN: 1573-1510. DOI: 10.1007/s10652-010-9188-6.
- Bung, Daniel (2011). “Developing flow in skimming flow regime on embankment stepped spillways”. In: *Journal of Hydraulic Research* 49.5, pp. 639–648. ISSN: 0022-1686. DOI: 10.1080/00221686.2011.584372.
- Bung, Daniel and Daniel Valero (2015). “Hybrid investigation of air transport processes in moderately sloped stepped spillway flows”. In: URL: www.iahr.org/library/infor?pid=7825.

- Bung, Daniel and Daniel Valero (2016). “Optical flow estimation in aerated flows”. In: *Journal of Hydraulic Research* 54.5, pp. 575–580. ISSN: 0022-1686. DOI: 10.1080/00221686.2016.1173600.
- Calitz, G. and G. R. Basson (2018). “The effect of aeration through an internal gallery of a dam on the cavitation risk of Roberts splitters”. In: *Journal of the South African Institution of Civil Engineering* 60.1. Publisher: South African Institution of Civil Engineering (SAICE), pp. 31–43. ISSN: 1021-2019. DOI: 10.17159/2309-8775/2018/v60n1a4. (Visited on 04/20/2023).
- Catucci, Daniele, Riccardo Briganti, and Valentin Heller (2021). “Numerical validation of novel scaling laws for air entrainment in water”. In: *Proceedings of the Royal Society A: Mathematical, Physical and Engineering Sciences* 477.2255, p. 20210339. DOI: 10.1098/rspa.2021.0339.
- CCC (2009). *Wadi Dayqah Main & Saddle Dams*. Consolidated Contractors Company. URL: www.ccc.net/project/wadi-dayqah-main-saddle-dams/.
- Chamani, Mohammad R. (2000). “Air inception in skimming flow regime over stepped spillways”. In: *Hydraulics of Stepped Spillways*. ISBN: 978-1-00-307860-9.
- Chanson, Hubert (1994a). “Comparison of energy dissipation between nappe and skimming flow regimes on stepped chutes”. In: *Journal of Hydraulic Research* 32.2, pp. 213–218. ISSN: 0022-1686. DOI: 10.1080/00221686.1994.10750036.
- (2021a). “Hydraulics and energy dissipation on stepped spillways-prototype and laboratory experiences”. In: Sichuan University Press.
- (1994b). “Hydraulics of skimming flows over stepped channels and spillways”. In: *Journal of Hydraulic Research* 32.3, pp. 445–460. ISSN: 0022-1686. DOI: 10.1080/00221689409498745.
- (2021b). “Stepped Spillway Prototype Operation and Air Entrainment: Toward a Better Understanding of the Mechanisms Leading to Air Entrainment in Skimming Flows”. In: URL: <https://ascelibrary.org/doi/10.1061/%28ASCE%29HY.1943-7900.0002015>.
- (2021c). *Stepped spillway prototype operation, spillway flow and air entrainment: the Hinze Dam, Australia*. CH123/21. ISBN: 9781742723549. The University of Queensland. DOI: 10.14264/c8d5280.
- (2003). “The Hydraulics of Stepped Chutes and Spillways”. In: *Applied Mechanics Reviews* 56. DOI: 10.1115/1.1523365.
- Chanson, Hubert and Frederic Murzyn (2008). “Froude Similitude and Scale Effects Affecting Air Entrainment in Hydraulic Jumps”. In: DOI: 10.1061/40976(316)240.
- Chanson, Hubert, Youichi Yasuda, and Iwao Ohtsu (2002). “Flow resistance in skimming flows in stepped spillways and its modelling”. In: *Canadian Journal of Civil Engineering* 29.6, pp. 809–819. ISSN: 0315-1468. DOI: 10.1139/102-083.
- Chatila, Jean G and Bassam R Jurdi (2004). “Stepped Spillway as an Energy Dissipater”. In: *Canadian Water Resources Journal / Revue canadienne des ressources hydriques* 29.3. Publisher: Taylor & Francis, pp. 147–158. ISSN: 0701-1784. DOI: 10.4296/cwrj147.
- Chinnarasri, C. (2002). *Assessing the flow resistance of skimmed flow on the step faces of stepped spillways - NS Energy*. In: *Dam Engineering*. URL: www.dam-engineering.com.

- nsenergybusiness.com/news/newsassessing-the-flow-resistance-of-skimmed-flow-on-the-step-faces-of-stepped-spillways/.
- Christodoulou, George (1993). “Energy Dissipation on Stepped Spillways”. In: *Journal of Hydraulic Engineering* 119.5. Publisher: American Society of Civil Engineers, pp. 644–650. DOI: 10.1061/(ASCE)0733-9429(1993)119:5(644).
- Dong, Zongshi et al. (2019). “Numerical Simulation of Air–Water Two-Phase Flow on Stepped Spillways behind X-Shaped Flaring Gate Piers under Very High Unit Discharge”. In: *Water* 11.10. Number: 10 Publisher: Multidisciplinary Digital Publishing Institute, p. 1956. ISSN: 2073-4441. DOI: 10.3390/w11101956.
- Emiroglu, Muhammet and Ahmet Baylar (2003). “An Investigation of Effect of Stepped Chutes with End Sill on Aeration Performance”. In: *Water Qual. Res. J. Can.* 38. DOI: 10.2166/wqrj.2003.034.
- Estrella, S. et al. (2015). “Physical modeling of a stepped spillway without side-walls”. In: *Canadian Journal of Civil Engineering* 42.5. Publisher: NRC Research Press, pp. 311–318. ISSN: 0315-1468. DOI: 10.1139/cjce-2014-0427. URL: <https://cdnsiencepub.com/doi/10.1139/cjce-2014-0427> (visited on 06/01/2023).
- Felder, Stefan and Hubert Chanson (2014). “Air–water flows and free-surface profiles on a non-uniform stepped chute”. In: *Journal of Hydraulic Research* 52.2. Publisher: Taylor & Francis, pp. 253–263. ISSN: 0022-1686. DOI: 10.1080/00221686.2013.841780.
- (2011). “Energy Dissipation down a Stepped Spillway with Nonuniform Step Heights”. In: *Journal of Hydraulic Engineering* 137.11, pp. 1543–1548. ISSN: 0733-9429, 1943-7900. DOI: 10.1061/(ASCE)HY.1943-7900.0000455.
- (2009). “Turbulence, dynamic similarity and scale effects in high-velocity free-surface flows above a stepped chute”. In: *Experiments in Fluids* 47.1, pp. 1–18. ISSN: 1432-1114. DOI: 10.1007/s00348-009-0628-3.
- Frizell, Kathleen (1992). “Hydraulics of Stepped Spillways for RCC Dams and Dam Rehabilitations”. In: URL: www.usbr.gov/tsc/techreferences/hydraulics_lab/pubs/PAP/PAP-0596.pdf.
- Frizell, Warren, Renna Floriana, and Matos Jorge (2015). “Cavitation Potential of Flow on Stepped Spillways”. In: *Journal of Hydraulic Engineering* 141.8. Publisher: American Society of Civil Engineers, p. 07015009. DOI: 10.1061/(ASCE)HY.1943-7900.0001009.
- Guenther, Philipp, Stefan Felder, and Hubert Chanson (2013). “Flow aeration, cavity processes and energy dissipation on flat and pooled stepped spillways for embankments”. In: *Environmental Fluid Mechanics* 13.5, pp. 503–525. ISSN: 1573-1510. DOI: 10.1007/s10652-013-9277-4.
- Henderson, Francis (1966). *Open Channel Flow*. Google-Books-ID: 4whSAAAA-MAAJ. Macmillan. 552 pp. ISBN: 978-0-02-353510-9.
- Hohermuth, Benjamin, Robert M. Boes, and Stefan Felder (2021). “High-Velocity Air–Water Flow Measurements in a Prototype Tunnel Chute: Scaling of Void Fraction and Interfacial Velocity”. In: *Journal of Hydraulic Engineering* 147.11. Publisher: American Society of Civil Engineers, p. 04021044. ISSN: 1943-7900. DOI: 10.1061/(ASCE)HY.1943-7900.0001936.
- Ikinciogullari, Erdinc (2023). “Stepped spillway design for energy dissipation”. In: *Water Supply*, ws2023016. ISSN: 1606-9749. DOI: 10.2166/ws.2023.016.

- Khatsuria, Rajnikant M. (2004). *Hydraulics of Spillways and Energy Dissipators*. Boca Raton: CRC Press. ISBN: 978-0-429-22501-7. DOI: 10.1201/9780203996980.
- Kobus, Helmut (1984). “Local air entrainment and detrainment”. In: Universität Stuttgart. DOI: 10.18419/OPUS-559.
- Kramer, Matthias (2023). “Velocities and Turbulent Stresses of Free-Surface Skimming Flows over Triangular Cavities”. In: 149. DOI: 10.1061/JHEND8.HYENG-13209.
- Kramer, Matthias and Stefan Felder (2021). “Remote Sensing of Aerated Flows at Large Dams: Proof of Concept”. In: *Remote Sensing* 13. DOI: 10.3390/rs13142836.
- Li, Shuai, Zhang Jianmin, and Weilin Xu (2017). “Numerical investigation of air–water flow properties over steep flat and pooled stepped spillways”. In: *Journal of Hydraulic Research* 56, pp. 1–14. DOI: 10.1080/00221686.2017.1286393.
- Lysne, Dagfinn Kåre et al. (2003). *Hydropower Development. Vol. no. 8 : Hydraulic Design*. Hydraulic Design. Vol. 8. 17 vols. Trondheim: Norwegian Institute of Technology. Department of Hydraulic Engineering. ISBN: 82-7598-027-5.
- Matos, Jorge (2000). “Hydraulic design of stepped spillways over RCC dams”. In: *Hydraulics of Stepped Spillways*. ISBN: 978-1-00-307860-9.
- Meireles, Ines C., Fabian A. Bombardelli, and Jorge Matos (2014). “Air entrainment onset in skimming flows on steep stepped spillways: an analysis”. In: *Journal of Hydraulic Research* 52.3, pp. 375–385. ISSN: 0022-1686, 1814-2079. DOI: 10.1080/00221686.2013.878401.
- Microsonic (2023). *mic+130/IU/TC | ultrasonic sensor in M30 | microsonic*. URL: www.microsonic.de/en/distance-sensors/cylindrical/micplus/standard-sensors/standard-sensors/micplus130iutc.htm.
- Mikalsen, Lars Marius (2022). *Alternativer for energidreper ved Chute de Tsamba*. Mulighetsstudie. Trondheim: NTNU.
- Nina, Yvan Arosquipa et al. (2022). “Intrusive and non-intrusive two-phase air-water measurements on stepped spillways: A physical study”. In: *Experimental Thermal and Fluid Science* 131, p. 110545. ISSN: 0894-1777. DOI: 10.1016/j.expthermflusci.2021.110545.
- Ohtsu, I., Y. Yasuda, and M. Takahashi (2004). “Flow Characteristics of Skimming Flows in Stepped Channels”. In: *Journal of Hydraulic Engineering* 130.9, pp. 860–869. ISSN: 0733-9429, 1943-7900. DOI: 10.1061/(ASCE)0733-9429(2004)130:9(860).
- Olsen, Nils Reidar Bøe (2015). *Numerisk modellering av kapasitet på flomløp et litteraturstudium*. Trondheim: NTNU. ISBN: 978-82-7598-094-4. URL: <https://docplayer.me/24593843-Numerisk-modellering-av-kapasitet-pa-flomlop-et-litteraturstudium.html> (visited on 09/14/2022).
- Pegram, Geoffrey G. S., Andrew K. Officer, and Samuel R. Mottram (1999). “Hydraulics of Skimming Flow on Modeled Stepped Spillways”. In: *Journal of Hydraulic Engineering* 125.5. Publisher: American Society of Civil Engineers, pp. 500–510. ISSN: 0733-9429. DOI: 10.1061/(ASCE)0733-9429(1999)125:5(500).
- Peterka, Alvin J. (1958). *Hydraulic Design of Stilling Basins and Energy Dissipators*. United States Bureau of Reclamation. URL: www.usbr.gov/tsc/techreferences/hydraulics_lab/pubs/EM/EM25.pdf.

- Peyras, L., P. Royet, and G. Degoutte (1992). “Flow and Energy Dissipation over Stepped Gabion Weirs”. In: *Journal of Hydraulic Engineering* 118.5. Publisher: American Society of Civil Engineers, pp. 707–717. ISSN: 0733-9429. DOI: 10.1061/(ASCE)0733-9429(1992)118:5(707).
- Pfister, Michael, Willi H. Hager, and Hans-Erwin Minor (2006). “Bottom Aeration of Stepped Spillways”. In: *Journal of Hydraulic Engineering* 132.8. Publisher: American Society of Civil Engineers, pp. 850–853. ISSN: 0733-9429. DOI: 10.1061/(ASCE)0733-9429(2006)132:8(850).
- Rajaratnam, Nallamuthu (1990). “Skimming flow in stepped spillways”. In: *Journal of Hydraulic Engineering* 116.4. ISBN: 0733-9429, pp. 587–591.
- Roberts, D. F. (1943). “The dissipating of the energy of a flood passing over a high dam”. In: pp. 48–92. URL: https://journals.co.za/doi/pdf/10.10520/AJA10212019_20965.
- Ruff, James F. and Jason P. Ward (2002). *Hydraulic Design of Stepped Spillways*. Report 951. Denver, Colorado: United States Bureau of Reclamation. URL: www.usbr.gov/tsc/techreferences/hydraulics_lab/pubs/PAP/PAP-0951.pdf.
- Sánchez-Juny, Martí and J. Dolz (2003). “Characterization of the pressure field over a stepped spillway in Roller Compacted Concrete dams”. In: *Roller Compacted Concrete Dams Proceedings of the IV International Symposium on Roller Compacted Concrete Dams, Madrid, Spain, 17-19 November 2003- 2 Vol set*. Ed. by L. Berga et al. 1st ed. London: Routledge, pp. 697–700. ISBN: 978-0-203-74127-6. DOI: 10.1201/9780203741276.
- Sánchez-Juny, Martí, Soledad Estrella, et al. (2022). “Velocity Measurements in Highly Aerated Flow on a Stepped Chute without Sidewall Constraint Using a BIV Technique”. In: *Water* 14.16. Number: 16 Publisher: Multidisciplinary Digital Publishing Institute, p. 2587. ISSN: 2073-4441. DOI: 10.3390/w14162587.
- Siemens (2023a). *SITRANS FM MAG 5000*. siemens.com Global Website. URL: [siemens.com/global/en/products/automation/process-instrumentation/flow-measurement/electromagnetic/sitrans-f-m-mag-5000.html](https://www.siemens.com/global/en/products/automation/process-instrumentation/flow-measurement/electromagnetic/sitrans-f-m-mag-5000.html) (visited on 04/18/2023).
- (2023b). *SITRANS FM MAG 5100 W*. siemens.com Global Website. URL: [siemens.com/global/en/products/automation/process-instrumentation/flow-measurement/electromagnetic/sitrans-f-m-mag-5100-w-for-water-applications.html](https://www.siemens.com/global/en/products/automation/process-instrumentation/flow-measurement/electromagnetic/sitrans-f-m-mag-5100-w-for-water-applications.html) (visited on 04/18/2023).
- Sorensen, Robert M. (1985). “Stepped Spillway Hydraulic Model Investigation”. In: *Journal of Hydraulic Engineering* 111.12. Publisher: American Society of Civil Engineers, pp. 1461–1472. ISSN: 0733-9429. DOI: 10.1061/(ASCE)0733-9429(1985)111:12(1461).
- Takahashi, Masayuki and Iwao Ohtsu (2012). “Aerated flow characteristics of skimming flow over stepped chutes”. In: *Journal of Hydraulic Research* 50.4, pp. 427–434. ISSN: 0022-1686. DOI: 10.1080/00221686.2012.702859. (Visited on 06/04/2023).
- Thielicke, William and René Sonntag (2021). “Particle Image Velocimetry for MATLAB: Accuracy and enhanced algorithms in PIVlab”. In: 9.1. Number: 1 Publisher: Ubiquity Press, p. 12. ISSN: 2049-9647. DOI: 10.5334/jors.334.
- Thielicke, William and Eize J. Stamhuis (2014). “PIVlab – Towards User-friendly, Affordable and Accurate Digital Particle Image Velocimetry in MATLAB”. In:

- 2.1. Number: 1 Publisher: Ubiquity Press, e30. ISSN: 2049-9647. DOI: 10.5334/jors.bl.
- Toro, Juan Pablo, Fabián A. Bombardelli, and Joongcheol Paik (2017). “Detached Eddy Simulation of the Nonaerated Skimming Flow over a Stepped Spillway”. In: *Journal of Hydraulic Engineering* 143.9. Publisher: American Society of Civil Engineers, p. 04017032. ISSN: 1943-7900. DOI: 10.1061/(ASCE)HY.1943-7900.0001322.
- USBR (1987). *Design of Small Dams*. Water resources technical publication. Third edition. United States Bureau of Reclamation. 910 pp. ISBN: 978-81-903098-0-6. URL: www.usbr.gov/tsc/techreferences/mands/mands-pdfs/SmallDams.pdf.
- Wood, Ian R. (1983). “Uniform Region of Self-Aerated Flow”. In: *Journal of Hydraulic Engineering* 109.3. Publisher: American Society of Civil Engineers, pp. 447–461. ISSN: 0733-9429. DOI: 10.1061/(ASCE)0733-9429(1983)109:3(447).
- Wright, Henry-John (2006). “Improved Energy Dissipation on Stepped Spillways with the Addition of Triangular Protrusions”. In: URL: www.researchgate.net/publication/44139361.
- Wright, Henry-John and D G Cameron-Ellis (2018). “Energy Dissipation Provisions for Stepped Spillways Are Additional Measures Necessary? a Southern African perspective”. In: URL: www.researchgate.net/publication/333645060.
- Yiguo, Deng, Lin Keji, and Han Li (2003). “Design and prototype test of stepped overflow surface at Dachaoshan hydropower station in China”. In: *Roller Compacted Concrete Dams Proceedings of the IV International Symposium on Roller Compacted Concrete Dams, Madrid, Spain, 17-19 November 2003- 2 Vol set*. Ed. by L. Berga et al. 1st ed. London: Routledge, pp. 431–432. ISBN: 978-0-203-74127-6. DOI: 10.1201/9780203741276.
- Zabaleta, Federico, Fabián A. Bombardelli, and Juan Pablo Toro (2020). “Towards an understanding of the mechanisms leading to air entrainment in the skimming flow over stepped spillways”. In: *Environmental Fluid Mechanics* 20.2, pp. 375–392. ISSN: 1573-1510. DOI: 10.1007/s10652-019-09729-2.
- Zare, H.K. and J.C. Doering (2012). “Effect of rounding edges of stepped spillways on the flow characteristics”. In: *Canadian Journal of Civil Engineering* 39.2, pp. 140–153. ISSN: 0315-1468. DOI: 10.1139/111-121.
- Zhang, Gangfu (2017). “Free-Surface Aeration, Turbulence, and Energy Dissipation on Stepped Chutes with Triangular Steps, Chamfered Steps, and Partially Blocked Step Cavities”. In: DOI: 10.14264/uql.2017.906.
- Zhang, Gangfu and Hubert Chanson (2018). “Application of local optical flow methods to high-velocity free-surface flows: Validation and application to stepped chutes”. In: *Experimental Thermal and Fluid Science* 90, pp. 186–199. ISSN: 0894-1777. DOI: 10.1016/j.expthermflusci.2017.09.010.
- (2015). “Broad-Crested Weir Operation Upstream of a Steep Stepped Spillway”. In: URL: www.iahr.org/library/infor?pid=7755.

APPENDICES

LABORATORY DATA

A.1 D-flume measurements

Table A.1.1: D-flume water depth and inception point data - series 1 - basecase. Measured 14.04.2023.

Q_{red}	Q_{blue}	q_w	V	Y_2	u_2	Fr_2	Y_1	u_1	Fr_1	ΔE_0	ΔE_1	ΔE	$\frac{h_c}{h_s}$	IP
0.0000	0.0393	0.0393	-	-	-	-	-	-	-	-	-	-	0.60	II
0.0000	0.0494	0.0494	-	-	-	-	-	-	-	-	-	-	0.70	II
0.0000	0.0605	0.0605	-	-	-	-	-	-	-	-	-	-	0.80	III
0.0000	0.0722	0.0722	0.898	0.178	0.41	0.31	0.03	2.50	4.69	74 %	46 %	86 %	0.90	III/IV
0.0000	0.0845	0.0845	1.032	0.199	0.42	0.30	0.03	2.66	4.77	71 %	47 %	84 %	1.00	III/IV
0.0000	0.0976	0.0976	1.201	0.225	0.43	0.29	0.03	2.93	5.13	65 %	50 %	83 %	1.10	IV
0.0110	0.1002	0.1112	1.276	0.237	0.47	0.31	0.04	2.89	4.70	66 %	46 %	82 %	1.20	IV/V
0.0253	0.1000	0.1253	1.370	0.252	0.50	0.32	0.04	2.91	4.48	65 %	44 %	81 %	1.30	V
0.0410	0.1000	0.1410	1.481	0.269	0.52	0.32	0.05	2.97	4.35	64 %	43 %	80 %	1.41	VI
0.0554	0.1000	0.1554	1.592	0.287	0.54	0.32	0.05	3.06	4.34	62 %	43 %	78 %	1.50	VI/VII
0.0712	0.1000	0.1712	1.705	0.305	0.56	0.32	0.05	3.14	4.29	61 %	42 %	77 %	1.60	VII
0.0874	0.1000	0.1874	1.878	0.332	0.56	0.31	0.06	3.37	4.56	56 %	45 %	76 %	1.70	VII/VIII
0.1000	0.1042	0.2042	1.937	0.341	0.60	0.33	0.06	3.31	4.25	57 %	42 %	75 %	1.80	VIII
0.1000	0.1215	0.2215	2.082	0.364	0.61	0.32	0.06	3.46	4.36	54 %	43 %	74 %	1.90	IX
0.1000	0.1392	0.2392	2.209	0.384	0.62	0.32	0.07	3.56	4.38	52 %	43 %	73 %	2.00	X
0.1000	0.1574	0.2574	2.355	0.407	0.63	0.32	0.07	3.70	4.48	48 %	44 %	71 %	2.10	XI
0.1000	0.1760	0.2760	2.457	0.423	0.65	0.32	0.07	3.74	4.39	47 %	43 %	70 %	2.20	-
0.1500	0.1450	0.2950	2.549	0.438	0.67	0.33	0.08	3.76	4.28	47 %	42 %	69 %	2.30	-
0.1500	0.1644	0.3144	2.714	0.464	0.68	0.32	0.08	3.93	4.44	43 %	44 %	68 %	2.40	-
0.1500	0.1843	0.3343	2.849	0.485	0.69	0.32	0.08	4.04	4.49	40 %	44 %	67 %	2.50	-
0.2000	0.1545	0.3545	2.878	0.490	0.72	0.33	0.09	3.93	4.17	43 %	41 %	67 %	2.60	-
0.2000	0.1752	0.3752	3.046	0.516	0.73	0.32	0.09	4.10	4.32	39 %	43 %	65 %	2.70	-
0.2000	0.1962	0.3962	3.188	0.538	0.74	0.32	0.09	4.22	4.39	37 %	43 %	64 %	2.80	-
0.2176	0.2000	0.4176	3.267	0.551	0.76	0.33	0.10	4.21	4.26	37 %	42 %	64 %	2.90	-
0.2394	0.2000	0.4394	3.323	0.560	0.79	0.34	0.11	4.16	4.08	39 %	40 %	63 %	3.00	-
0.2616	0.2000	0.4616	3.564	0.598	0.77	0.32	0.10	4.45	4.41	31 %	44 %	61 %	3.10	-
0.2841	0.2000	0.4841	3.586	0.601	0.81	0.33	0.11	4.34	4.15	34 %	41 %	61 %	3.20	-
0.2900	0.2170	0.5070	3.817	0.637	0.80	0.32	0.11	4.61	4.44	28 %	44 %	59 %	3.30	-

Table A.1.2: D-flume water depth and inception point data - series 2 - basecase. Measured 17.04.2023.

Q_{red}	Q_{blue}	q_w	V	Y_2	u_2	Fr_2	Y_1	u_1	Fr_1	ΔE_0	ΔE_1	ΔE	$\frac{h_c}{h_s}$	IP
0.0000	0.0393	0.0393	-	-	-	-	-	-	-	-	-	-	0.60	II
0.0000	0.0495	0.0495	-	-	-	-	-	-	-	-	-	-	0.70	II
0.0000	0.0605	0.0605	-	-	-	-	-	-	-	-	-	-	0.80	III
0.0000	0.0722	0.0722	0.926	0.185	0.39	0.29	0.03	2.67	5.17	71 %	50 %	85 %	0.90	III/IV
0.0000	0.0846	0.0846	1.058	0.205	0.41	0.29	0.03	2.81	5.16	68 %	50 %	84 %	1.00	IV
0.0000	0.0976	0.0976	1.214	0.230	0.43	0.28	0.03	3.02	5.37	63 %	52 %	82 %	1.10	IV
0.1112	0.0000	0.1112	1.256	0.236	0.47	0.31	0.04	2.86	4.64	66 %	46 %	82 %	1.20	IV/V
0.1000	0.0253	0.1253	1.399	0.258	0.49	0.30	0.04	3.03	4.75	63 %	47 %	80 %	1.30	V
0.1000	0.0401	0.1401	1.519	0.277	0.51	0.31	0.04	3.12	4.70	61 %	46 %	79 %	1.40	V/VI
0.1000	0.0554	0.1554	1.623	0.293	0.53	0.31	0.05	3.16	4.56	60 %	45 %	78 %	1.50	VI
0.1000	0.0712	0.1712	1.742	0.311	0.55	0.31	0.05	3.25	4.52	58 %	45 %	77 %	1.60	VII/VI
0.1000	0.0874	0.1874	1.876	0.332	0.56	0.31	0.06	3.37	4.57	56 %	45 %	76 %	1.70	VII/VIII
0.1042	0.1000	0.2042	2.011	0.353	0.58	0.31	0.06	3.49	4.61	53 %	46 %	74 %	1.80	VIII
0.1215	0.1000	0.2215	2.141	0.373	0.59	0.31	0.06	3.59	4.62	51 %	46 %	73 %	1.90	IX
0.1392	0.1000	0.2392	2.275	0.394	0.61	0.31	0.06	3.70	4.65	48 %	46 %	72 %	2.00	X
0.1574	0.1000	0.2574	2.396	0.413	0.62	0.31	0.07	3.78	4.63	46 %	46 %	71 %	2.10	XI
0.1760	0.1000	0.2760	2.514	0.431	0.64	0.31	0.07	3.85	4.59	45 %	45 %	70 %	2.20	-
0.1950	0.1000	0.2950	2.675	0.456	0.65	0.31	0.07	4.01	4.73	41 %	47 %	68 %	2.30	-
0.2144	0.1000	0.3144	2.771	0.471	0.67	0.31	0.08	4.03	4.61	41 %	46 %	68 %	2.40	-
0.2343	0.1000	0.3343	2.932	0.496	0.67	0.31	0.08	4.19	4.73	37 %	47 %	66 %	2.50	-
0.2545	0.1000	0.3545	3.047	0.514	0.69	0.31	0.08	4.24	4.69	35 %	46 %	65 %	2.60	-
0.2752	0.1000	0.3752	3.169	0.533	0.70	0.31	0.09	4.31	4.67	34 %	46 %	64 %	2.70	-
0.2962	0.1000	0.3962	3.277	0.549	0.72	0.31	0.09	4.35	4.61	33 %	46 %	64 %	2.80	-
0.3176	0.1000	0.4176	3.422	0.572	0.73	0.31	0.09	4.47	4.66	30 %	46 %	62 %	2.90	-
0.2894	0.1500	0.4394	3.500	0.584	0.75	0.31	0.10	4.45	4.52	31 %	45 %	62 %	3.00	-
0.3116	0.1500	0.4616	3.631	0.604	0.76	0.31	0.10	4.53	4.53	29 %	45 %	61 %	3.10	-
0.2841	0.2000	0.4841	3.679	0.612	0.79	0.32	0.11	4.46	4.32	31 %	43 %	61 %	3.20	-
0.3070	0.2000	0.5070	3.787	0.628	0.81	0.33	0.11	4.50	4.29	30 %	42 %	60 %	3.30	-

Table A.1.3: D-flume water depth data - series 3 - basecase. Measured 18.04.2023.

q_w	h_c	V	Y_2	u_2	Fr_2	Y_1	u_1	Fr_1	ΔE_0	ΔE_1	ΔE	$\frac{h_c}{h_s}$
0.0393	0.054	-	0.130	0.30	0.27	0.017	2.38	5.90	76 %	56 %	89 %	0.60
0.0495	0.063	-	0.160	0.31	0.25	0.018	2.81	6.77	67 %	61 %	87 %	0.70
0.0605	0.072	-	0.170	0.36	0.28	0.023	2.66	5.62	71 %	54 %	87 %	0.80
0.0722	0.081	0.929	0.185	0.39	0.29	0.027	2.68	5.21	70 %	51 %	85 %	0.90
0.0846	0.090	1.041	0.203	0.42	0.30	0.031	2.75	5.00	69 %	49 %	84 %	1.00
0.0976	0.099	1.166	0.222	0.44	0.30	0.034	2.86	4.95	66 %	49 %	83 %	1.10
0.1112	0.108	1.270	0.238	0.47	0.31	0.038	2.91	4.75	66 %	47 %	82 %	1.20
0.1253	0.117	1.394	0.258	0.49	0.31	0.042	3.01	4.72	63 %	47 %	80 %	1.30
0.1401	0.126	1.516	0.276	0.51	0.31	0.045	3.11	4.68	61 %	46 %	79 %	1.40
0.1554	0.135	1.620	0.293	0.53	0.31	0.049	3.16	4.54	60 %	45 %	78 %	1.50
0.1712	0.144	1.799	0.320	0.53	0.30	0.050	3.40	4.84	55 %	48 %	76 %	1.60
0.1874	0.153	1.898	0.336	0.56	0.31	0.055	3.43	4.68	54 %	46 %	75 %	1.70
0.2042	0.162	1.996	0.351	0.58	0.31	0.059	3.45	4.53	54 %	45 %	74 %	1.80
0.2215	0.171	2.099	0.367	0.60	0.32	0.063	3.49	4.43	53 %	44 %	74 %	1.90
0.2392	0.180	2.243	0.389	0.61	0.31	0.066	3.63	4.52	50 %	45 %	72 %	2.00
0.2574	0.189	2.381	0.410	0.63	0.31	0.069	3.75	4.57	47 %	45 %	71 %	2.10
0.2760	0.198	2.527	0.433	0.64	0.31	0.071	3.88	4.64	44 %	46 %	70 %	2.20
0.2950	0.207	2.639	0.450	0.65	0.31	0.075	3.94	4.59	43 %	45 %	69 %	2.30
0.3144	0.216	2.781	0.472	0.67	0.31	0.078	4.05	4.64	40 %	46 %	68 %	2.40
0.3343	0.225	2.869	0.486	0.69	0.32	0.082	4.05	4.51	40 %	45 %	67 %	2.50
0.3545	0.234	3.016	0.509	0.70	0.31	0.085	4.18	4.58	37 %	45 %	66 %	2.60
0.3752	0.243	3.107	0.523	0.72	0.32	0.090	4.19	4.47	37 %	44 %	65 %	2.70
0.3962	0.252	3.245	0.544	0.73	0.32	0.092	4.29	4.51	35 %	45 %	64 %	2.80
0.4176	0.261	3.337	0.559	0.75	0.32	0.097	4.30	4.41	35 %	44 %	63 %	2.90
0.4394	0.270	3.437	0.574	0.77	0.32	0.102	4.33	4.34	34 %	43 %	62 %	3.00
0.4616	0.279	3.549	0.591	0.78	0.32	0.105	4.38	4.31	33 %	43 %	62 %	3.10
0.4841	0.288	3.656	0.608	0.80	0.33	0.110	4.42	4.26	32 %	42 %	61 %	3.20
0.5070	0.297	3.779	0.627	0.81	0.33	0.113	4.49	4.26	31 %	42 %	60 %	3.30

Table A.1.4: D-flume water depth and inception point data - series 1 - splitters configuration. Measured 21.04.2023.

q_w	h_c	V	Y_2	u_2	Fr_2	Y_1	u_1	Fr_1	ΔE_0	ΔE_1	ΔE	$\frac{h_c}{h_s}$	IP
0.0393	0.054	-	0.118	0.33	0.31	0.019	2.02	4.64	82 %	46 %	90 %	0.60	II
0.0495	0.063	-	0.148	0.33	0.28	0.020	2.46	5.55	75 %	53 %	88 %	0.70	II
0.0605	0.072	-	0.168	0.36	0.28	0.023	2.60	5.46	72 %	53 %	87 %	0.80	II
0.0722	0.081	0.881	0.178	0.41	0.31	0.029	2.50	4.71	74 %	46 %	86 %	0.90	II
0.0846	0.090	1.034	0.202	0.42	0.30	0.031	2.72	4.93	69 %	48 %	84 %	1.00	II
0.0976	0.099	1.168	0.223	0.44	0.30	0.034	2.87	4.97	66 %	49 %	83 %	1.10	II
0.1112	0.108	1.281	0.240	0.46	0.30	0.038	2.94	4.83	65 %	48 %	82 %	1.20	II
0.1253	0.117	1.408	0.260	0.48	0.30	0.041	3.06	4.82	62 %	47 %	80 %	1.30	II
0.1401	0.126	1.538	0.280	0.50	0.30	0.044	3.17	4.82	60 %	47 %	79 %	1.40	II
0.1554	0.135	1.631	0.294	0.53	0.31	0.049	3.18	4.60	60 %	45 %	78 %	1.50	II
0.1712	0.144	1.761	0.314	0.54	0.31	0.052	3.30	4.62	57 %	46 %	77 %	1.60	II
0.1874	0.153	1.881	0.333	0.56	0.31	0.055	3.38	4.59	55 %	45 %	76 %	1.70	II
0.2042	0.162	1.966	0.346	0.59	0.32	0.060	3.38	4.39	55 %	43 %	75 %	1.80	IV
0.2225	0.172	2.068	0.362	0.61	0.33	0.065	3.41	4.26	55 %	42 %	74 %	1.91	IV
0.2392	0.180	2.249	0.390	0.61	0.31	0.066	3.64	4.54	50 %	45 %	72 %	2.00	V
0.2574	0.189	2.331	0.403	0.64	0.32	0.071	3.63	4.36	50 %	43 %	71 %	2.10	VI
0.2760	0.198	2.462	0.423	0.65	0.32	0.074	3.74	4.39	48 %	43 %	70 %	2.20	VII
0.2950	0.207	2.607	0.445	0.66	0.32	0.076	3.87	4.47	45 %	44 %	69 %	2.30	VIII
0.3144	0.216	2.714	0.462	0.68	0.32	0.080	3.91	4.40	44 %	44 %	68 %	2.40	IX
0.3343	0.225	2.898	0.491	0.68	0.31	0.081	4.12	4.61	39 %	46 %	67 %	2.50	X
0.3545	0.234	2.956	0.499	0.71	0.32	0.087	4.06	4.38	40 %	43 %	66 %	2.60	XI
0.3752	0.243	3.088	0.520	0.72	0.32	0.090	4.15	4.41	38 %	44 %	65 %	2.70	-
0.3962	0.252	3.134	0.527	0.75	0.33	0.097	4.07	4.17	40 %	41 %	65 %	2.80	-
0.4176	0.261	3.245	0.544	0.77	0.33	0.101	4.13	4.14	39 %	41 %	64 %	2.90	-
0.4394	0.270	3.369	0.564	0.78	0.33	0.105	4.20	4.15	37 %	41 %	63 %	3.00	-
0.4616	0.279	3.492	0.582	0.79	0.33	0.108	4.27	4.15	36 %	41 %	62 %	3.10	-
0.4841	0.288	3.573	0.595	0.81	0.34	0.113	4.27	4.05	36 %	40 %	61 %	3.20	-
0.5070	0.297	3.746	0.622	0.82	0.33	0.114	4.43	4.18	32 %	41 %	60 %	3.30	-

Table A.1.5: D-flume water depth and inception point data - series 2 - splitters configuration. Measured 24.04.2023.

q_w	h_c	V	Y_2	u_2	Fr_2	Y_1	u_1	Fr_1	ΔE_0	ΔE_1	ΔE	$\frac{h_c}{h_s}$	IP
0.0393	0.054	-	0.130	0.30	0.27	0.017	2.38	5.90	76 %	56 %	89 %	0.60	II
0.0495	0.063	-	0.148	0.33	0.28	0.020	2.46	5.55	75 %	53 %	88 %	0.70	II
0.0605	0.072	-	0.165	0.37	0.29	0.024	2.53	5.22	73 %	51 %	87 %	0.80	II
0.0717	0.081	0.906	0.180	0.40	0.30	0.028	2.56	4.87	73 %	48 %	86 %	0.90	II
0.0846	0.090	1.057	0.203	0.42	0.30	0.031	2.75	5.00	69 %	49 %	84 %	1.00	II
0.0976	0.099	1.116	0.212	0.46	0.32	0.037	2.65	4.40	71 %	43 %	83 %	1.10	II
0.1112	0.108	1.189	0.223	0.50	0.34	0.043	2.61	4.04	71 %	40 %	83 %	1.20	II
0.1253	0.117	1.401	0.255	0.49	0.31	0.042	2.97	4.62	64 %	46 %	81 %	1.30	II
0.1410	0.127	1.554	0.279	0.51	0.31	0.045	3.14	4.72	61 %	47 %	79 %	1.41	II
0.1554	0.135	1.589	0.284	0.55	0.33	0.052	3.01	4.23	63 %	42 %	79 %	1.50	II
0.1712	0.144	1.784	0.314	0.55	0.31	0.052	3.29	4.60	57 %	45 %	77 %	1.60	II
0.1874	0.153	1.827	0.320	0.59	0.33	0.059	3.18	4.18	60 %	41 %	76 %	1.70	II
0.2042	0.162	1.988	0.345	0.59	0.32	0.061	3.36	4.35	56 %	43 %	75 %	1.80	IV
0.2215	0.171	2.146	0.369	0.60	0.32	0.063	3.53	4.50	52 %	44 %	73 %	1.90	IV
0.2392	0.180	2.246	0.384	0.62	0.32	0.067	3.56	4.38	52 %	43 %	73 %	2.00	V
0.2574	0.189	2.343	0.399	0.65	0.33	0.072	3.58	4.26	51 %	42 %	72 %	2.10	VI
0.2760	0.198	2.479	0.420	0.66	0.32	0.075	3.69	4.31	49 %	43 %	70 %	2.20	VII
0.2950	0.207	2.583	0.436	0.68	0.33	0.079	3.73	4.23	48 %	42 %	70 %	2.30	VIII
0.3144	0.216	2.668	0.449	0.70	0.33	0.084	3.73	4.10	48 %	40 %	69 %	2.40	IX
0.3343	0.225	2.841	0.475	0.70	0.33	0.086	3.91	4.26	44 %	42 %	67 %	2.50	X
0.3545	0.234	2.933	0.489	0.72	0.33	0.090	3.92	4.16	44 %	41 %	67 %	2.60	XI
0.3752	0.243	3.094	0.514	0.73	0.33	0.092	4.07	4.28	40 %	42 %	65 %	2.70	-
0.3962	0.252	3.174	0.526	0.75	0.33	0.098	4.06	4.15	41 %	41 %	65 %	2.80	-
0.4176	0.261	3.260	0.539	0.77	0.34	0.103	4.06	4.04	41 %	40 %	64 %	2.90	-
0.4394	0.270	3.364	0.555	0.79	0.34	0.107	4.10	4.00	40 %	39 %	63 %	3.00	-
0.4616	0.279	3.485	0.573	0.81	0.34	0.111	4.17	4.00	38 %	39 %	63 %	3.10	-
0.4841	0.288	3.556	0.584	0.83	0.35	0.117	4.15	3.88	39 %	38 %	62 %	3.20	-
0.5070	0.297	3.668	0.601	0.84	0.35	0.121	4.20	3.86	38 %	37 %	61 %	3.30	-

Table A.1.6: D-flume water depth and inception point data - series 3 - splitters configuration. Measured 25.04.2023.

q_w	h_c	V	Y_2	u_2	Fr_2	Y_1	u_1	Fr_1	ΔE_0	ΔE_1	ΔE	$\frac{h_c}{h_s}$	IP
0.0393	0.054	-	0.120	0.33	0.30	0.019	2.08	4.83	81 %	48 %	90 %	0.60	II
0.0495	0.063	-	0.148	0.33	0.28	0.020	2.46	5.55	75 %	53 %	88 %	0.70	II
0.0600	0.072	-	0.163	0.37	0.29	0.024	2.49	5.13	74 %	50 %	87 %	0.80	II
0.0722	0.081	0.876	0.175	0.41	0.31	0.030	2.44	4.52	75 %	45 %	86 %	0.90	II
0.0846	0.090	0.964	0.189	0.45	0.33	0.035	2.44	4.18	75 %	41 %	85 %	1.00	II
0.0976	0.099	1.145	0.216	0.45	0.31	0.036	2.74	4.63	69 %	46 %	83 %	1.10	II
0.1112	0.108	1.268	0.235	0.47	0.31	0.039	2.84	4.59	67 %	45 %	82 %	1.20	II
0.1253	0.117	1.405	0.256	0.49	0.31	0.042	2.98	4.65	64 %	46 %	81 %	1.30	II
0.1401	0.126	1.490	0.269	0.52	0.32	0.047	2.97	4.37	64 %	43 %	80 %	1.40	II
0.1554	0.135	1.644	0.292	0.53	0.31	0.049	3.15	4.53	60 %	45 %	78 %	1.50	II
0.1712	0.144	1.727	0.305	0.56	0.32	0.055	3.14	4.30	61 %	42 %	77 %	1.60	II
0.1874	0.153	1.849	0.324	0.58	0.32	0.058	3.23	4.29	59 %	42 %	76 %	1.70	II
0.2042	0.162	1.960	0.341	0.60	0.33	0.062	3.29	4.22	57 %	42 %	75 %	1.80	IV
0.2215	0.171	2.046	0.354	0.63	0.34	0.067	3.30	4.06	57 %	40 %	74 %	1.90	IV
0.2392	0.180	2.235	0.383	0.63	0.32	0.068	3.53	4.33	52 %	43 %	73 %	2.00	V
0.2574	0.189	2.326	0.396	0.65	0.33	0.073	3.54	4.20	52 %	41 %	72 %	2.10	VI
0.2760	0.198	2.487	0.421	0.66	0.32	0.074	3.71	4.34	48 %	43 %	70 %	2.20	VII
0.2950	0.207	2.577	0.435	0.68	0.33	0.079	3.72	4.21	48 %	42 %	70 %	2.30	VIII
0.3144	0.216	2.710	0.455	0.69	0.33	0.082	3.82	4.25	46 %	42 %	69 %	2.40	IX
0.3343	0.225	2.806	0.470	0.71	0.33	0.087	3.84	4.15	46 %	41 %	68 %	2.50	X
0.3545	0.234	2.943	0.491	0.72	0.33	0.090	3.94	4.19	43 %	41 %	67 %	2.60	XI
0.3752	0.243	3.031	0.504	0.74	0.33	0.095	3.95	4.09	43 %	40 %	66 %	2.70	-
0.3962	0.252	3.169	0.525	0.75	0.33	0.098	4.05	4.13	41 %	41 %	65 %	2.80	-
0.4176	0.261	3.225	0.534	0.78	0.34	0.104	4.00	3.95	42 %	39 %	65 %	2.90	-
0.4394	0.270	3.393	0.559	0.79	0.34	0.106	4.15	4.07	39 %	40 %	63 %	3.00	-
0.4616	0.279	3.494	0.575	0.80	0.34	0.110	4.18	4.02	38 %	39 %	62 %	3.10	-
0.4841	0.288	3.544	0.582	0.83	0.35	0.117	4.13	3.85	40 %	37 %	62 %	3.20	-
0.5070	0.297	3.639	0.597	0.85	0.35	0.122	4.15	3.79	39 %	37 %	61 %	3.30	-

A.2 C-flume measurements

Table A.2.1: C-flume water depth data - series 1 - basecase. Measured 24.03.2023.

Q_{in}	q_w	h_c	Y_2	u_2	Fr_2	Y_1	u_1	Fr_1	$\Delta E0$	$\Delta E1$	ΔE	$\frac{h_c}{h_s}$
0.0047	0.0077	0.018	0.034	0.23	0.39	0.008	0.92	3.20	88 %	29 %	91 %	0.61
0.0057	0.0093	0.021	0.045	0.21	0.31	0.008	1.24	4.57	80 %	45 %	89 %	0.69
0.0072	0.0117	0.024	0.054	0.22	0.30	0.008	1.41	4.92	75 %	48 %	87 %	0.80
0.0087	0.0143	0.027	0.060	0.24	0.31	0.010	1.44	4.63	74 %	46 %	86 %	0.92
0.0100	0.0164	0.030	0.066	0.25	0.31	0.011	1.52	4.66	71 %	46 %	84 %	1.00
0.0120	0.0196	0.034	0.076	0.26	0.30	0.012	1.67	4.92	66 %	48 %	82 %	1.13
0.0133	0.0218	0.036	0.080	0.27	0.31	0.013	1.67	4.68	66 %	46 %	82 %	1.22
0.0148	0.0243	0.039	0.086	0.28	0.31	0.014	1.74	4.70	63 %	46 %	80 %	1.30
0.0166	0.0271	0.042	0.095	0.29	0.30	0.014	1.88	4.99	58 %	49 %	79 %	1.41
0.0183	0.0300	0.045	0.100	0.30	0.30	0.016	1.89	4.80	58 %	47 %	78 %	1.50
0.0194	0.0318	0.047	0.104	0.31	0.30	0.016	1.93	4.80	56 %	47 %	77 %	1.56
0.0203	0.0333	0.048	0.110	0.30	0.29	0.016	2.05	5.13	51 %	50 %	76 %	1.61
0.0219	0.0358	0.051	0.114	0.31	0.30	0.017	2.05	4.96	51 %	49 %	75 %	1.69
0.0246	0.0403	0.055	0.123	0.33	0.30	0.019	2.13	4.93	48 %	48 %	73 %	1.83
0.0257	0.0420	0.056	0.127	0.33	0.30	0.019	2.17	4.97	47 %	49 %	73 %	1.88
0.0271	0.0443	0.059	0.130	0.34	0.30	0.020	2.16	4.83	47 %	48 %	72 %	1.95
0.0295	0.0484	0.062	0.136	0.36	0.31	0.022	2.18	4.68	46 %	46 %	71 %	2.07
0.0320	0.0525	0.065	0.145	0.36	0.30	0.023	2.28	4.79	42 %	47 %	70 %	2.18
0.0343	0.0562	0.069	0.152	0.37	0.30	0.024	2.34	4.81	40 %	47 %	68 %	2.28
0.0368	0.0603	0.072	0.158	0.38	0.31	0.026	2.36	4.71	39 %	46 %	67 %	2.40
0.0387	0.0634	0.074	0.166	0.38	0.30	0.026	2.46	4.89	35 %	48 %	66 %	2.48
0.0407	0.0667	0.077	0.170	0.39	0.30	0.027	2.46	4.78	35 %	47 %	65 %	2.56
0.0416	0.0682	0.078	0.173	0.39	0.30	0.027	2.49	4.81	33 %	47 %	65 %	2.60
0.0435	0.0713	0.080	0.177	0.40	0.31	0.029	2.50	4.73	33 %	47 %	64 %	2.68
0.0460	0.0754	0.083	0.184	0.41	0.31	0.030	2.56	4.75	31 %	47 %	63 %	2.78
0.0490	0.0803	0.087	0.190	0.42	0.31	0.031	2.57	4.63	31 %	46 %	62 %	2.90
0.0516	0.0846	0.090	0.197	0.43	0.31	0.032	2.62	4.65	29 %	46 %	61 %	3.00
0.0538	0.0882	0.093	0.202	0.44	0.31	0.033	2.64	4.62	28 %	46 %	61 %	3.09
0.0554	0.0908	0.094	0.206	0.44	0.31	0.034	2.67	4.62	27 %	46 %	60 %	3.15
0.0580	0.0951	0.097	0.211	0.45	0.31	0.035	2.68	4.55	26 %	45 %	59 %	3.24

Table A.2.2: C-flume water depth and inception point data - series 2 - basecase. Measured 17.04.2023.

Q_{in}	q_w	h_c	Y_2	u_2	Fr_2	Y_1	u_1	Fr_1	$\Delta E0$	$\Delta E1$	ΔE	$\frac{h_c}{h_s}$	IP
0.0046	0.0076	0.018	0.037	0.20	0.34	0.007	1.06	4.01	85 %	39 %	91 %	0.60	II
0.0057	0.0094	0.021	0.045	0.21	0.31	0.008	1.24	4.55	80 %	45 %	89 %	0.69	II
0.0072	0.0118	0.024	0.055	0.21	0.29	0.008	1.45	5.12	74 %	50 %	87 %	0.81	III/IV
0.0084	0.0138	0.027	0.061	0.23	0.29	0.009	1.52	5.11	71 %	50 %	86 %	0.89	IV
0.0099	0.0162	0.030	0.066	0.25	0.31	0.011	1.53	4.74	71 %	47 %	84 %	1.00	V/IV
0.0114	0.0187	0.033	0.074	0.25	0.30	0.011	1.66	4.97	66 %	49 %	83 %	1.10	V
0.0130	0.0214	0.036	0.080	0.27	0.30	0.013	1.70	4.84	65 %	48 %	82 %	1.20	VI
0.0145	0.0238	0.039	0.087	0.27	0.30	0.013	1.80	4.99	61 %	49 %	80 %	1.29	VI/VII
0.0168	0.0275	0.043	0.095	0.29	0.30	0.015	1.86	4.87	59 %	48 %	79 %	1.42	VII
0.0184	0.0302	0.045	0.100	0.30	0.31	0.016	1.88	4.75	58 %	47 %	78 %	1.51	VIII
0.0200	0.0327	0.048	0.105	0.31	0.31	0.017	1.92	4.70	57 %	46 %	77 %	1.59	IX
0.0219	0.0358	0.051	0.114	0.31	0.30	0.017	2.05	4.96	51 %	49 %	75 %	1.69	X
0.0238	0.0390	0.054	0.117	0.33	0.31	0.019	2.01	4.60	53 %	45 %	74 %	1.79	X/XI
0.0257	0.0422	0.057	0.125	0.34	0.30	0.020	2.11	4.75	49 %	47 %	73 %	1.89	XI
0.0281	0.0460	0.060	0.134	0.34	0.30	0.021	2.21	4.90	45 %	48 %	71 %	2.00	-
0.0299	0.0490	0.063	0.140	0.35	0.30	0.022	2.27	4.93	43 %	48 %	70 %	2.08	-
0.0323	0.0530	0.066	0.144	0.37	0.31	0.024	2.24	4.64	44 %	46 %	70 %	2.20	-
0.0345	0.0566	0.069	0.152	0.37	0.30	0.024	2.32	4.75	40 %	47 %	68 %	2.30	-
0.0368	0.0602	0.072	0.158	0.38	0.31	0.026	2.36	4.72	39 %	47 %	67 %	2.39	-
0.0383	0.0629	0.074	0.161	0.39	0.31	0.027	2.36	4.61	39 %	46 %	67 %	2.46	-
0.0399	0.0654	0.076	0.166	0.39	0.31	0.027	2.40	4.66	37 %	46 %	66 %	2.53	-
0.0412	0.0675	0.077	0.170	0.40	0.31	0.028	2.44	4.69	36 %	46 %	66 %	2.58	-
0.0433	0.0710	0.080	0.177	0.40	0.30	0.028	2.51	4.77	33 %	47 %	64 %	2.67	-
0.0464	0.0761	0.084	0.184	0.41	0.31	0.030	2.54	4.68	32 %	46 %	63 %	2.80	-
0.0488	0.0799	0.087	0.190	0.42	0.31	0.031	2.58	4.67	30 %	46 %	62 %	2.89	-
0.0516	0.0846	0.090	0.196	0.43	0.31	0.033	2.60	4.60	30 %	45 %	62 %	3.00	-
0.0535	0.0877	0.092	0.203	0.43	0.31	0.033	2.68	4.72	26 %	47 %	61 %	3.07	-
0.0560	0.0918	0.095	0.207	0.44	0.31	0.034	2.67	4.60	27 %	45 %	60 %	3.17	-
0.0578	0.0948	0.097	0.211	0.45	0.31	0.035	2.69	4.57	26 %	45 %	59 %	3.24	-

Table A.2.3: C-flume water depth data - series 3 - basecase. Measured 20.04.2023.

Q_{in}	q_w	h_c	Y_2	u_2	Fr_2	Y_1	u_1	Fr_1	$\Delta E0$	$\Delta E1$	ΔE	$\frac{h_c}{h_s}$
0.0048	0.0078	0.018	0.038	0.21	0.34	0.007	1.08	4.03	84 %	39 %	91 %	0.61
0.0059	0.0096	0.021	0.046	0.21	0.31	0.008	1.26	4.62	79 %	46 %	89 %	0.70
0.0071	0.0116	0.024	0.054	0.22	0.30	0.008	1.42	4.99	75 %	49 %	87 %	0.80
0.0084	0.0138	0.027	0.060	0.23	0.30	0.009	1.48	4.89	73 %	48 %	86 %	0.90
0.0100	0.0163	0.030	0.069	0.24	0.29	0.010	1.64	5.22	67 %	51 %	84 %	1.00
0.0116	0.0190	0.033	0.074	0.26	0.30	0.012	1.63	4.84	67 %	48 %	83 %	1.11
0.0131	0.0215	0.036	0.081	0.27	0.30	0.012	1.72	4.93	64 %	48 %	81 %	1.21
0.0148	0.0242	0.039	0.086	0.28	0.31	0.014	1.74	4.71	63 %	47 %	80 %	1.30
0.0164	0.0268	0.042	0.094	0.29	0.30	0.014	1.86	4.96	59 %	49 %	79 %	1.39
0.0183	0.0299	0.045	0.100	0.30	0.30	0.016	1.90	4.83	57 %	48 %	78 %	1.50
0.0201	0.0329	0.048	0.105	0.31	0.31	0.017	1.91	4.65	57 %	46 %	77 %	1.60
0.0220	0.0361	0.051	0.111	0.33	0.31	0.018	1.95	4.59	55 %	45 %	76 %	1.70
0.0240	0.0393	0.054	0.119	0.33	0.31	0.019	2.05	4.74	51 %	47 %	74 %	1.80
0.0261	0.0428	0.057	0.126	0.34	0.31	0.020	2.11	4.74	49 %	47 %	73 %	1.91
0.0281	0.0461	0.060	0.131	0.35	0.31	0.022	2.13	4.61	49 %	46 %	72 %	2.00
0.0301	0.0493	0.063	0.140	0.35	0.30	0.022	2.25	4.86	43 %	48 %	70 %	2.09
0.0326	0.0535	0.066	0.147	0.36	0.30	0.023	2.30	4.80	42 %	47 %	69 %	2.21
0.0345	0.0566	0.069	0.152	0.37	0.30	0.024	2.32	4.76	40 %	47 %	68 %	2.29
0.0371	0.0608	0.072	0.160	0.38	0.30	0.025	2.39	4.79	38 %	47 %	67 %	2.41
0.0387	0.0634	0.074	0.165	0.38	0.30	0.026	2.44	4.82	36 %	48 %	66 %	2.48
0.0406	0.0666	0.077	0.170	0.39	0.30	0.027	2.47	4.80	35 %	47 %	65 %	2.56
0.0416	0.0682	0.078	0.173	0.39	0.30	0.027	2.49	4.81	33 %	47 %	65 %	2.60
0.0441	0.0723	0.081	0.179	0.40	0.30	0.029	2.52	4.76	32 %	47 %	64 %	2.70
0.0465	0.0762	0.084	0.184	0.41	0.31	0.030	2.53	4.67	32 %	46 %	63 %	2.80
0.0490	0.0803	0.087	0.190	0.42	0.31	0.031	2.57	4.63	31 %	46 %	62 %	2.90
0.0520	0.0852	0.090	0.196	0.43	0.31	0.033	2.58	4.54	30 %	45 %	62 %	3.02
0.0540	0.0885	0.093	0.201	0.44	0.31	0.034	2.62	4.54	29 %	45 %	61 %	3.09
0.0560	0.0918	0.095	0.208	0.44	0.31	0.034	2.69	4.65	26 %	46 %	60 %	3.17
0.0578	0.0948	0.097	0.210	0.45	0.31	0.036	2.67	4.52	27 %	45 %	60 %	3.24

Table A.2.4: C-flume water depth and inception point data - series 1 - splitters. Measured 20.04.2023.

Q_{in}	q_w	h_c	Y_2	u_2	Fr_2	Y_1	u_1	Fr_1	$\Delta E0$	$\Delta E1$	ΔE	$\frac{h_c}{h_s}$	IP
0.0045	0.0073	0.018	0.035	0.21	0.36	0.007	0.99	3.70	86 %	36 %	91 %	0.59	II
0.0057	0.0093	0.021	0.041	0.23	0.36	0.009	1.07	3.68	84 %	35 %	90 %	0.69	II
0.0070	0.0115	0.024	0.049	0.23	0.34	0.009	1.22	4.01	80 %	39 %	88 %	0.79	II
0.0084	0.0138	0.027	0.059	0.23	0.31	0.010	1.44	4.71	74 %	47 %	86 %	0.89	II
0.0098	0.0161	0.030	0.064	0.25	0.32	0.011	1.46	4.44	73 %	44 %	85 %	0.99	II
0.0114	0.0187	0.033	0.071	0.26	0.31	0.012	1.55	4.51	70 %	45 %	83 %	1.10	II
0.0130	0.0213	0.036	0.080	0.27	0.30	0.013	1.70	4.86	65 %	48 %	82 %	1.20	II
0.0149	0.0244	0.039	0.089	0.27	0.29	0.013	1.83	5.08	60 %	50 %	80 %	1.31	II
0.0164	0.0269	0.042	0.094	0.29	0.30	0.014	1.86	4.93	59 %	48 %	79 %	1.40	II
0.0182	0.0299	0.045	0.102	0.29	0.29	0.015	1.96	5.08	55 %	50 %	77 %	1.50	IV
0.0201	0.0330	0.048	0.106	0.31	0.31	0.017	1.94	4.74	56 %	47 %	77 %	1.60	IV
0.0221	0.0363	0.051	0.111	0.33	0.31	0.019	1.95	4.55	56 %	45 %	76 %	1.71	V
0.0238	0.0390	0.054	0.118	0.33	0.31	0.019	2.03	4.69	52 %	46 %	74 %	1.79	VI/V
0.0260	0.0426	0.057	0.125	0.34	0.31	0.020	2.09	4.68	50 %	46 %	73 %	1.90	VI
0.0282	0.0462	0.060	0.130	0.36	0.31	0.022	2.10	4.51	50 %	45 %	72 %	2.00	VII
0.0303	0.0497	0.063	0.138	0.36	0.31	0.023	2.19	4.64	46 %	46 %	71 %	2.10	VIII
0.0322	0.0528	0.066	0.144	0.37	0.31	0.024	2.24	4.66	44 %	46 %	70 %	2.19	IX
0.0346	0.0567	0.069	0.150	0.38	0.31	0.025	2.27	4.58	43 %	45 %	69 %	2.30	X
0.0370	0.0606	0.072	0.159	0.38	0.31	0.026	2.37	4.75	38 %	47 %	67 %	2.40	XI
0.0389	0.0637	0.075	0.162	0.39	0.31	0.027	2.36	4.58	39 %	45 %	67 %	2.48	-
0.0406	0.0666	0.077	0.166	0.40	0.31	0.028	2.37	4.53	39 %	45 %	66 %	2.56	-
0.0419	0.0687	0.078	0.167	0.41	0.32	0.029	2.34	4.36	40 %	43 %	66 %	2.61	-
0.0441	0.0723	0.081	0.174	0.42	0.32	0.030	2.41	4.44	38 %	44 %	65 %	2.70	-
0.0466	0.0764	0.084	0.180	0.42	0.32	0.031	2.44	4.41	36 %	44 %	64 %	2.80	-
0.0490	0.0803	0.087	0.185	0.43	0.32	0.033	2.46	4.34	36 %	43 %	63 %	2.90	-
0.0515	0.0844	0.090	0.192	0.44	0.32	0.034	2.52	4.39	33 %	43 %	62 %	3.00	-
0.0546	0.0895	0.093	0.199	0.45	0.32	0.035	2.55	4.35	32 %	43 %	61 %	3.12	-
0.0568	0.0931	0.096	0.203	0.46	0.33	0.036	2.56	4.29	32 %	42 %	61 %	3.20	-
0.0590	0.0967	0.098	0.206	0.47	0.33	0.038	2.55	4.18	33 %	41 %	60 %	3.28	-

Table A.2.5: C-flume water depth and inception point data - series 2 - splitters.
Measured 21.04.2023.

Q_{in}	q_w	h_c	Y_2	u_2	Fr_2	Y_1	u_1	Fr_1	$\Delta E0$	$\Delta E1$	ΔE	$\frac{h_c}{h_s}$	IP
0.0048	0.0078	0.018	0.037	0.21	0.35	0.008	1.03	3.80	85 %	37 %	91 %	0.61	II
0.0056	0.0092	0.020	0.042	0.22	0.34	0.008	1.13	3.99	83 %	39 %	90 %	0.68	II
0.0070	0.0114	0.024	0.050	0.23	0.33	0.009	1.27	4.28	79 %	42 %	88 %	0.79	II
0.0083	0.0136	0.027	0.057	0.24	0.32	0.010	1.38	4.43	76 %	44 %	86 %	0.89	II
0.0098	0.0161	0.030	0.063	0.26	0.33	0.011	1.42	4.28	74 %	42 %	85 %	0.99	II
0.0113	0.0185	0.033	0.072	0.26	0.31	0.012	1.59	4.72	69 %	47 %	83 %	1.09	II
0.0132	0.0217	0.036	0.080	0.27	0.31	0.013	1.68	4.72	66 %	47 %	82 %	1.21	II
0.0144	0.0237	0.039	0.085	0.28	0.30	0.014	1.74	4.75	63 %	47 %	81 %	1.28	II
0.0163	0.0267	0.042	0.091	0.29	0.31	0.015	1.78	4.63	62 %	46 %	79 %	1.39	II
0.0183	0.0300	0.045	0.100	0.30	0.30	0.016	1.89	4.80	58 %	47 %	78 %	1.50	IV
0.0198	0.0324	0.048	0.105	0.31	0.30	0.017	1.93	4.77	56 %	47 %	77 %	1.58	IV
0.0217	0.0356	0.051	0.110	0.32	0.31	0.018	1.95	4.59	56 %	45 %	76 %	1.68	V
0.0241	0.0396	0.054	0.119	0.33	0.31	0.019	2.04	4.68	52 %	46 %	74 %	1.81	VI/V
0.0260	0.0426	0.057	0.125	0.34	0.31	0.020	2.09	4.68	50 %	46 %	73 %	1.90	VI
0.0278	0.0456	0.060	0.130	0.35	0.31	0.022	2.12	4.61	49 %	46 %	72 %	1.99	VII
0.0302	0.0494	0.063	0.139	0.36	0.30	0.022	2.22	4.76	45 %	47 %	71 %	2.10	VIII
0.0324	0.0531	0.066	0.143	0.37	0.31	0.024	2.21	4.54	45 %	45 %	70 %	2.20	IX
0.0347	0.0569	0.069	0.150	0.38	0.31	0.025	2.27	4.57	43 %	45 %	69 %	2.30	X
0.0368	0.0602	0.072	0.156	0.39	0.31	0.026	2.31	4.57	41 %	45 %	68 %	2.39	XI
0.0393	0.0644	0.075	0.164	0.39	0.31	0.027	2.39	4.64	38 %	46 %	66 %	2.50	-
0.0410	0.0672	0.077	0.167	0.40	0.31	0.028	2.38	4.52	39 %	45 %	66 %	2.57	-
0.0416	0.0682	0.078	0.169	0.40	0.31	0.028	2.40	4.54	38 %	45 %	66 %	2.60	-
0.0439	0.0720	0.081	0.175	0.41	0.31	0.030	2.44	4.53	36 %	45 %	65 %	2.69	-
0.0470	0.0770	0.085	0.182	0.42	0.32	0.031	2.47	4.47	35 %	44 %	64 %	2.82	-
0.0492	0.0807	0.087	0.185	0.44	0.32	0.033	2.45	4.32	36 %	43 %	63 %	2.91	-
0.0509	0.0834	0.089	0.189	0.44	0.32	0.034	2.48	4.31	35 %	43 %	63 %	2.97	-
0.0542	0.0889	0.093	0.196	0.45	0.33	0.035	2.50	4.25	34 %	42 %	62 %	3.10	-
0.0570	0.0934	0.096	0.200	0.47	0.33	0.037	2.49	4.11	35 %	40 %	61 %	3.21	-
0.0586	0.0961	0.098	0.204	0.47	0.33	0.038	2.52	4.12	34 %	41 %	61 %	3.27	-

Table A.2.6: C-flume water depth and inception point data - series 3 - splitters.
Measured 25.04.2023.

Q_{in}	q_w	h_c	Y_2	u_2	Fr_2	Y_1	u_1	Fr_1	$\Delta E0$	$\Delta E1$	ΔE	$\frac{h_c}{h_s}$	IP
0.0046	0.0075	0.018	0.036	0.21	0.35	0.007	1.02	3.82	86 %	37 %	91 %	0.60	II
0.0059	0.0097	0.021	0.043	0.23	0.35	0.009	1.12	3.85	83 %	37 %	89 %	0.71	II
0.0069	0.0113	0.024	0.050	0.23	0.32	0.009	1.28	4.33	79 %	43 %	88 %	0.78	II
0.0084	0.0138	0.027	0.055	0.25	0.34	0.011	1.28	3.94	79 %	38 %	87 %	0.90	II
0.0100	0.0164	0.030	0.062	0.26	0.34	0.012	1.37	4.01	76 %	39 %	85 %	1.00	II
0.0115	0.0189	0.033	0.070	0.27	0.33	0.013	1.50	4.27	72 %	42 %	84 %	1.10	II
0.0131	0.0215	0.036	0.079	0.27	0.31	0.013	1.66	4.64	66 %	46 %	82 %	1.20	II
0.0147	0.0240	0.039	0.086	0.28	0.30	0.014	1.75	4.76	63 %	47 %	80 %	1.30	II
0.0163	0.0267	0.042	0.093	0.29	0.30	0.015	1.84	4.86	60 %	48 %	79 %	1.39	II
0.0182	0.0298	0.045	0.099	0.30	0.31	0.016	1.87	4.75	58 %	47 %	78 %	1.50	IV
0.0200	0.0328	0.048	0.105	0.31	0.31	0.017	1.92	4.68	57 %	46 %	77 %	1.60	IV
0.0218	0.0358	0.051	0.111	0.32	0.31	0.018	1.97	4.65	55 %	46 %	76 %	1.69	V
0.0240	0.0393	0.054	0.118	0.33	0.31	0.019	2.03	4.64	52 %	46 %	74 %	1.80	VI/V
0.0261	0.0428	0.057	0.124	0.35	0.31	0.021	2.06	4.55	51 %	45 %	73 %	1.91	VI
0.0280	0.0459	0.060	0.130	0.35	0.31	0.022	2.11	4.56	49 %	45 %	72 %	2.00	VII
0.0300	0.0492	0.063	0.136	0.36	0.31	0.023	2.15	4.55	47 %	45 %	71 %	2.09	VIII
0.0326	0.0534	0.066	0.145	0.37	0.31	0.024	2.25	4.65	44 %	46 %	70 %	2.21	IX
0.0345	0.0565	0.069	0.150	0.38	0.31	0.025	2.28	4.62	43 %	46 %	69 %	2.29	X
0.0369	0.0604	0.072	0.157	0.38	0.31	0.026	2.33	4.62	40 %	46 %	68 %	2.40	XI
0.0392	0.0643	0.075	0.163	0.39	0.31	0.027	2.36	4.58	39 %	45 %	67 %	2.50	-
0.0411	0.0673	0.077	0.168	0.40	0.31	0.028	2.40	4.57	38 %	45 %	66 %	2.58	-
0.0420	0.0689	0.078	0.170	0.41	0.31	0.029	2.41	4.54	38 %	45 %	66 %	2.62	-
0.0440	0.0721	0.081	0.172	0.42	0.32	0.030	2.37	4.33	39 %	43 %	65 %	2.70	-
0.0460	0.0754	0.083	0.180	0.42	0.32	0.031	2.47	4.50	35 %	44 %	64 %	2.78	-
0.0490	0.0803	0.087	0.185	0.43	0.32	0.033	2.46	4.34	36 %	43 %	63 %	2.90	-
0.0513	0.0841	0.090	0.190	0.44	0.32	0.034	2.48	4.30	35 %	42 %	63 %	2.99	-
0.0540	0.0885	0.093	0.195	0.45	0.33	0.036	2.49	4.22	35 %	42 %	62 %	3.09	-
0.0555	0.0910	0.094	0.201	0.45	0.32	0.036	2.56	4.34	32 %	43 %	61 %	3.15	-

PIVLAB SETTINGS

Table B.0.1: Overview of settings in PIVlab.

Main process	Sub process	Settings	Choice
Image settings	Mask	Mask irrelevant regions	On
		Image pre-processing	CLAHE
	Highpass		15 px
	Wiener2 denoise and low pass		3 px
	Auto contrast stretch		On
	Background subtraction	Subtract mean intensity	On
Analysis	PIV algorithm Pass 1	FFT window deformation	On
		Interrogation area	64 px
	Pass 2	Step	32 px
		Interrogation area	32 px
	Sub-pixel estimator	Step	16 px
		Gauss 2x3-point	-
Correlation robustness	Standard	-	
Calibration	Measured reference length	-	-
Post-processing	Velocity based	Standard deviation filter	8
		Threshold [n*stdev]	
		Local median filter	3
		Threshold	
	Image based	Magnitude notch filter	Off
		Filter low contrast	Off
		Filter bright objects	Off
		Correlation contrast filter	Off
	Interpolate missing data	On	
Plot	Temporal	Derive Parameters	Calculate mean



 **NTNU**

Norwegian University of
Science and Technology